Functional characterization of the *Ustilago maydis* effector protein Ten1

Dissertation

zur
Erlangung des Doktorgrades
der Naturwissenschaften
(Dr. rer. nat.)

Dem Fachbereich Biologie
der Philipps-Universität Marburg
vorgelegt von

Philipp Erchinger
aus Villingen-Schwenningen

Marburg/Lahn, 2017

Die Untersuchungen zur vorliegenden Arbeit wurden von Oktober 2013 bis September 2017 unter Betreuung von Frau Prof. Dr. Regine Kahmann in Marburg am Max-Planck-Institut für terrestrische Mikrobiologie in der Abteilung Organismische Interaktionen durchgeführt.

Vom Fachbereich Biologie der Philipps-Universität Marburg
als Dissertation angenommen am: 24.10.2017

Erstgutachterin: Frau Prof. Dr. Regine Kahmann
Zweitgutachter: Herr Prof. Dr. Alfred Batschauer

Tag der mündlichen Prüfung: 09.11.2017

Erklärung

Ich versichere, dass ich meine Dissertation mit dem Titel „Functional characterization of the *Ustilago maydis* effector protein Ten1“ selbstständig, ohne unerlaubte Hilfe angefertigt und mich dabei keiner anderen als der von mir ausdrücklich bezeichneten Quellen und Hilfsmittel bedient habe.

Diese Dissertation wurde in der jetzigen oder einer ähnlichen Form noch bei keiner anderen Hochschule eingereicht und hat noch keinen sonstigen Prüfungszwecken gedient.

_____ _____

(Ort, Datum) (Philipp Erchinger)

Wir sind auf einer Mißion: zur Bildung der Erde sind wir berufen
(Novalis)

Table of contents

Abbreviations

ABA	Abscisic acid
Approx.	Approximately
bp	Base pairs
BSA	Bovine serum albumin
cDNA	Complementary DNA
cfu	Colony-forming unit
Co-IP	Co-immunoprecipitation
C-terminal	Carboxy-terminal
ddH_2O	Double-distilled water
Δ	Deletion
DIC	Differential interface contrast
DNA	Deoxyribonucleic acid
dNTP	Deoxyribonucleoside triphosphate
dpi	Days post-infection/infiltration
DTT	Dithiothreitol
e.g.	*Exempli gratia* (for example)
EDTA	Ethylenediaminetetraacetic acid
EM	Electron microscopy
et al.	*Et alii* (and others)
Fig.	Figure
GFP	Green fluorescent protein
GST	Glutathione S-transferase
h	Hours(s)
HA	Hemagglutinin
HEPES	4-(2-Hydroxyethyl)-1-piperazineethanesulfonic acid
His	Histidine
hpi	Hours post-infection
i.e.	*Id est* (that is)
IPTG	Isopropyl β-D-1-thiogalactopyranoside
kb	Kilobase pairs
kDa	Kilodalton
M	Molar
MES	2-(N-morpholino)ethanesulfonic acid
mg	Milligram
min	Minute(s)
mL	Millilitre
MOPS	3-(N-morpholino)propanesulfonic acid
mRNA	Messenger RNA
MW	Molecular weight
µg	Microgram
µL	Microlitre
µM	Micromolar
µm	Micrometer
ng	Nanogram
nm	Nanometer
N-terminal	Amino-terminal
OD_{600}	Optical density at 600 nm
ORF	Open reading frame
PAGE	Polyacrylamide gel electrophoresis
PCR	Polymerase chain reaction
PP2C	Type 2C protein phosphatase
qRT-PCR	Quantitative reverse transcription PCR
RNA	Ribonucleic acid
rpm	Revolutions per minute
SA	Salicylic acid
SDS	Sodium dodecyl sulfate
TCA	Trichloroacetic acid
TCEP	Tris(2-carboxyethyl)phosphine
TEMED	Tetramethylethylenediamine
Tris	Trishydroxymethylaminomethane
UV	Ultraviolet
v/v	Volume fraction
w/v	Mass concentration
WGA	Wheat germ agglutinin

Summary

Ustilago maydis, the causal agent of corn smut disease, is a pathogen that establishes a biotrophic interaction with *Zea mays*. The interaction with the host plant is largely governed by a plethora of secreted effector proteins, many of which are encoded in gene clusters. The deletion of cluster 10A consisting of 10 effector-encoding genes results in strongly reduced virulence after maize seedling infection. In the present study, the gene *UMAG_03744* (termed *ten1*) could be identified as a major virulence factor of gene cluster 10A. Via quantitative reverse transcription PCR an induction of *ten1* during the biotrophic development of the fungus was detected. *ten1* deletion strains showed a virulence phenotype mainly reflected by a reduced tumor size on seedling leaves. Moreover, by complementing the cluster 10A deletion strain for *ten1*, the strong virulence defect of the cluster mutant was partially rescued. After overexpression in *U. maydis* hyphae, secreted Ten1 protein could be detected in axenic culture supernatant. Furthermore, using immunoelectron microscopy, the translocation of secreted Ten1 to plant cells could be shown after maize seedling infection, manifested by a significant accumulation of the protein in the plant cytoplasm and especially in plant nuclei.

Through a yeast two-hybrid screen ZmPP26, a type 2C maize protein phosphatase (PP2C) could be identified as interaction partner of Ten1. This interaction was supported by co-immunoprecipitation experiments after transient co-expression of Ten1 and ZmPP26 in *Nicotiana benthamiana*. Moreover, ZmPP26 could be detected by mass spectrometry after immunoprecipitation of Ten1 from *U. maydis*-infected leaf tissue. Via yeast two-hybrid assays the ZmPP26-interacting domain of Ten1 was mapped. The engineered protein Ten1m, harboring amino acid substitutions in the interacting domain, showed no interaction with ZmPP26 in yeast two-hybrid assays. By complementing the cluster 10A deletion strain with Ten1m, the virulence defect of the cluster mutant could not be rescued, suggesting that the interaction of Ten1 and ZmPP26 may be biologically relevant.

Zusammenfassung

Der Pilz *Ustilago maydis* ist der Erreger des Maisbeulenbrandes. Die biotrophe Interaktion mit der Wirtspflanze Mais wird hauptsächlich durch eine Vielzahl sekretierter Effektorproteine ermöglicht, die oftmals in Genclustern codiert werden. Die Deletion von Cluster 10A resultiert in einer stark verringerten Virulenz nach Infektion von Maissetzlingen. In der vorliegenden Arbeit konnte das Gen *UMAG_03744* (umbenannt zu *ten1*) als wesentlicher Virulenzfaktor von Cluster 10A bestimmt werden. Mittels quantitativer Reverse-Transkriptase-PCR wurde eine Induzierung von *ten1* während der biotrophen Entwicklung des Pilzes festgestellt. *ten1* Deletionsmutanten zeigten einen Virulenzphänotyp, der sich überwiegend in einer Reduktion der Tumorgröße auf Blättern äußerte. Des Weiteren führte die Komplementation der Cluster 10A Deletionsmutante mit *ten1* zu einer teilweisen Wiederherstellung der Virulenz. Nach Überexpression in Hyphen von *U. maydis* konnte sekretiertes Ten1 Protein im Überstand von axenischer Kultur detektiert werden. Darüber hinaus wurde, nach Infektion von Maispflanzen, sekretiertes Ten1 Protein in Pflanzenzellen mittels Immunelektronenmikroskopie nachgewiesen, wobei eine Akkumulation des Proteins im Zytoplasma und besonders in Zellkernen beobachtet werden konnte.

Mittels Hefe-Zwei-Hybrid-System wurde ZmPP26, eine Typ 2C Protein-Phosphatase (PP2C) als Interaktionspartner von Ten1 identifiziert. Diese Interaktion konnte bestätigt werden durch Koimmunpräzipitation von Ten1 und ZmPP26 nach transienter Koexpression beider Proteine in *Nicotiana benthamiana*. Darüber hinaus wurde, nach Immunpräzipitation von Ten1 aus infiziertem Maispflanzenmaterial, ZmPP26 mittels Massenspektrometrie als Interaktor nachgewiesen. Durch Hefe-Zwei-Hybrid-Analysen wurde die Interaktionsdomäne von Ten1 kartiert. Das modifizierte Protein Ten1m, das Aminosäureaustausche in der Interaktionsdomäne besitzt, zeigte keine Interaktion mit ZmPP26 in Hefe-Zwei-Hybrid-Analysen. Die Komplementation der Cluster 10A Deletionsmutante mit Ten1m führte nicht zu einer Wiederherstellung der Virulenz, was dafür spricht, dass die Interaktion von Ten1 und ZmPP26 biologisch relevant sein könnte.

1. Introduction

Plants encounter a variety of microbes, resulting in interactions that can be neutral, mutually beneficial, or detrimental. Accordingly, plant-associated microbes are commonly referred to as endophytes, symbionts, or pathogens, respectively (Spanu and Panstruga, 2017). Of these, plant pathogens are of particular interest for economic and environmental reasons because they pose a major threat to crop plants grown for human consumption, resulting in yield reduction (Oerke, 2006). Microbial plant pathogens comprise viruses, bacteria, protozoa, fungi, and oomycetes (Bebber *et al.*, 2014) and are commonly characterized by their lifestyle: biotrophic pathogens extract nutrients from living host tissue, whereas necrotrophs kill their hosts and feed on the remains (Glazebrook, 2005). Hemibiotrophic pathogens share characteristics of both lifestyles, as they first establish a biotrophic interaction with their hosts but switch to necrotrophy at a later stage of infection (Vleeshouwers and Oliver, 2014). In order to establish a parasitic interaction with their hosts, plant pathogens depend on the manipulation of plant defense responses (Dodds and Rathjen, 2010; Lanver *et al.*, 2017; Toruño *et al.*, 2016).

1.1. Plant defense responses against pathogens

As sessile organisms that lack specialized immune cells or organs, plants rely on a two-tier innate immune system to perceive and fend off pathogenic microbes (Zipfel, 2014). The first layer of defense is called pattern-triggered immunity (PTI) and represents a robust immune response against most non-host pathogens (Macho and Zipfel, 2014; Ranf, 2017). PTI is induced upon perception of conserved microbe- or pathogen-associated molecular patterns (MAMPs or PAMPs) which are released during the infection (Macho and Zipfel, 2014). Moreover, plant-derived damage-associated molecular patterns (DAMPs) are also considered elicitors of PTI. They are primarily generated by pathogen-secreted plant cell wall degrading enzymes and can co-occur with MAMPs at the infection site (Souza *et al.*, 2017). The perception of MAMPs/DAMPs is mediated by cell surface-localized pattern recognition receptors (PRRs). Typical PRRs are either transmembrane receptor kinases (RKs) with an extracellular domain and a cytoplasmic kinase domain, or transmembrane receptor-like proteins (RLPs) which are structurally similar to RKs but which do not contain a kinase domain

(Zipfel, 2014). To be able to sense molecular patterns, PRRs display a variety of extracellular domains such as leucine-rich repeat (LRR), lysin motif (LysM), or lectin domains for the binding of diverse ligands (Ranf, 2017).

A number of MAMPs have been identified from bacteria, fungi, and oomycetes. One well-studied MAMP is bacterial flagellin from *Pseudomonas* species which is recognized by *Arabidopsis thaliana* and other plants (Chinchilla *et al.*, 2007; Gómez-Gómez and Boller, 2000; Hind *et al.*, 2016). Another example is peptidoglycan, a bacterial cell wall component, which is recognized by *A. thaliana* and rice plants (Liu *et al.*, 2013a; Willmann *et al.*, 2011). Of fungal pathogens, the cell wall component chitin is recognized by host plants (Shinya *et al.*, 2015). In *A. thaliana*, chitin is sensed via a complex formed by the LysM-containing receptor CERK1 and the receptor kinase LYK5 (Cao *et al.*, 2014; Liu *et al.*, 2012). B-glucan, the most abundant cell wall component in the majority of fungi is also considered to serve as a MAMP (Fesel and Zuccaro, 2016). However, the mechanism(s) of its perception in plants remain elusive (Fesel and Zuccaro, 2016). Recently, progress has been made in the identification of oomycete elicitors of plant immunity: INF1, a secreted elicitin of *Phytophthora infestans* was shown to be recognized extracellularly by the receptor-like protein ELR from the wild potato *Solanum microdontum* (Du *et al.*, 2015). Additionally, Albert *et al.* (2015) described the activation of PTI in *A. thaliana* via a tripartite receptor complex that recognizes a unique group of proteins which are produced not only by oomycetes, but by numerous prokaryotic and eukaryotic species.

Upon pattern recognition a set of defense responses is initiated which are hallmarks of PTI (Fig. 1). A very early response is an increase of the cytosolic Ca^{2+} concentration, primarily regulating defense gene expression together with MAPK cascade activation (Boudsocq *et al.*, 2010). An efflux of K^+, NO_3^-, Cl^- as well as an influx of H^+ ions is observed upon MAMP perception, generally leading to membrane depolarization and extracellular alkalinization (Jeworutzki *et al.*, 2010). A crucial early defense response is the reactive oxygen species (ROS) burst, involving the generation of hydrogen peroxide (H_2O_2), superoxide (O_2^-), and hydroxyl radicals ($^{\bullet}OH$) in the apoplast. ROS are able to inhibit pathogen spread by inducing the hypersensitive response (HR), but they also function as signaling molecules and contribute to the strengthening of cell walls (Torres, 2006).

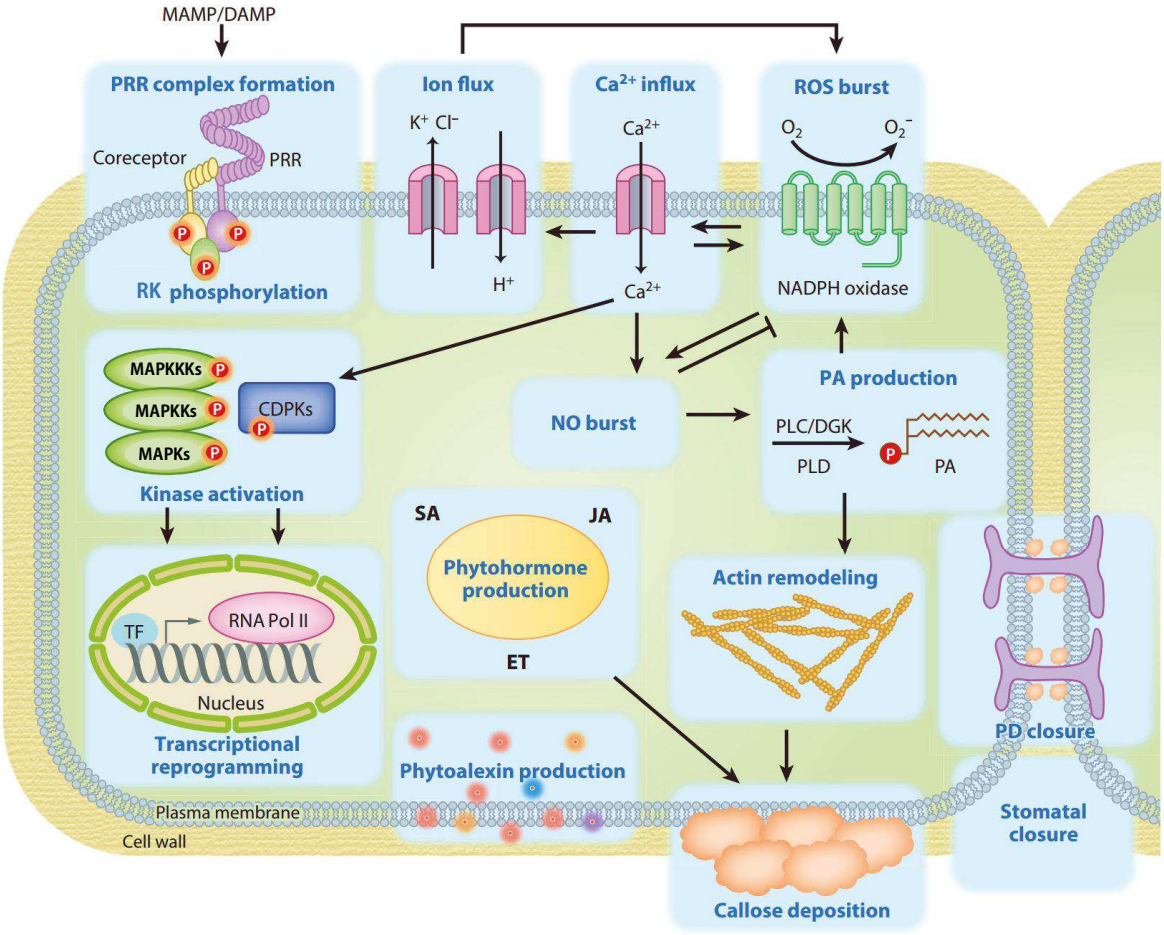

Fig. 1: Pattern-triggered immunity (PTI) responses in plants. Schematically depicted are partially intertwined cellular processes, elicited upon the extracellular perception of molecular patterns. Abbreviations: CDPK, calcium-dependent protein kinase; DAMP, damage-associated molecular pattern; DGK, diacylglycerol kinase; ET, ethylene; JA, jasmonic acid; MAMP, microbe-associated molecular pattern; MAPK, mitogen-activated protein kinase; NADPH, reduced nicotinamide adenine dinucleotide phosphate; NO, nitric oxide; PA, phosphatidic acid; PD, plasmodesmata; PLC, phospholipase C; PLD, phospholipase D; PRR, pattern recognition receptor; RK, receptor kinase; ROS, reactive oxygen species; SA, salicylic acid; TF, transcription factor (modified from Yu *et al.*, 2017).

PTI also triggers the production of plant defense hormones such as salicylic acid (SA), ethylene (ET), and jasmonic acid (JA; Halim *et al.*, 2009; Liu *et al.*, 2013b). Moreover, antimicrobial compounds referred to as phytoalexins have been implicated in defense responses (Ahuja *et al.*, 2012). As one prime route for pathogen entry, plant stomata close during infection. This MAMP-triggered stomatal closure is regulated by ROS, ET, and the early signaling molecule nitric oxide (NO; Melotto *et al.*, 2006). The production of NO is in turn closely connected to the burst of ROS (Scheler *et al.*, 2013) and to the formation of phosphatidic acid (PA; Raho *et al.*, 2011), which is considered a key signaling molecule for the regulation of cellular activities

such as actin remodeling (Testerink and Munnik, 2011). Transient changes in actin filament organization were observed upon MAMP perception (Day *et al.*, 2011) and are important for the formation of callose (Henty-Ridilla *et al.*, 2014). This β-1,3 glucan polymer is deposited at the cell wall and is able to strengthen damaged sections of the cell wall (Voigt, 2014). Although regulated at multiple levels, the biosynthesis of callose is strongly correlated to the production of ROS (Luna *et al.*, 2011). Analogous to stomatal closure, the permeability of plasmodesmata is regulated to prevent intercellular spread of pathogens and to mediate defense-related signaling from infected to neighboring host cells (Lee and Lu, 2011).

1.1.1. The interplay between pathogen effectors and plant defense

Plant pathogens produce a plethora of secreted effector proteins that act either in the apoplast or inside plant cells (Dodds and Rathjen, 2010). Modes of effector action comprise the dampening of plant immune responses, the shielding of the pathogen itself, and the modulation of plant physiology to promote pathogen growth (reviewed by Toruño *et al.*, 2016; Varden *et al.*, 2017). As a consequence of the deployment of effectors by pathogens, plants evolved a second layer of defense known as effector-triggered immunity (ETI) which is based on the recognition of secreted effectors by plant cells (Macho and Zipfel, 2014). ETI amplifies the basal antimicrobial defense responses of PTI and often culminates in localized plant cell death referred to as hypersensitive response (HR; Cui *et al.*, 2015). The detection of microbial effectors in plant cells is mediated by NLR receptor proteins. They were originally referred to as NOD-like receptors, but are more precisely part of the [nucleotide binding domain (NBD) and leucine-rich repeat (LRR)] superfamily of receptors (Jones *et al.*, 2016). There are two major subclasses of NLRs that have distinct N-terminal domains: those with a Toll-interleukin 1 receptor (TIR) domain, restricted to dicot plants, and those with a coiled-coil (CC) domain, found in both dicots and monocots (Cui *et al.*, 2015). In most cases the recognition of effectors is indirect: NLRs guard effector-mediated modifications of plant target proteins, so-called guardees, or of mimics of plant target proteins, so-called decoys (Jones *et al.*, 2016). However, NLRs are also able to detect pathogen effectors by direct interaction or via integrated domains from effector targets, so-called "integrated decoy domains" (Jones *et al.*, 2016). Recently, NLR networks were described consisting of "sensor" and "helper" NLRs which confer an increased robustness of plant immune signaling against pathogens (Wu *et al.*, 2017).

Because of the ability of NLRs to elicit these strong defense responses upon effector recognition, they were described as resistance (R) proteins. Furthermore, effectors which are recognized by NLRs and hence trigger defense responses were referred to as avirulence (Avr) proteins (Petit-Houdenot and Fudal, 2017). This concept goes back to Flor (1971) who proposed a gene-for-gene model for the elicitation of plant resistance in response to a pathogen. From an evolutionary point of view, Jones and Dangl (2006) described the plant immune system as a zigzag model: pathogens evolve effectors to overcome PTI; R proteins evolve in resistant plants to counteract effectors; selection pressure leads to evolution of pathogen *Avr* genes that evade R protein recognition; new plant *R* genes are favored by selection to counteract previously unrecognized effectors. However, as studies revealed the complexity of the interactions between effectors and plant defense, the limitations of this model in describing the plant immune system became evident. The biggest concern is the dichotomy between MAMPs and effectors (and consequently between PTI and ETI), as it is often hard to clearly classify pathogen molecules into either group (Thomma *et al.*, 2011). Cook *et al.* (2015) suggest an alternative, so-called invasion model for the plant immune system. Accordingly, MAMPs and effectors are considered as "invasion patterns" which are perceived by both PRRs and R proteins, collectively referred to as "IP receptors".

1.2. The *Ustilago maydis*/maize pathosystem

Within the phylum *Basidiomycota* and the order *Ustilaginales*, the group of smut fungi comprises important plant pathogens, infecting approx. 4,000 species of angiosperms (Martínez-Espinoza *et al.*, 2002). The biotrophic smut fungus *Ustilago maydis* parasitizes on maize and causes corn smut disease. The symptoms of the disease are tumors which can develop in all above-ground organs of the plant, and which contain a huge quantity of fungal spores (Matei and Doehlemann, 2016). With about 271 million tonnes harvest in 2010, maize is among the five major crops that feed the world's population (Fisher *et al.*, 2012). In the same year, worldwide yield losses due to corn smut were estimated to range between 2% and 20%, equaling a loss of food for 26 to 262 million people (Fisher *et al.*, 2012).

In the field, *U. maydis* infections of maize seedlings occur rarely and are characterized by hypertrophy of the stem and of leaves (Christensen, 1963). More apparent is the formation of tumors in ears of older plants, potentially leading to the destruction of ears and to yield loss (Fig. 2A; Christensen, 1963). Disrupted plant tumors release diploid teliospores of *U. maydis* which germinate under favorable conditions, undergo meiosis, and produce haploid progeny (Fig. 2B). Haploid cells can grow saprophytically by budding, however, they are not able to cause disease. To generate the pathogenic form, haploid cells need to mate.

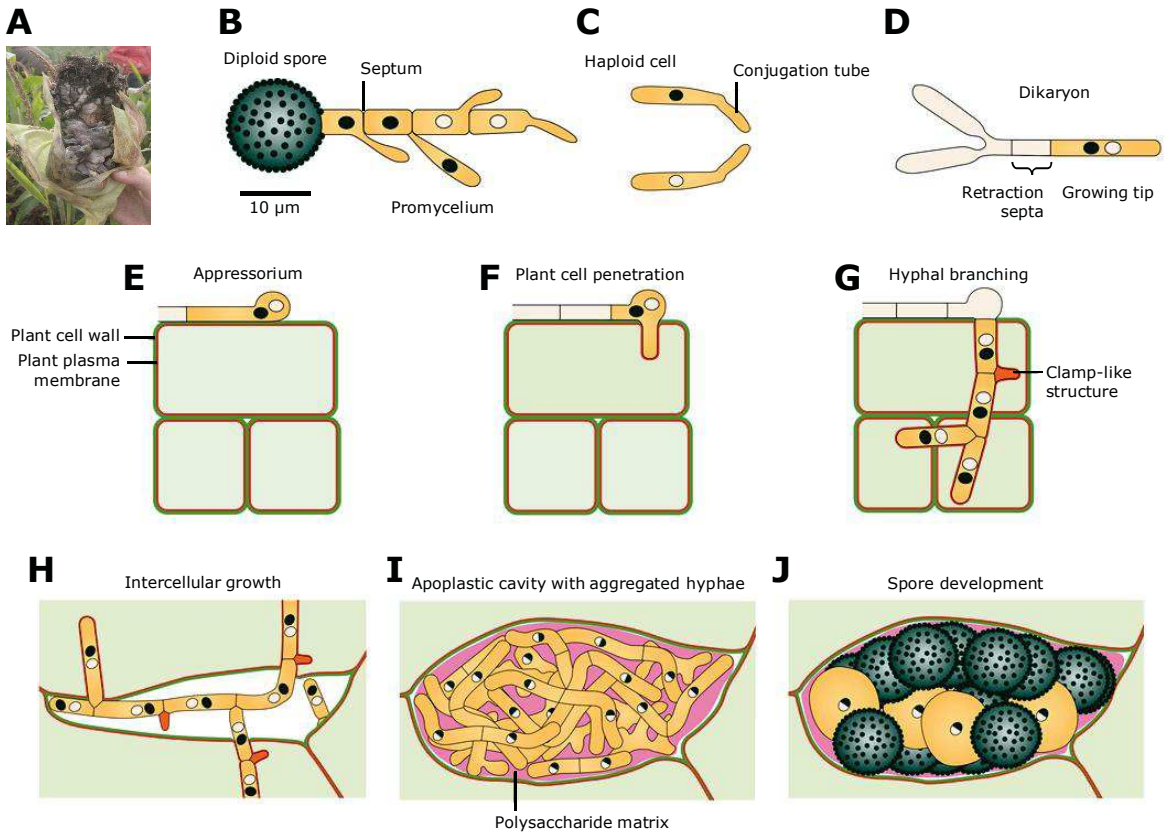

Fig. 2: Stages of the *U. maydis* life cycle. (A) Infected maize cob collected near Bauerbach, Germany, showing black teliospores. **(B)** Diploid teliospores give rise to a promycelium containing four haploid nuclei. **(C)** Haploid cells of compatible mating types form conjugation tubes for cell fusion. **(D)** Cell cycle-arrested dikaryon with a growing tip filled with cytoplasm (yellow) and with older, vacuolated parts (grey). **(E, F)** Hyphal tip cells develop appressoria on the leaf surface and penetrate the epidermal plant cell. **(G)** Hyphae start to branch and develop clamp-like structures (orange) to ensure correct segregation of nuclei. **(H)** Hyphae grow mainly intercellularly at the beginning of plant tumor formation. **(I)** After karyogamy diploid cells proliferate massively in tumor tissue and form aggregates. Aggregated hyphae become embedded in a gelatinous polysaccharide matrix (pink). **(J)** Hyphae undergo fragmentation and form spores. Black and white nuclei represent haploid nuclei harboring different mating-type genes. Half black and half white nuclei indicate diploid nuclei after karyogamy (modified from Lanver *et al.* 2017).

The process of mating is governed by a tetrapolar system represented by a biallelic *a* locus and a multiallelic *b* locus. On the leaf surface, haploid cells of compatible mating types (two strains that differ in *a* and *b*) form conjugation tubes (Fig. 2C), fuse, and form a filamentous dikaryon which represents the pathogenic form of *U. maydis* (Fig. 2D). Crucial for filamentation and pathogenic development is the formation of the heterodimer bE/bW, a transcription factor complex encoded by different *b* alleles. The hyphal tip develops appressoria in specific locations on the leaf surface, resulting in the penetration of plant epidermal cells (Fig. 2E, F). Following this, dikaryotic filamentous hyphae grow intracellularly and invade the underlying tissue (Fig. 2G). At a later stage of infection the fungus grows intercellularly in mesophyll tissue (Fig. 2H) and the plant cell starts to enlarge, culminating in the formation of tumors (Fig. 2I). After karyogamy, hyphae show massive fungal proliferation in tumor tissue, aggregate in a polysaccharide matrix, and subsequently undergo fragmentation. Eventually, black teliospores are formed (Fig. 2J) which can survive harsh conditions and which reinitiate an new disease cycle (reviewed by Banuett and Herskowitz, 1996; Brefort *et al.*, 2009; Lanver *et al.*, 2017).

U. maydis is widely used as a model organism for biotrophic plant pathogenic fungi. Since more than a decade, a completely sequenced genome (Kämper *et al.*, 2006) and established tools for genetic modification (Brachmann *et al.*, 2004; Kämper, 2004; Schuster *et al.*, 2015) are available. The possibility to cultivate *U. maydis* in synthetic medium together with the ability of the fungus to cause tumors in leaves of maize seedlings, allows rapid assessments of virulence for phenotypical analyses of mutant strains (Brefort *et al.*, 2009; Djamei and Kahmann, 2012). The engineered haploid solopathogenic strain SG200, encoding compatible *bE1* and *bW2* alleles, allows plant infections without the need for a compatible mating partner (Kämper *et al.*, 2006). This has speeded up reverse genetics of virulence determinants considerably.

1.2.1. Effectors of *U. maydis*

As a biotrophic pathogen, *U. maydis* depends on a living host for feeding and growth. For this, it needs to suppress host defense reactions (Giraldo and Valent, 2013). The fungus is able to achieve this by secreting effector proteins which can be distinguished by their target site: apoplastic effectors act at the so-called biotrophic interaction zone between fungal tip and plant plasma membrane, whereas cytoplasmic effectors are translocated into the plant cytoplasm (Matei and Doehlemann, 2016). The proteome of *U. maydis* harbors 467 potentially secreted proteins, *i.e.*, they have a predicted secretion signal sequence and no predicted transmembrane domains. Of these, 203 are novel, *i.e.*, they lack a predicted functional or structural domain. Furthermore, about 25% of all putative effectors of *U. maydis* are encoded in gene clusters (Schuster *et al.*, 2017). SG200 deletion strains for five of those clusters exhibit an altered virulence after maize seedling infection, ranging from non-pathogenicity to hypervirulence (Kämper *et al.*, 2006). Secreted proteins of *U. maydis* have been classified as either core or accessory effector proteins. Core effectors are detected in all secretomes of the five related smut fungi *S. reilianum* f. sp. *zeae*, *Sporisorium scitamineum*, *Ustilago hordei*, and *Melanopsichium pennsylvanicum*. In contrast, secreted proteins that have orthologs only in a subset of these species are considered accessory effectors (Schuster *et al.*, 2017). To date, five *U. maydis* effectors have been functionally characterized (Lanver *et al.*, 2017).

One of these is the *U. maydis* core effector Pep1 (Lanver *et al.*, 2017). Doehlemann *et al.* (2009) could show that this protein is secreted to the apoplastic space and that it is essential for penetration. *pep1* deletion mutants arrest during penetration of the epidermal cells and induce strong plant defense responses. The function of Pep1 for the establishment of biotrophy was later elucidated by Hemetsberger *et al.* (2012). The infection with *pep1* mutants elicits a strong accumulation of hydrogen peroxide (H_2O_2), accompanied by a massive transcriptional upregulation of the secreted maize peroxidase POX12 which is one major generator of H_2O_2 in the apoplast. Hemetsberger *et al.* (2012) have shown that Pep1 directly interacts with POX12 and inhibits its peroxidase activity. This shows that Pep1 is a crucial effector for the suppression of early plant defense responses.

Another apoplastic core effector is Pit2 (Lanver *et al.*, 2017). Doehlemann *et al*. (2011) could show that strains deleted for *pit2* are able to penetrate plant cells but fail to spread in the infected leaf and are unable to induce tumor formation. The concomitant upregulation of maize defense genes during an infection with *pit2* mutants suggests an inability of the deletion mutants to suppress plant immune responses. Later, Mueller *et al.* (2013) revealed that Pit2 functions as an inhibitor of a group of four apoplastic maize cysteine proteases, whose activity is linked to salicylate-dependent plant defense responses.

Cmu1, a secreted active chorismate mutase, was described by Djamei *et al.* (2011) as the first translocated *U. maydis* effector. Chorismate is a metabolite of the shikimate pathway and is also a precursor for aromatic amino acids and the plant defense hormone salicylic acid. Plants infected with a deletion strain for *cmu1* accumulate considerably higher levels of salicylic acid. It is suggested that Cmu1 in the plant cytosol redirects the shikimate pathway away from the production of salicylic acid. The ability of Cmu1 to spread to neighboring, yet uninfected cells, is considered a metabolic priming for those cells for the upcoming infection by *U. maydis*.

Tin2, an accessory secreted effector of *U. maydis*, was determined by Tanaka *et al.* (2014) to act inside plant cells and to target the anthocyanin pathway in maize. Tin2 interacts with the maize protein kinase ZmTTK1 and protects it from proteasome-dependent inactivation. Active ZmTTK1 controls the transcription factor ZmR1 which in turn triggers expression of genes involved in the anthocyanin biosynthesis pathway. In the absence of Tin2, ZmTTK1 is degraded and by this the anthocyanin pathway is shut down. As a consequence, 4-coumaric acid, a common precursor for both anthocyanin and lignin biosynthesis, is increasingly available for the synthesis of lignin in plant cells. This is supported by the fact that leaves infected with a strain deleted for *tin2* show enhanced lignin biosynthesis, culminating in strongly lignified vascular bundles. Under these conditions, *U. maydis* is considered to have only restricted access to plant nutrients. Tin2 is thus supposed to channel metabolites into the anthocyanin pathway to make them unavailable for other plant defense responses (Tanaka *et al.*, 2014).

More recently, See1, a seedling-specific effector was described by Redkar *et al.* (2015). This secreted protein localizes to the plant cytoplasm and to plant nuclei where it activates host DNA synthesis and cell division, both of which are necessary for the formation of leaf tumors and for the massive proliferation of *U. maydis* hyphae therein. In contrast, See1 is not needed for tumor induction in immature tassels because this floral tissue is highly proliferating and reactivation of cell division is not required for the formation of tumors. See1 was shown to interact with the maize cell cycle regulator SGT1 in the plant cytoplasm and nucleus. This interaction inhibits MAPK-triggered phosphorylation of SGT1. In other plant systems, SGT1 proteins play important roles in host and non-host resistance and some bacterial effectors also target SGT1 to suppress plant defense responses. Taken together, See1 is important for tumor formation specifically in maize leaves by reactivation of host DNA synthesis and likely modulates defense responses in leaves by the interaction with SGT1.

1.2.2. *ten1* and the effector gene cluster 10A

The deletion of cluster 10A, residing on chromosome 10 and consisting of 10 protein-encoding genes, resulted in a strongly attenuated virulence on seedling leaves (Kämper *et al.*, 2006). Furthermore, Skibbe *et al.* (2010) showed that the deletion of the cluster significantly reduced the frequency and size of tumors in adult leaves and virtually abolished tumor formation in tassels, accompanied with a developmental arrest of the fungus in tassels. A recent comparative secretome analysis of *U. maydis* and related basidiomycetes provided new insights into the organization of gene cluster 10A (Schuster *et al.*, 2017). Accordingly, two of the genes, *UMAG_03746* and *UMAG_03747*, encode proteins for which the prediction of an N-terminal secretion signal was ambiguous. Therefore, these genes were not considered secreted protein-encoding genes. Of the residual eight candidate effector genes of the cluster, seven are part of two different gene families, both of which are also present in six other related fungal species. In contrast, the first gene of the cluster, *UMAG_03744*, is not part of any gene family (Fig. 3).

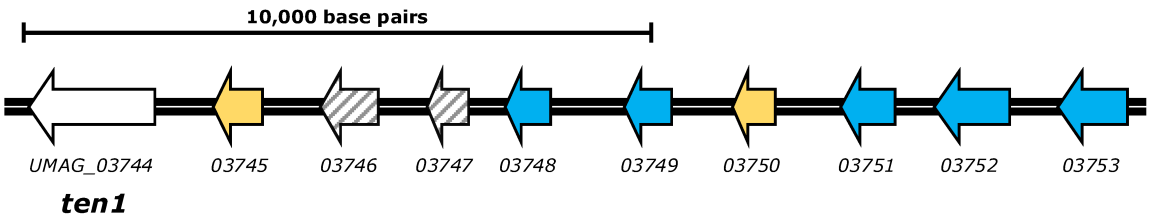

Fig. 3: Organization of the *U. maydis* gene cluster 10A for secreted proteins. Arrows depict the genomic localization of each gene on chromosome 10 as well as the transcriptional orientation and the relative length of the ORF. The affiliation to gene families according to Schuster *et al.* (2017) is marked by yellow and blue arrows. Shaded arrows indicate genes encoding proteins not predicted to be secreted (modified from Kämper *et al.*, 2006).

Earlier work on gene cluster 10A suggested that *UMAG_03744* is an important virulence factor of *U. maydis* (J. Wu, personal communication). This gene was hence considered a highly interesting effector candidate for a functional analysis and designated *ten1*. The gene encodes 680 amino acids with an expected molecular weight of 75.6 kDa and a predicted N-terminal secretion signal within the first 33 residues. However, Ten1 harbors no predicted functional domains.

1.3. Aims and objectives of this study

The aim of the present study is a functional analysis of the putative effector protein Ten1, in the course of which the following main questions will be addressed:

- When is *ten1* expressed during *U. maydis* infection of maize?
- What is the virulence phenotype of a *ten1* deletion strain? Is *ten1* a major virulence factor of gene cluster 10A?
- Is Ten1 a secreted protein and, if so, where does it localize after secretion?
- What are the plant interactors of Ten1?
- What is the biological function of this interaction and is it relevant for biotrophic development of *U. maydis*?

2. Results

2.1. Ten1 is weakly conserved among related fungi

Over the last years, several genomes of grass-infecting smut fungi related to *U. maydis* have been sequenced: *Sporisorium reilianum* f. sp. *zeae*, causing maize head smut (Schirawski *et al.*, 2010); *Sporisorium scitamineum*, infecting sugarcane (Que *et al.*, 2014; Taniguti *et al.*, 2015); and *Ustilago bromivora*, infecting *Brachypodium* spp. (Rabe *et al.*, 2016). Moreover, the genome of the dicot-infecting smut fungus *Melanopsichium pennsylvanicum* was sequenced by Sharma *et al.* (2014). In all of these species proteins related to Ten1 were identified by a comparative analysis of the proteomes, displaying between 20.7% and 29.8% amino acid identity with Ten1 in pairwise sequence alignments. *Pseudozyma* spp. are related to smut fungi but not known to infect plants (Schuster *et al.*, 2017). The genomes of *P. hubeiensis* (Konishi *et al.*, 2013), *P. aphidis* (Lorenz *et al.*, 2014) and *P. antarctica* (Morita *et al.*, 2014) all encode proteins related to Ten1, displaying between 22.5% and 37.5% amino acid identity with Ten1 in pairwise sequence alignments (Table 1).

Table 1: Conservation of Ten1 among related fungi.

Organism	Protein name[1]	UniProtKB entry[2]	amino acid identity with Ten1 [%]
P. hubeiensis	PHSY_000082	R9NVL1	37.5
P. antarctica	PANT_10d00070	M9LVY3	31.3
S. reilianum f. sp. *zeae*	sr11226	E6ZM96	29.8
U. bromivora	UBRO_20117	A0A1K0G9H8	29.6
S. scitamineum	SPSC_05103	A0A0F7SCG8	28.8
S. scitamineum	SPSC_05104	A0A0F7RY63	25.1
S. reilianum f. sp. *zeae*	sr11227	E6ZM97	22.9
P. aphidis	PaG_01412	W3VTR2	22.5
M. pennsylvanicum	mp06537	A0A077RAV4	20.7

[1] Protein names according to the respective genome publications

[2] UniProt Knowledgebase (http://www.uniprot.org/)

The lengths of most of the identified related proteins differ strongly from Ten1, *e.g.*, with sr11227 from *S. reilianum* f. sp. *zeae* being the shortest protein (322 amino acids) and PaG_01412 from *P. aphidis* being the largest protein (1,275 amino acids). This leads to the insertion of gaps into pairwise sequence alignments (for an alignment of Ten1 and sr11226 see Fig. 33, appendix).

2.2. *ten1* is induced during biotrophic development of *U. maydis*

One hallmark of *U. maydis* effector genes is their strong upregulation following plant colonization (Lanver *et al.*, 2017). To examine the expression of *ten1* throughout disease development, mRNA levels during axenic growth and at different time points after syringe-inoculation of maize seedlings were determined by quantitative reverse transcription PCR (qRT-PCR). To this end, total RNA was extracted from exponentially grown cells of the compatible wild type strains FB1 and FB2 (Banuett and Herskowitz, 1989), cultivated in $YEPS_{light}$ medium. Furthermore, leaves infected with a mixture of FB1 and FB2 were subjected to RNA extraction at eight time points between twelve hours and twelve days post-infection (dpi; RNA samples kindly provided by N. Ludwig and A. Müller). After cDNA synthesis from total RNA via reverse transcription, quantitative PCR was performed. The constitutively expressed gene *ppi* (*UMAG_03726*), encoding a peptidylprolyl isomerase, was used as reference (Bohlmann, 1996). Whereas minimal expression levels were determined in axenic culture, *ten1* expression peaked at 2 dpi with an approximate 4,700-fold increase compared to the level of expression in axenic culture. At 4 dpi, relative *ten1* expression was still elevated about 2,800-fold. At later time points of the infection the level of expression decreased, but remained upregulated compared to axenic culture (Fig. 4). This expression profile was also confirmed via RNAseq analysis of the same RNA samples (D. Lanver, personal communication; Fig. 34, appendix). These analyses show that *ten1* is strongly induced at the onset of intracellular fungal development in the plant (2 dpi) and that the gene remains upregulated until 12 dpi.

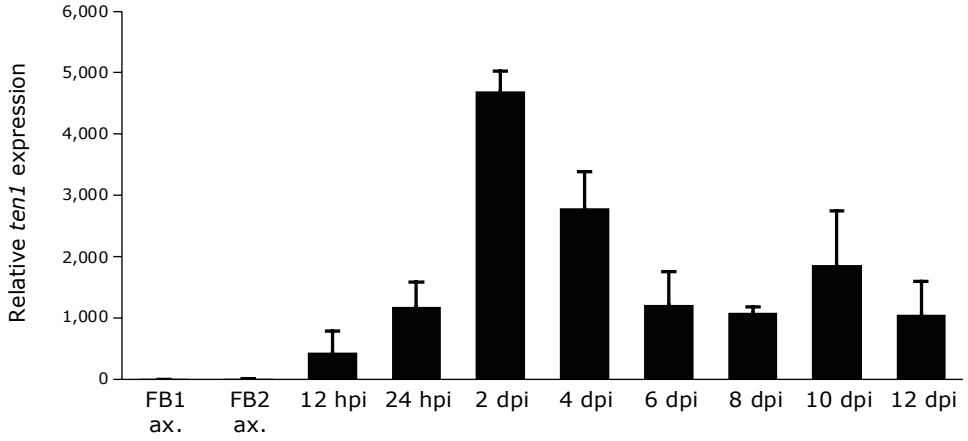

Fig. 4: Relative *ten1* expression in axenic culture and during biotrophic development of *U. maydis*. Bars represent the fold change of *ten1* expression normalized against the expression of *ppi* and the average expression level in axenic culture (ax.) of FB1 and FB2, based on the $2^{-\Delta\Delta C}{}_{T}$ method (Livak and Schmittgen, 2001). Shown are mean values after three independent biological replicates with standard deviations. qRT-PCR was performed in two technical replicates showing identical results. hpi, hours post-infection; dpi, days post-infection.

2.3. *ten1* is a virulence factor of *U. maydis*

To assess the contribution of *ten1* to mating, virulence, and spore production of *U. maydis*, the gene was deleted in the compatible strains FB1 and FB2. When dropped on charcoal-supplemented solid medium, mixtures of FB1 and FB2 strains form white and fuzzy dikaryotic filaments after successful mating (Banuett and Herskowitz, 1989; Day and Anagnostakis, 1971). Compatible mixtures of FB1, FB2, and of the corresponding *ten1* deletion strains all formed white and fuzzy dikaryotic filaments 24 hours after dropping on charcoal plates (Fig. 5A). After syringe-inoculation of maize seedlings, the mixture of FB1Δten1 and FB2Δten1 showed a reduction of virulence in comparison to the mixture of FB1 and FB2 at 12 dpi. No dead plants were observed after the infection with compatible *ten1* deletion strains, and, compared to the infection with compatible wild type, fewer heavy tumors near the base of the stem, but more large leaf tumors were observed (Fig. 5B). At a later stage of infection (at 13 dpi to 14 dpi) teliospores maturate in stem and leaf tumors and acquire a dark coloration (Banuett and Herskowitz, 1996). Fig. 5C illustrates the production of teliospores in heavy stem tumors, caused by *ten1* mutant as well as by wild type crosses at 15 dpi.

Taken together, the deletion of *ten1* in the compatible wild type strains FB1 and FB2 results in a reduction of virulence not originating from a defect in mating. Moreover, the production of teliospores at a later infection stage likely is not affected by the deletion of *ten1*.

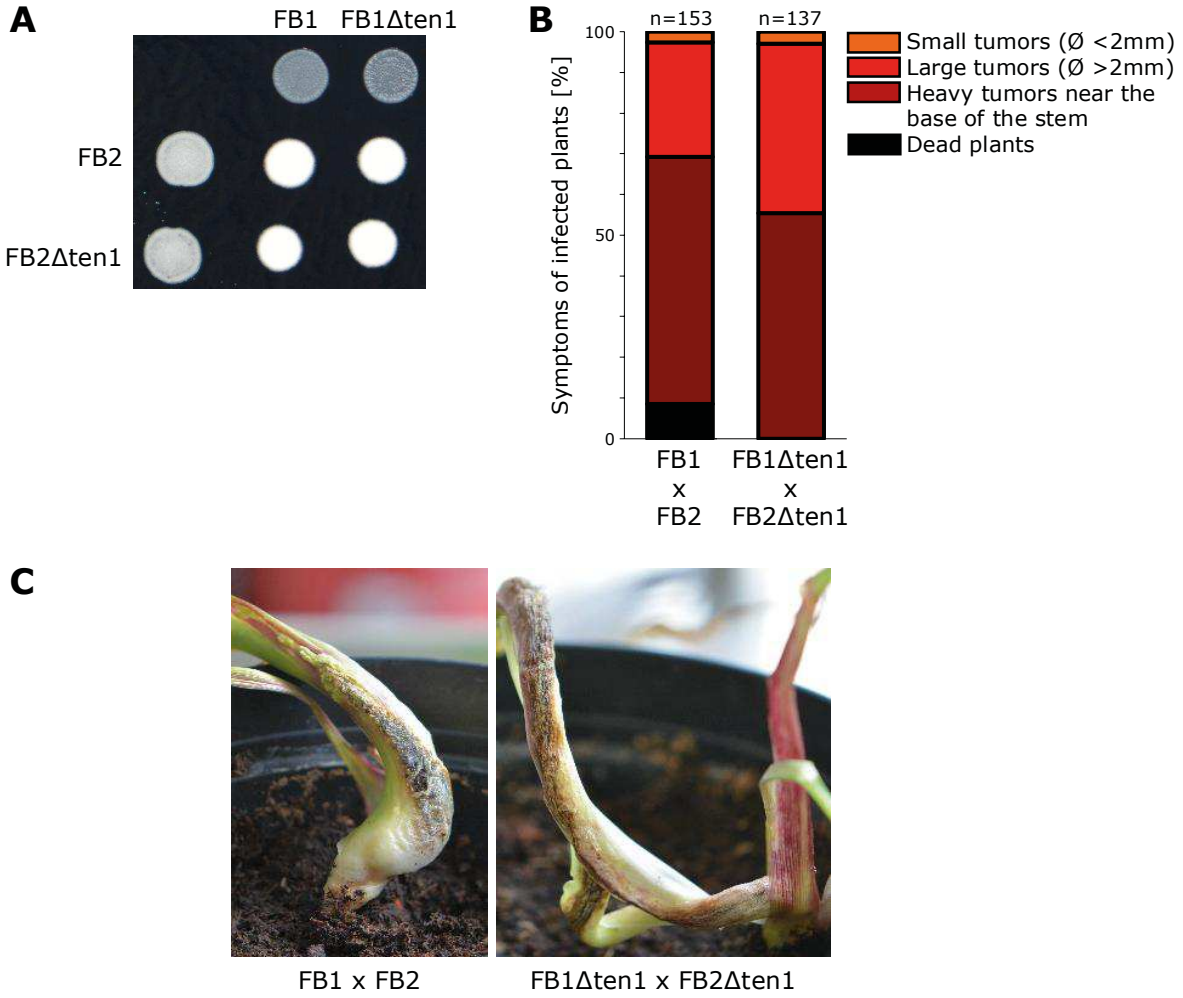

Fig. 5: Mating, virulence, and teliospore production of FB1Δten1 and FB2Δten1 crosses. (A) Mating analysis on PD-charcoal plate after dropping of the indicated strains alone or as a mixture with compatible mating partners at a 1:1 ratio. **(B)** Infection symptoms on maize seedlings at 12 dpi caused by crosses of the indicated strains. Symptoms are classified into disease categories modified from Kämper *et al.* (2006). Shown are average values of three independent biological replicates. n, total number of infected plants. **(C)** Heavy tumors near the base of the stem caused by crosses of the indicated strains at 15 dpi, showing the production of black teliospores.

2.4. *ten1* is a major virulence factor of gene cluster 10A

To determine the relevance of *ten1* for virulence of the solopathogenic *U. maydis* strain SG200 (Kämper *et al.*, 2006), the gene was deleted and the mutant strain was tested for virulence by syringe-inoculation of maize seedlings. Compared to SG200, SG200Δten1 showed a virulence phenotype mainly reflected by a decrease in leaf tumor size and by the absence of heavy tumors near the base of the stem at 12 dpi (Fig. 6).

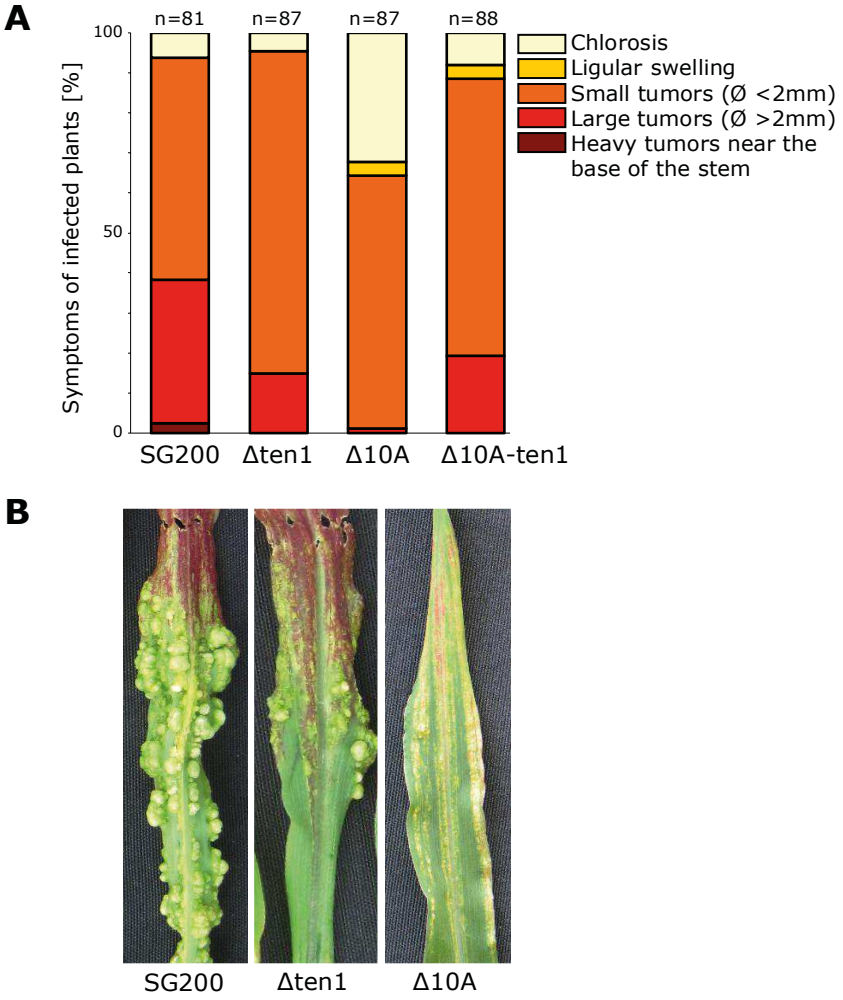

Fig. 6: Virulence of *ten1* and gene cluster 10A deletion strains in SG200 background. (A) Infection symptoms on maize seedlings at 12 dpi caused by SG200, SG200Δten1, SG200Δ10A, and SG200Δ10A-ten1. Symptoms are classified into disease categories modified from Kämper *et al.* (2006). Shown are average values of three independent biological replicates. n, total number of infected plants. **(B)** Infected maize seedling leaves with representative disease symptoms caused by SG200, SG200Δten1, and SG200Δ10A at 12 dpi.

Previous data showed a strongly reduced virulence of a SG200 mutant strain deleted for all genes of cluster 10A (Kämper *et al.*, 2006). In the present study, the virulence phenotype of the respective strain SG200Δ10A on maize seedlings was reproduced, which is characterized by a strong reduction of large tumors at 12 dpi, compared to SG200 (Fig. 6). To determine the extent to which this virulence defect could be rescued by the expression of *ten1* under its native promoter, SG200Δ10A was complemented for *ten1* via *ip* locus integration of a single copy of *ten1*. After seedling infection, this complementation strain SG200Δ10A-ten1 showed an increased frequency of large tumors compared to SG200Δ10A at 12 dpi (Fig. 6A). In conclusion, these seedling infections show that the deletion of *ten1* also leads to a virulence phenotype in SG200. Moreover, the expression of *ten1* alone partially rescues the virulence defect of the cluster mutant SG200Δ10A. This suggests that *ten1* is a major virulence factor of gene cluster 10A.

2.5. The deletion of *ten1* does not affect early pathogenic development of SG200

The fact that no expression of *ten1* was detected in axenic culture (Fig. 4), indicated that the observed virulence phenotype of SG200Δten1 does not originate from a defect in saprophytic growth. In support of this, cells of SG200Δten1 displayed neither morphological alterations, nor delayed growth during axenic growth in $YEPS_{light}$ medium, compared to SG200 (not shown). To examine whether the deletion of *ten1* affects the formation of appressoria *in vitro*, the gene was deleted in the appressorial marker strain SG200AM1 (Mendoza-Mendoza *et al.*, 2009). This strain harbors the *AM1* marker construct, a triple *gfp* gene expressed under the appressorium-specific promoter of *UMAG_01779*. Cells of SG200AM1Δten1 and SG200AM1 were grown in $YEPS_{light}$ medium and supplemented with hydroxy fatty acids (HFA, 16-hydroxyhexadecanoic acid). This allowed the enhanced induction of appressoria after the cells were sprayed on Parafilm M, an artificial hydrophobic surface mimicking the plant cuticle (Mendoza-Mendoza *et al.*, 2009). The expression of the appressorial marker *AM1* was analyzed by fluorescence microscopy in filaments that were attached to the hydrophobic surface 16 hours after spraying.

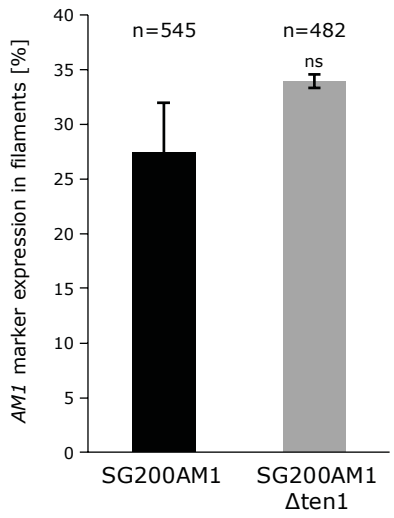

Fig. 7: *In vitro* appressoria formation of SG200AM1Δten1 on Parafilm M. Quantification of filaments expressing the *AM1* marker 16 hours after spraying in relation to the total number of analyzed filaments (n). Shown are mean values with standard deviations after two independent biological replicates. ns, not significantly different based on a two-tailed *t* test at the confidence level of 0.1.

On average, GFP-specific fluorescence indicating expression of *AM1* was detected in 27.4% of SG200AM1 filaments. Filaments of SG200AM1Δten1 showed a higher average *AM1* marker expression of 33.9% (Fig. 7). However, the observed difference of marker expression proved to be not statistically significant. This result shows that the deletion of *ten1* has no effect on the ability of *U. maydis* to form appressoria *in vitro*.

To analyze whether SG200Δten1 shows a defect in intracellular proliferation compared to SG200, seedlings were infected with the respective strains and microscopic analyses with infected leaf tissue were performed at 4 dpi. For this purpose, fungal hyphae were stained with WGA-AF488. This is a green fluorescein-conjugated lectin that binds to fungal cell walls (Robin *et al.*, 1986). Moreover, plant cell walls were stained by propidium iodide (PI; Running *et al.*, 1995). In SG200Δten1-infected maize leaves, epidermal cells displayed an intracellular proliferation of hyphae comparable to SG200-infected tissue at the same stage (Fig. 8). In summary, the described experiments show that the deletion of *ten1* neither affects saprophytic growth, nor *in vitro* appressoria formation of SG200. Moreover, at a microscopic level no significant difference in proliferation at 4 dpi was observed for SG200Δten1, relative to SG200.

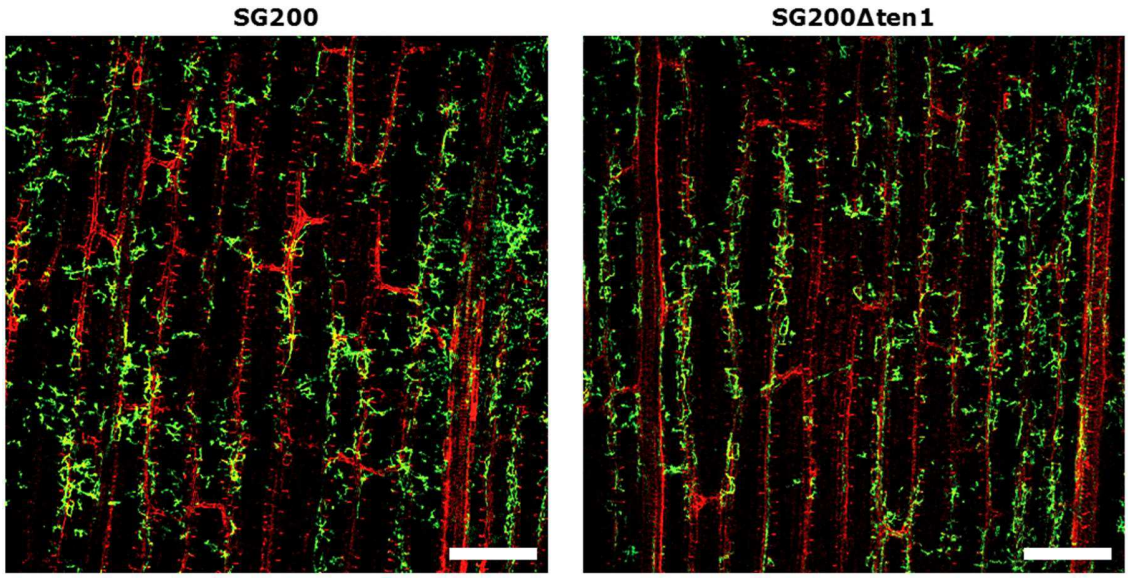

Fig. 8: WGA-AF488/PI staining of leaf tissue infected with SG200 and SG200Δten1 at 4 dpi. Fungal hyphae growing inside maize epidermal cells were visualized using WGA-AF488 (green) and plant cell walls were visualized using propidium iodide (PI, red). Pictures are maximum projections of confocal z-stacks. Scale bars equal 250 µm.

2.6. Ten1 interacts with ZmPP26, a maize type 2C protein phosphatase (PP2C)

2.6.1. ZmPP26 was identified via yeast two-hybrid screen

To identify maize proteins that interact with Ten1, a yeast two-hybrid screen was performed using Ten1$_{34-680}$ (without its predicted signal peptide) as bait and a cDNA library generated from *U. maydis*-infected maize leaves as prey. For this analysis, the yeast strain AH109 was used, harboring the marker genes *ADE2* and *HIS3* under the control of GAL4-responsive UAS (upstream activating sequences) and promoter elements. Moreover, this strain is auxotrophic for adenine, histidine, leucine, tryptophan, and uracil (Clontech/Takara, Saint-Germain-en-Laye, France). AH109 was transformed with the plasmid pGBKT7-ten1$_{34-680}$, allowing the expression of the bait protein BD-Ten1$_{34-680}$. This fusion protein contains the GAL4 binding domain (BD) fused to a Myc epitope tag. In lysates of six independent yeast transformants BD-Ten1$_{34-680}$ was detected at approx. 120 kDa via anti-Myc Western blot analysis (Fig. 9).

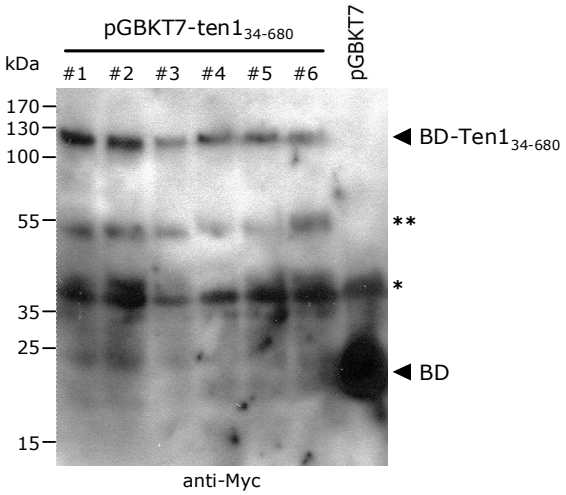

Fig. 9: Expression of the bait fusion protein BD-Ten1$_{34-680}$ in yeast strain AH109. SDS-PAGE followed by anti-Myc Western blot using cell lysates of AH109 transformed with pGBKT7-ten1$_{34-680}$ and pGBKT7, respectively. *, non-specific bands. **, products of protein degradation. BD, GAL4 binding domain; AD, GAL4 activation domain.

The displayed molecular weight of BD-Ten1$_{34-680}$ differed considerably from the expected molecular weight of 91.8 kDa (MW of BD-Myc: 19.9 kDa; MW of Ten1$_{34-680}$: 71.9 kDa). Importantly, in all following immunodetection experiments involving denaturing protein electrophoresis, epitope-tagged Ten1 proteins were detected at a higher molecular weight than expected. As control an AH109 strain expressing only the BD was included in the analysis. In cell lysates of this strain the BD was detected at approx. 20 kDa (Fig. 9). In a second step the cDNA library was introduced into strain AH109-pGBKT7-ten1$_{34-680}$#1. Via this library GAL4 activation domain (AD) fusion proteins were expressed from the prey plasmid pAD-GAL4-2.1 (Farfsing, 2004). Co-transformed yeast cells were streaked out on “low stringency” SD medium lacking leucine and tryptophan (-Leu/-Trp). This allowed a nutritional selection for the correct integration of the bait and prey plasmids, carrying the yeast marker genes *TRP1* and *LEU2*, respectively. A co-transformation efficiency of about 3.72 x 10^4 cfu/µg DNA was determined. To screen for protein interaction, co-transformed yeast cells were streaked out on “high stringency” SD medium lacking leucine, tryptophan, adenine, and histidine (-Leu/-Trp/-Ade/-His). This allowed a nutritional selection for clones harboring interacting BD- and AD fusion proteins due to the GAL4-driven transcriptional activation of the yeast reporter genes *ADE2* and *HIS3*. A total of 35 yeast transformants grew on high stringency medium. For the identification of interacting proteins, the prey plasmids harbored by these yeast

transformants were isolated and the cDNA inserts were amplified via PCR. To eliminate identical cDNA inserts, the PCR products were digested using the endonuclease HaeIII and subsequently analyzed according to restriction fragment length polymorphisms (RFLP). As a result, 19 prey plasmids were sequenced encoding for three different maize proteins, in the following referred to as ZmPP26, PVA12, and VAP27-2 (Table 2).

Table 2: Maize interactors of Ten1 identified via yeast two-hybrid screen.

Description	Expected MW (residues)	MaizeGDB entry[1]	Encoded by
ZmPP26, cytosolic type 2C protein phosphatase (PP2C)	30.7 kDa (284)	GRMZM2G056572	16 prey plasmids
Homolog of *A. thaliana* **PVA12**, VAMP (vesicle-associated membrane protein)	25.1 kDa (225)	GRMZM5G868047	1 prey plasmid
Homolog of *A. thaliana* **VAP27-2**, VAMP (vesicle-associated membrane protein)	40.1 kDa (362)	GRMZM2G019596	2 prey plasmids

[1] Maize Genetics and Genomics Database (http://maizegdb.org/)

To verify the interaction of Ten1 with the identified proteins, *ZmPP26*, *PVA12*, and *VAP27-2* were amplified in full-length from maize cDNA via PCR and cloned into the vector pGADT7. This vector allows the expression of prey fusion proteins containing the GAL4 activation domain (AD) fused to an HA epitope tag. For the co-expression of bait and prey fusion proteins, AH109-pGBKT7-ten1$_{34\text{-}680}$#1 was transformed with the generated pGADT7 constructs. Moreover, the empty bait vector pGBKT7 was introduced into AH109. The resulting strain AH109-pGBKT7 was also transformed with the generated pGADT7 constructs to test for autoactivation of the GAL4 transcription factor by AD fusion proteins. Via anti-Myc Western blot using lysates of transformed yeast cells, BD-Ten1$_{34\text{-}680}$ and the BD alone were detected at approx. 120 kDa and 20 kDa, respectively (Fig. 10). Via anti-HA Western blot the AD fusion proteins of ZmPP26, PVA12, and VAP27-2 were detected at approx. 50 kDa, 45 kDa, and 90 kDa, respectively (Fig. 10). The displayed molecular weight of AD-VAP27-2 was considerably higher than the expected molecular weight of 57.6 kDa (MW of AD-HA: 17.5 kDa; MW of VAP27-2: 40.1 kDa).

Western signals for all AD fusion proteins showed enhanced intensity when BD-Ten1$_{34-680}$ was co-expressed (Fig. 10). This suggests that the interaction with BD-Ten1$_{34-680}$ has an effect on stability of these prey fusion proteins.

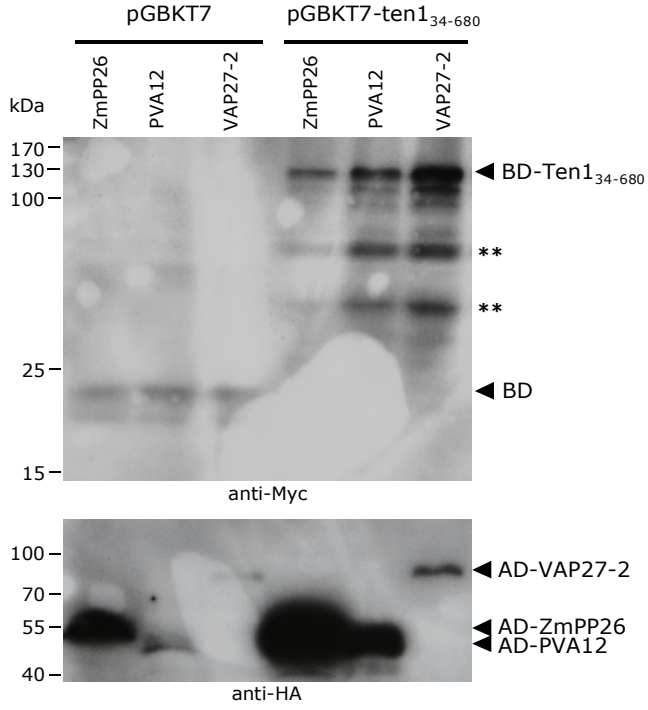

Fig. 10: Co-expression of BD-Ten1$_{34-680}$ and AD fusion proteins of maize interactors in AH109. SDS-PAGE followed by anti-Myc and anti-HA Western blots using yeast cell lysates. AH109 strains carrying pGBKT7 or pGBKT7-ten1$_{34-680}$ were transformed with pGADT7-ZmPP26, pGADT7-PVA12, and pGADT-VAP27-2, respectively. **, products of protein degradation. BD, GAL4 binding domain; AD, GAL4 activation domain.

To check for autoactivation of the GAL4 transcription factor by BD-Ten1$_{34-680}$, the empty vector pGADT7 was introduced into AH109-pGBKT7-ten1$_{34-680}$#1. Subsequently, all generated yeast strains were streaked out on low stringency and high stringency media to verify the integration of bait and prey plasmids and to test for interaction of fusion proteins, as described earlier. As negative control an AH109 strain expressing only the AD and BD was included in the analysis. Strains co-expressing BD-Ten1$_{34-680}$ and AD fusion proteins of maize interactors were able to grow on high stringency medium, suggesting interaction of fusion proteins (Fig. 11). Autoactivation of reporter genes was neither observed for BD-Ten1$_{34-680}$, nor for AD fusion proteins of ZmPP26, PVA12, and VAP27-2 (Fig. 11). This analysis confirms the interaction of Ten1 and full-length maize interactors in yeast two-hybrid assays.

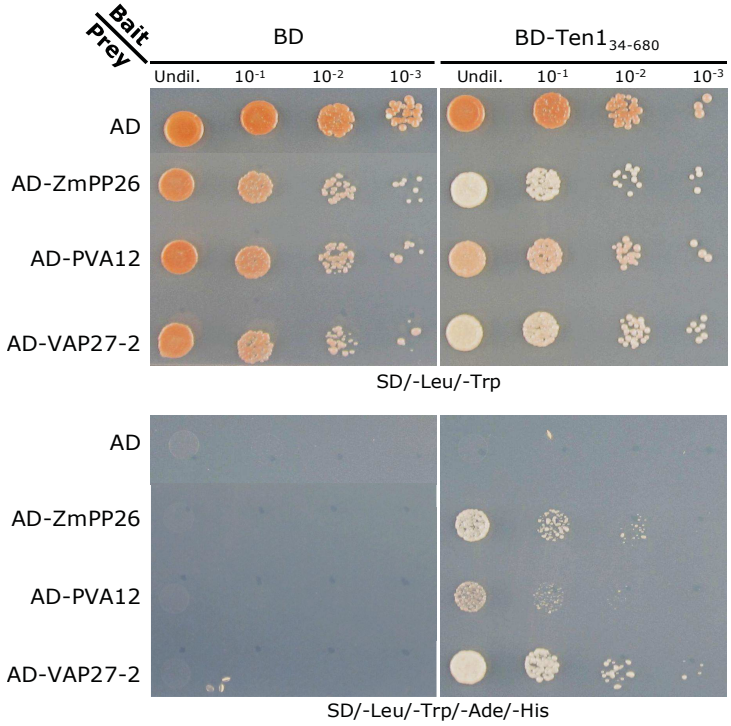

Fig. 11: Yeast two-hybrid assays with Ten1$_{34-680}$ and maize interactors. Low stringency (SD/-Leu/-Trp) and high stringency (SD/-Leu/-Trp/-Ade/-His) plates showing serial dilutions of AH109 strains co-expressing the indicated bait and prey proteins. BD, GAL4 binding domain; AD, GAL4 activation domain.

ZmPP26 is a homolog of WIN2 from *A. thaliana*, a type 2C protein phosphatase (PP2C) which is proposed to be involved in the regulation of biotic stress responses (Lee *et al.*, 2008). Interestingly, RNAseq analyses of maize seedling leaves infected with *U. maydis* wild type strains FB1 and FB2 revealed an upregulation of *ZmPP26* at 4 dpi, showing a 1.3-fold increase in detected mRNA reads compared to MOCK-infected samples (D. Lanver, personal communication; Fig. 12). In the following, the interaction of Ten1 and ZmPP26 hence was investigated in more detail.

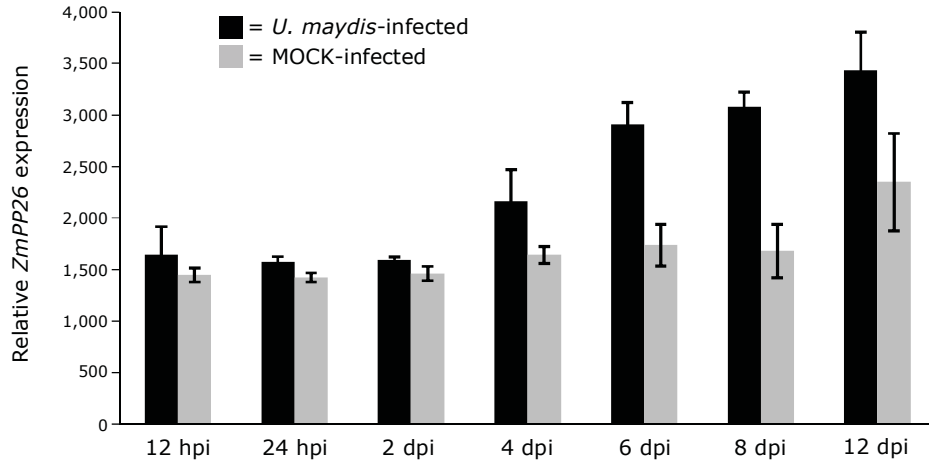

Fig. 12: Relative *ZmPP26* expression after *U. maydis* and MOCK infection of maize seedlings. Shown are DESeq-normalized gene counts determined by RNAseq analyses of maize seedling leaves infected with FB1 and FB2 or with water (MOCK). hpi, hours post-infection; dpi, days post-infection (data provided by D. Lanver).

2.6.2. Ten1 specifically interacts with ZmPP26

Wei and Pan (2014) classified ZmPP26 into group F2 of maize PP2Cs, containing eight related proteins. Among those, ZmPP76 (GRMZM2G166035) and ZmPP84 (GRMZM5G829894) are most closely related to ZmPP26, displaying 67.3% and 60.3% amino acid identity with ZmPP26, respectively. To estimate the specificity of the interaction of Ten1 and ZmPP26, ZmPP76 and ZmPP84 were tested for interaction with Ten1 in yeast two-hybrid assays. Furthermore, the distantly related group D PP2C ZmPP28 (GRMZM2G479665), displaying 27.4% amino acid identity with ZmPP26, was also included in the analysis. *ZmPP76*, *ZmPP84*, and *ZmPP28* were amplified from maize cDNA via PCR and cloned into the prey vector pGADT7. Subsequently, AH109-pGBKT7-ten1$_{34\text{-}680}$#1 was transformed with the generated pGADT7 constructs. Via anti-Myc and anti-HA Western blot analyses expression of the epitope-tagged fusion proteins was confirmed in cell lysates of transformed yeasts, whereas no signals were detected in cell lysates of untransformed AH109 (Fig. 13A). Subsequently, all generated yeast strains were streaked out on low stringency and high stringency media to verify the integration of bait and prey plasmids and to test for interaction of fusion proteins, as described in chapter 2.6.1.

Strains co-expressing BD-Ten1$_{34-680}$ and AD fusion proteins of ZmPP76, ZmPP84, and ZmPP28, respectively, did not grow on high stringency medium, indicating the absence of protein interactions (Fig. 13B). These results suggest that Ten1 specifically interacts with ZmPP26 and fails to interact with other members of the PP2C family of maize.

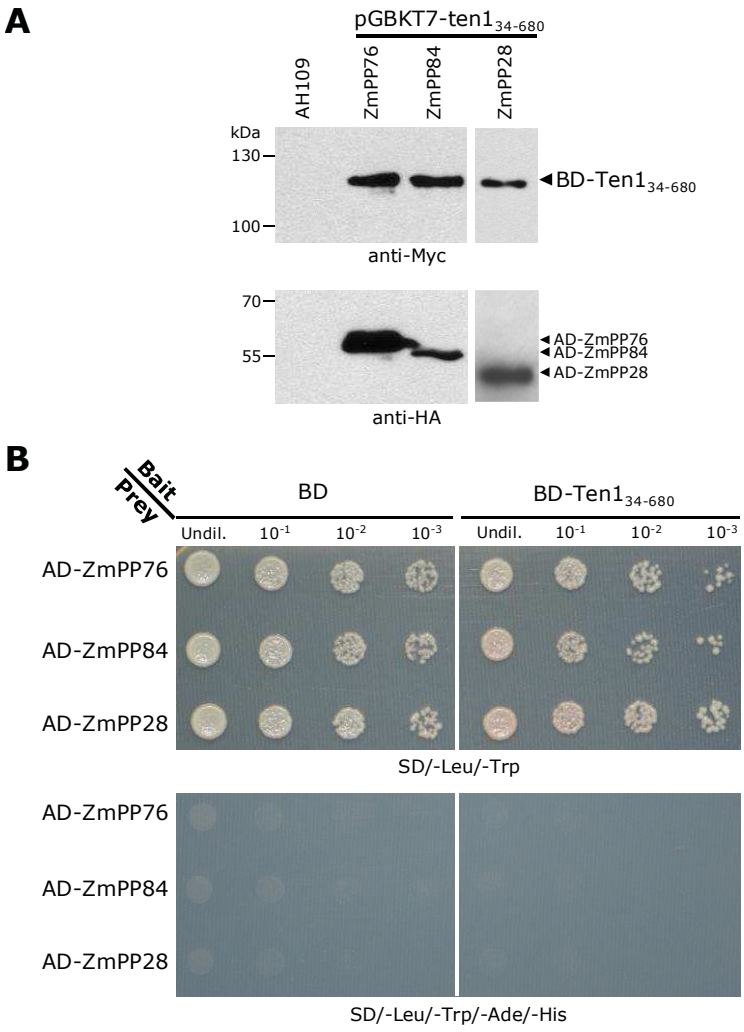

Fig. 13: Yeast two-hybrid assays with Ten1$_{34-680}$ and other maize PP2Cs. (A) SDS-PAGE followed by anti-Myc and anti-HA Western blots using yeast cell lysates. AH109-pGBKT7-ten1$_{34-680}$#1 was transformed with pGADT7-ZmPP76, pGADT7-ZmPP84, and pGADT7-ZmPP28, respectively. **(B)** Low stringency (SD/-Leu/-Trp) and high stringency (SD/-Leu/-Trp/-Ade/-His) plates showing serial dilutions of AH109 strains co-expressing the indicated bait and prey proteins. BD, GAL4 binding domain; AD, GAL4 activation domain.

2.6.3. Ten1 and ZmPP26 co-immunoprecipitate after transient expression in *N. benthamiana*

To corroborate the interaction of Ten1 and ZmPP26, co-immunoprecipitation (co-IP) of epitope-tagged proteins was performed in *Nicotiana benthamiana* after *Agrobacterium tumefaciens*-mediated DNA transfer. To this end, the fusion constructs *HA_3-ten1$_{34-680}$* and *ZmPP26-His_6* were generated and cloned into the binary expression vector pEZRK, containing the cauliflower mosaic virus (CaMV) 35S promoter. For the transient co-expression of proteins, *N. benthamiana* leaves were infiltrated with a mixture of *A. tumefaciens* strains harboring pEZRK-HA_3-ten1$_{34-680}$ and pEZRK-ZmPP26-His_6, respectively. As control, a strain harboring the empty plasmid pEZRK was co-infiltrated. Three days after infiltration, leaves were harvested and cell lysates were used for an IP of HA_3-Ten1$_{34-680}$ via anti-HA magnetic beads. Subsequent anti-His and anti-HA Western blot analyses using the IP samples showed a co-immunoprecipitation of ZmPP26-His_6 and HA_3-Ten1$_{34-680}$ (Fig. 14). This substantiates the interaction of Ten1 and ZmPP26 in a heterologous plant system.

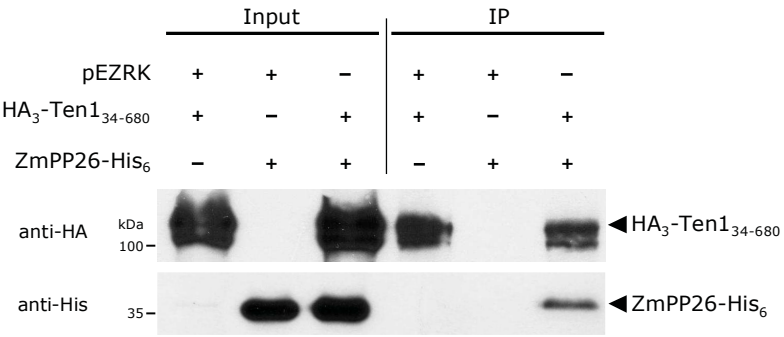

Fig. 14: Co-IP of ZmPP26-His_6 and HA_3-Ten1$_{34-680}$ after transient expression in *N. benthamiana*. SDS-PAGE followed by anti-HA and anti-His Western blots using leaves co-infiltrated with *A. tumefaciens* strains harboring pEZRK, pEZRK-HA_3-ten1$_{34-680}$, and pEZRK-ZmPP26-His_6, respectively. Input, soluble fraction of cell lysates from infiltrated leaves; IP, anti-HA immunoprecipitated proteins released from magnetic beads after boiling.

2.6.4. Ten1 and ZmPP26 interact during the biotrophic interaction of *U. maydis* and maize

To substantiate the evidence for interaction obtained from two heterologous systems, the interaction of Ten1 and ZmPP26 was further investigated in the *U. maydis*-maize pathosystem. Therefore, HA-tagged Ten1 was immunoprecipitated from *U. maydis*-infected leaf material and the IP sample was analyzed for interacting proteins via mass spectrometry.

For this purpose, a single copy of an *HA*-tag fusion construct of *ten1* was expressed under the *ten1* promoter in SG200Δ10A via *ip* locus integration. At first, an HA-tag was fused to the C-terminus of Ten1. This fusion protein was not biologically active, *i.e.*, the resulting complementation strain SG200Δ10A-ten1-HA was not able to rescue the virulence defect of SG200Δ10A (not shown). Therefore, the fusion protein HA_3-Ten1 was generated, harboring a triple HA-affinity tag at the N-terminus of Ten1, downstream of the predicted signal peptide sequence (Fig. 15A). Seedling infections with SG200Δ10A-HA_3-ten1 revealed a partial rescue of the SG200Δ10A virulence defect at 12 dpi, similar to SG200Δ10A-ten1 (Fig. 15B). This shows that the fusion of a triple HA-tag to the N-terminus of Ten1 results in a functional protein which, similar to the native Ten1 protein, is able to partially rescue the virulence defect of SG200Δ10A.

At 3 dpi, leaf material infected with SG200Δ10A-HA_3-ten1 was harvested and cell lysates were used for an IP of HA_3-Ten1 via anti-HA magnetic beads. As a control, the same experiment was performed using leaf material infected with SG200-SP-mCherry-HA. This strain expresses secreted mCherry with a C-terminal HA-tag, driven by the *cmu1* promoter, which is strongly active after plant penetration (Djamei *et al.*, 2011). Via anti-HA Western blot analyses, HA_3-Ten1 could not be detected in the lysate of infected leaves (Fig. 16A). However, after anti-HA IP via magnetic beads and Western blot, HA_3-Ten1 was detected at approx. 100 kDa (Fig. 16A). Western signals for mCherry-HA were detected in the lysate of infected leaves as well as after IP at approx. 35 kDa (Fig. 16B).

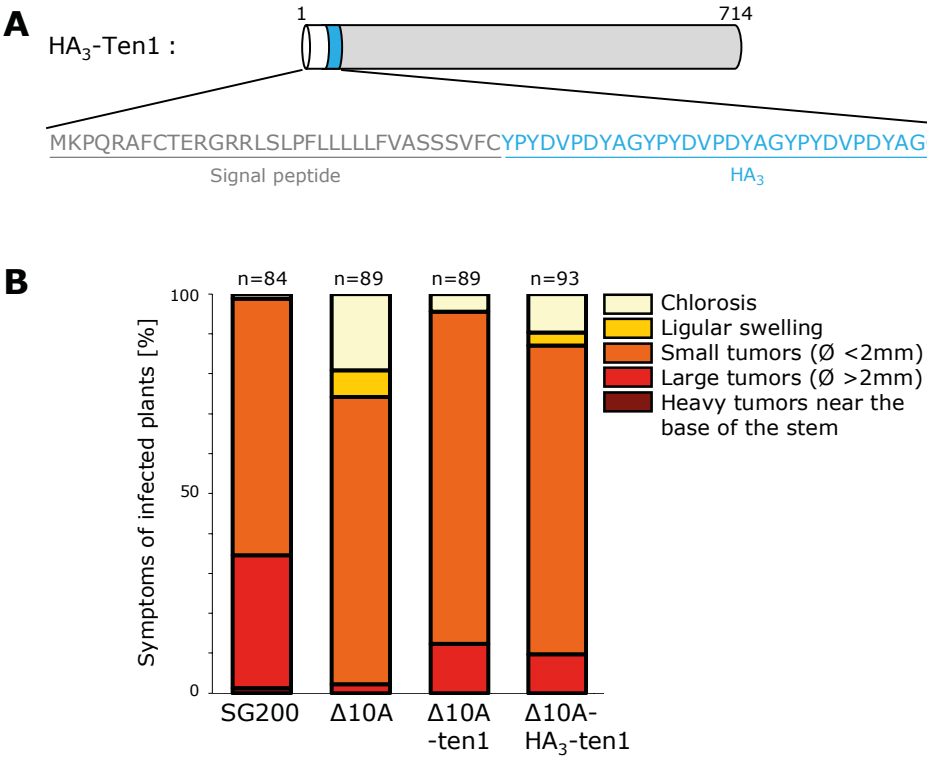

Fig. 15: Complementation of SG200Δ10A with HA3-Ten1. (A) Illustration of the full-length fusion protein HA3-Ten1 generated for complementation of SG200Δ10A. Numbers indicate amino acid positions. The white part indicates the N-terminal signal peptide of Ten1; blue indicates the triple HA-affinity tag including linker amino acids (HA3). **(B)** Infection symptoms on maize seedlings at 12 dpi caused by SG200, SG200Δ10A, SG200Δ10A-ten1, and SG200Δ10A-HA3-ten1. Symptoms are classified into disease categories modified from Kämper *et al.* (2006). Shown are average values of three independent biological replicates. n, total number of infected plants.

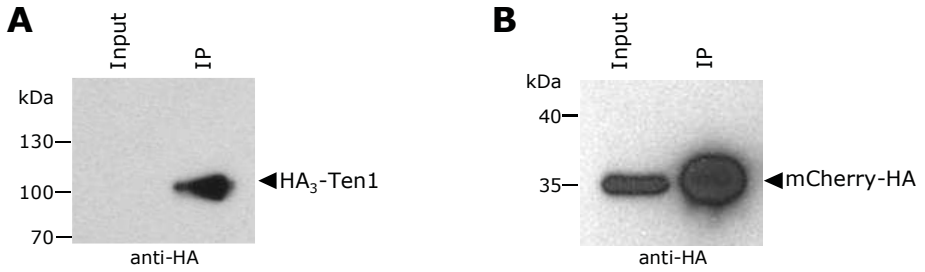

Fig. 16: IP of HA3-Ten1 and mCherry-HA from *U. maydis*-infected maize leaf tissue. SDS-PAGE followed by anti-HA Western blots using lysates of leaves infected with: **(A)** SG200Δ10A-HA3-ten1 and **(B)** SG200-SP-mCherry-HA at 3 dpi, respectively. Input, soluble fraction of cell lysate; IP, anti-HA immunoprecipitated proteins released from magnetic beads after boiling.

Subsequently, immunoprecipitated proteins were subjected to on-beads trypsin digestion. The resulting peptide mix was analyzed using liquid chromatography-mass spectrometry (LC-MS/MS) in collaboration with T. Glatter (Proteomics facility, MPI Marburg). The abundance of peptides from a given protein was determined by the total spectrum counts obtained. These spectra were searched against protein databases of *U. maydis* and maize which also contained the amino acid sequence of mCherry. In three biological replicates, peptides of mCherry were abundantly detected after IP of mCherry-HA, but not after IP of HA_3-Ten1 (Table 3). Moreover, peptides of both Ten1 and ZmPP26 were detected after IP of HA_3-Ten1, but not after IP of mCherry-HA (Table 3). Notably, the analysis of all detected peptides in both IP samples and over all three replicates determined ZmPP26 as the only specific interactor of Ten1. These experiments suggest that Ten1 and ZmPP26 specifically interact during the biotrophic interaction of *U. maydis* and maize.

Table 3: Total spectrum counts after LC-MS/MS analysis of IP samples over three biological replicates[1].

	IP replicate no. 1		IP replicate no. 2		IP replicate no. 3	
Protein	mCherry-HA	HA_3-Ten1	mCherry-HA	HA_3-Ten1	mCherry-HA	HA_3-Ten1
Ten1	-	9	-	1	-	3
ZmPP26	-	2	-	1	-	1
mCherry	48	-	41	-	26	-

[1] Shown are total numbers of spectra matching peptides from the indicated proteins.

2.6.5. Mutations in the interacting domain of Ten1 abolish interaction with ZmPP26 in yeast two-hybrid assays

For the identification of the interacting domain, truncated versions of $Ten1_{34-680}$ were tested for interaction with ZmPP26 in yeast two-hybrid assays. To avoid the disruption of alpha helices or beta sheets, truncation sites were chosen under the consideration of the secondary structure prediction of Ten1 by Phyre[2] (Kelley *et al.*, 2015; Fig. 35, appendix). Truncated parts of *ten1* were amplified via PCR and cloned into the bait plasmid pGBKT7, allowing the expression of truncated BD-$Ten1_{34-680}$ fusion proteins.

After co-transformation of AH109 with the generated bait constructs and pGADT7-ZmPP26, the expression of epitope-tagged fusion proteins was analyzed via anti-Myc and anti-HA Western blots. Subsequently, the generated yeast strains were tested for the interaction of fusion proteins as described in chapter 2.6.1.

At first, the truncated bait proteins BD-Ten1$_{133-680}$ and BD-Ten1$_{328-680}$ were tested for interaction with AD-ZmPP26 (Fig. 17A). Via anti-Myc and anti-HA Western blot analyses expression of the fusion proteins was confirmed in cell lysates of transformed yeasts (Fig. 17B). Co-expression of BD-Ten1$_{133-680}$ and AD-ZmPP26 allowed growth on high stringency medium, whereas co-expression of BD-Ten1$_{328-680}$ and AD-ZmPP26 did not (Fig. 17C). This suggested that the N-terminus of Ten1 is not necessary for interaction and that the interacting domain is located in a region between residue 133 and 327 of the protein.

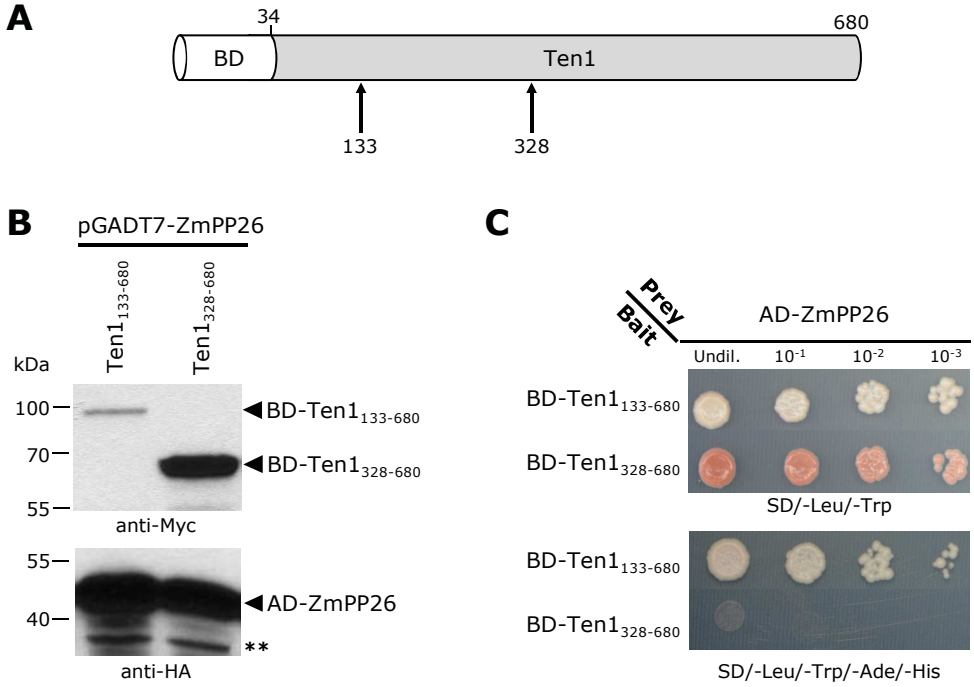

Fig. 17: Ten1$_{133-327}$ is necessary for interaction with ZmPP26 in yeast two-hybrid assays. (A) Illustration of the bait fusion protein BD-Ten1$_{34-680}$. Numbers indicate amino acid positions of the native Ten1 protein. Arrows depict residues meaningful for the truncated proteins analyzed in (B) and (C). **(B)** SDS-PAGE followed by anti-Myc and anti-HA Western blots using yeast cell lysates. AH109 was co-transformed with pGADT7-ZmPP26 and pGBKT7 constructs harboring *ten1$_{133-680}$* and *ten1$_{328-680}$*, respectively. **, products of protein degradation. **(C)** Low stringency (SD/-Leu/-Trp) and high stringency (SD/-Leu/-Trp/-Ade/-His) plates showing serial dilutions of AH109 strains co-expressing the indicated bait and prey proteins. BD, GAL4 binding domain; AD, GAL4 activation domain.

In the following it was investigated whether BD-Ten1$_{133-327}$ is sufficient to show interaction with AD-ZmPP26. Via anti-Myc and anti-HA Western blot analyses expression of the fusion proteins was confirmed in cell lysates of transformed yeasts (Fig. 18A). To check for autoactivation of the GAL4 transcription factor by BD-Ten1$_{133-327}$, the empty vector pGADT7 was co-expressed in AH109. In cell lysates of this strain, BD-Ten1$_{133-327}$ and the AD were detected via Western analyses (Fig. 18B). Co-expression of BD-Ten1$_{133-327}$ and AD-ZmPP26 allowed growth on high stringency medium and, moreover, autoactivation of reporter genes by BD-Ten1$_{133-327}$ was not observed (Fig. 18C).

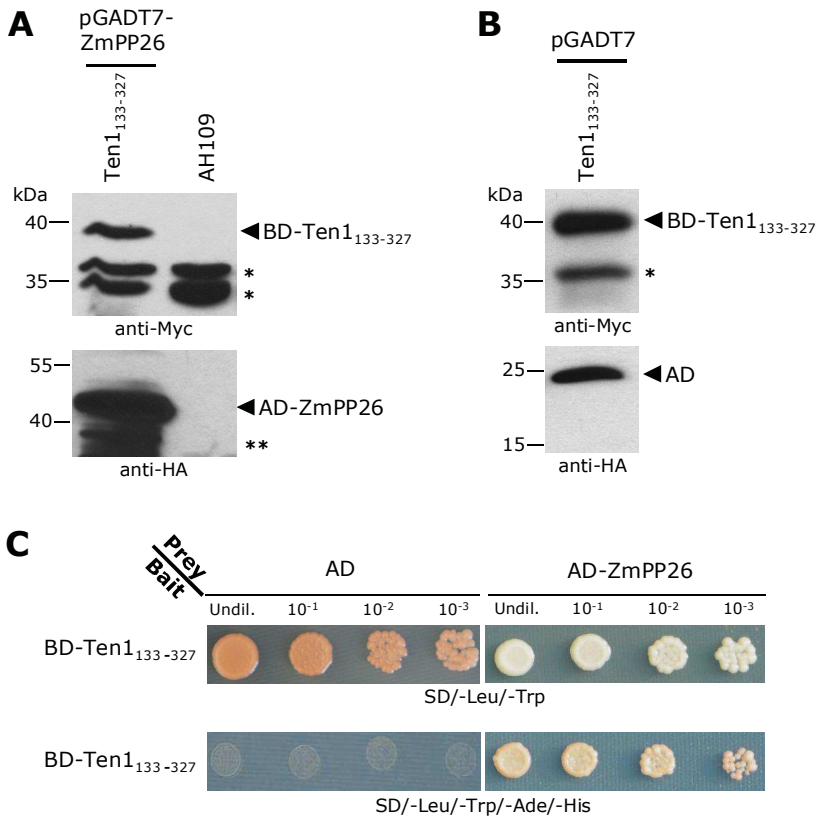

Fig. 18: Ten1$_{133-327}$ is sufficient for interaction with ZmPP26 in yeast two-hybrid assays. (A) SDS-PAGE followed by anti-Myc and anti-HA Western blots using cell lysates of untransformed AH109 and of AH109 co-transformed with pGADT7-ZmPP26 and pGBKT7-ten1$_{133-327}$. *, non-specific bands. **, products of protein degradation. **(B)** SDS-PAGE followed by anti-Myc and anti-HA Western blots using cell lysates of AH109 co-transformed with pGADT7 and pGBKT7-ten1$_{133-327}$. *, non-specific band. **(C)** Low stringency (SD/-Leu/-Trp) and high stringency (SD/-Leu/-Trp/-Ade/-His) plates showing serial dilutions of AH109 strains co-expressing the indicated bait and prey proteins. BD, GAL4 binding domain; AD, GAL4 activation domain.

To narrow down the interacting domain, BD-Ten1$_{133-327}$ was further truncated (Fig. 19A) and tested for interaction with AD-ZmPP26. Again, truncations were performed in regions of the protein which harbor no structural elements, based on the prediction by Phyre[2] (Fig. 35, appendix). Via anti-Myc and anti-HA Western blot analyses expression of the fusion proteins was confirmed in cell lysates of transformed yeasts (Fig. 19B).

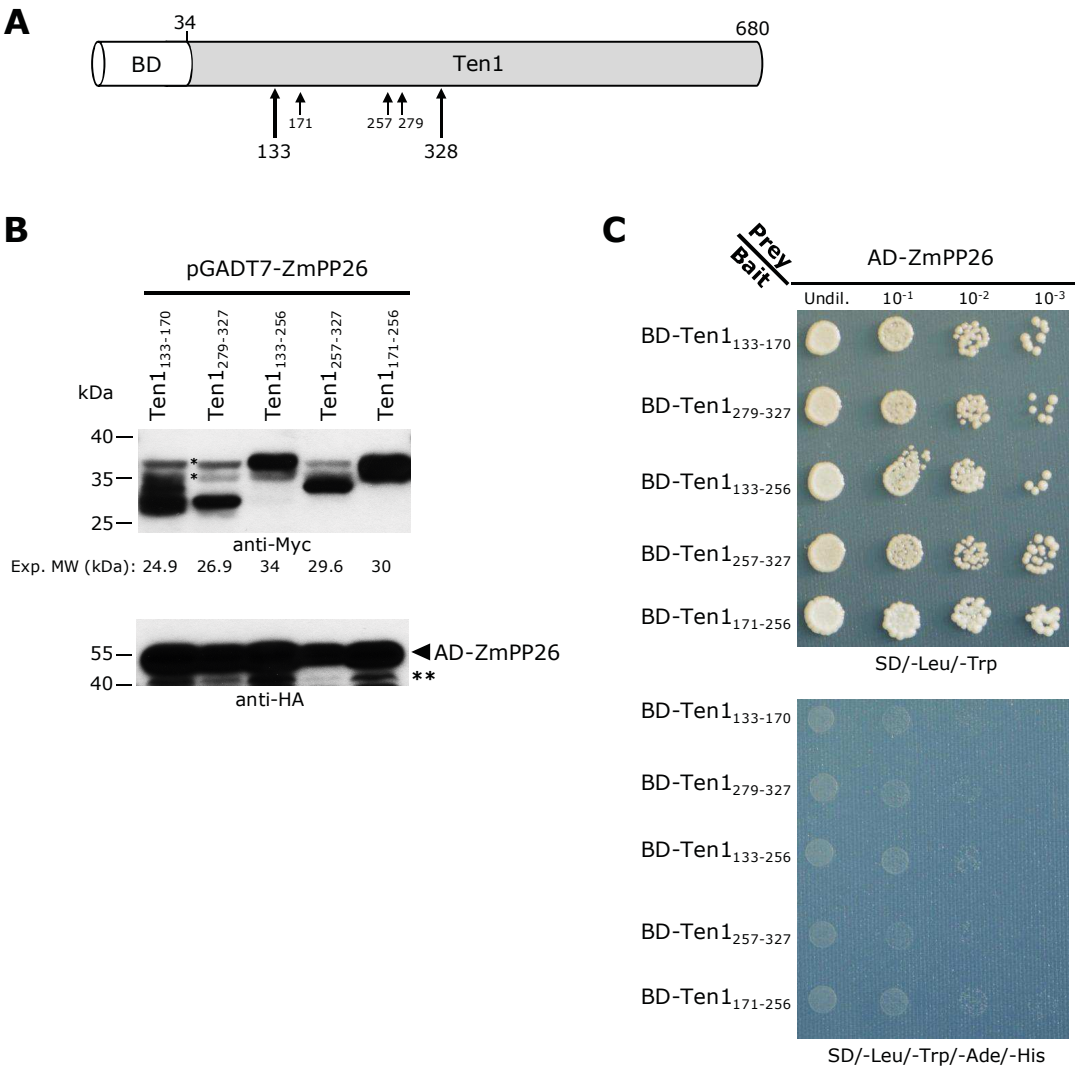

Fig. 19: Truncation of Ten1$_{133-327}$ eliminates the interaction with ZmPP26 in yeast two-hybrid assays. (A) Illustration of the bait fusion protein BD-Ten1$_{34-680}$. Numbers indicate amino acid positions of the native Ten1 protein. Arrows depict residues meaningful for the truncated proteins analyzed in (B) and (C). **(B)** SDS-PAGE followed by anti-Myc and anti-HA Western blots using yeast cell lysates. AH109 was co-transformed with pGADT7-ZmPP26 and pGBKT7 constructs harboring *ten1*$_{133-170}$, *ten1*$_{279-327}$, *ten1*$_{133-256}$, *ten1*$_{257-327}$, and *ten1*$_{171-256}$, respectively. *, non-specific bands. **, products of protein degradation. **(C)** Low stringency (SD/-Leu/-Trp) and high stringency (SD/-Leu/-Trp/-Ade/-His) plates showing serial dilutions of AH109 strains co-expressing the indicated bait and prey proteins. BD, GAL4 binding domain; AD, GAL4 activation domain.

However, the truncated bait proteins BD-Ten1$_{133-170}$, BD-Ten1$_{279-327}$, BD-Ten1$_{133-256}$, BD-Ten1$_{257-327}$, and BD-Ten1$_{171-256}$ showed no indication for interaction with AD-ZmPP26, respectively (Fig. 19C). In conclusion, via protein truncations it was not possible to further delimit key residues important for interaction. Therefore, amino acids 133 to 327 of Ten1 were determined as the ZmPP26-interacting domain.

To generate a Ten1 protein with a mutated interacting domain, error-prone PCR amplification of *ten1*$_{133-327}$ was performed, resulting in a library of randomly mutated sequences within the bait plasmid pGBKT7. After co-transformation of AH109 with the generated library constructs and pGADT7-ZmPP26, yeast cells were streaked out on low stringency and on high stringency media to verify the integration of bait and prey plasmids and to test for interaction of fusion proteins. Subsequently, 24 clones were analyzed which showed no growth on high stringency medium, indicating no interaction of a mutated BD-Ten1$_{133-327}$ fusion protein and AD-ZmPP26. From these clones plasmids were isolated and sequenced. Accordingly, 23 of the 24 clones harbored sequences encoding a premature stop codon in *ten1*$_{133-327}$, which resulted in the expression of truncated BD-Ten1$_{133-327}$ fusion proteins. In more than half of these cases a stop codon was generated already within the first 240 nucleotides of *ten1*$_{133-327}$ (considering a total of 582 nucleotides encoding Ten1$_{133-327}$). Nevertheless, these truncated sequences were analyzed, given the possibility that interaction of BD fusion proteins and AD-ZmPP26 was abolished not because of protein truncation, but because of substitutions of key residues in Ten1$_{133-327}$. After *in silico* translation of mutated sequences from all 24 clones, a multiple amino acid sequence alignment with native Ten1$_{133-327}$ was performed. However, no amino acid substitutions could be determined which occurred specifically in sequences from non-interacting clones. Therefore, the only mutated sequence not encoding a premature stop codon from a single yeast clone was used for following analyses. This sequence encoded a mutated Ten1$_{133-327}$ protein harboring 14 amino acid substitutions (Fig. 20A). In order to delimit the residues important for interaction with ZmPP26, BD-Ten1$_{133-327}$ proteins were produced that either harbored only the first seven or only the last seven of the 14 amino acid substitutions. However, both fusion proteins exhibited interaction with AD-ZmPP26, indicating that all 14 amino acid substitutions are necessary to eliminate interaction (not shown).

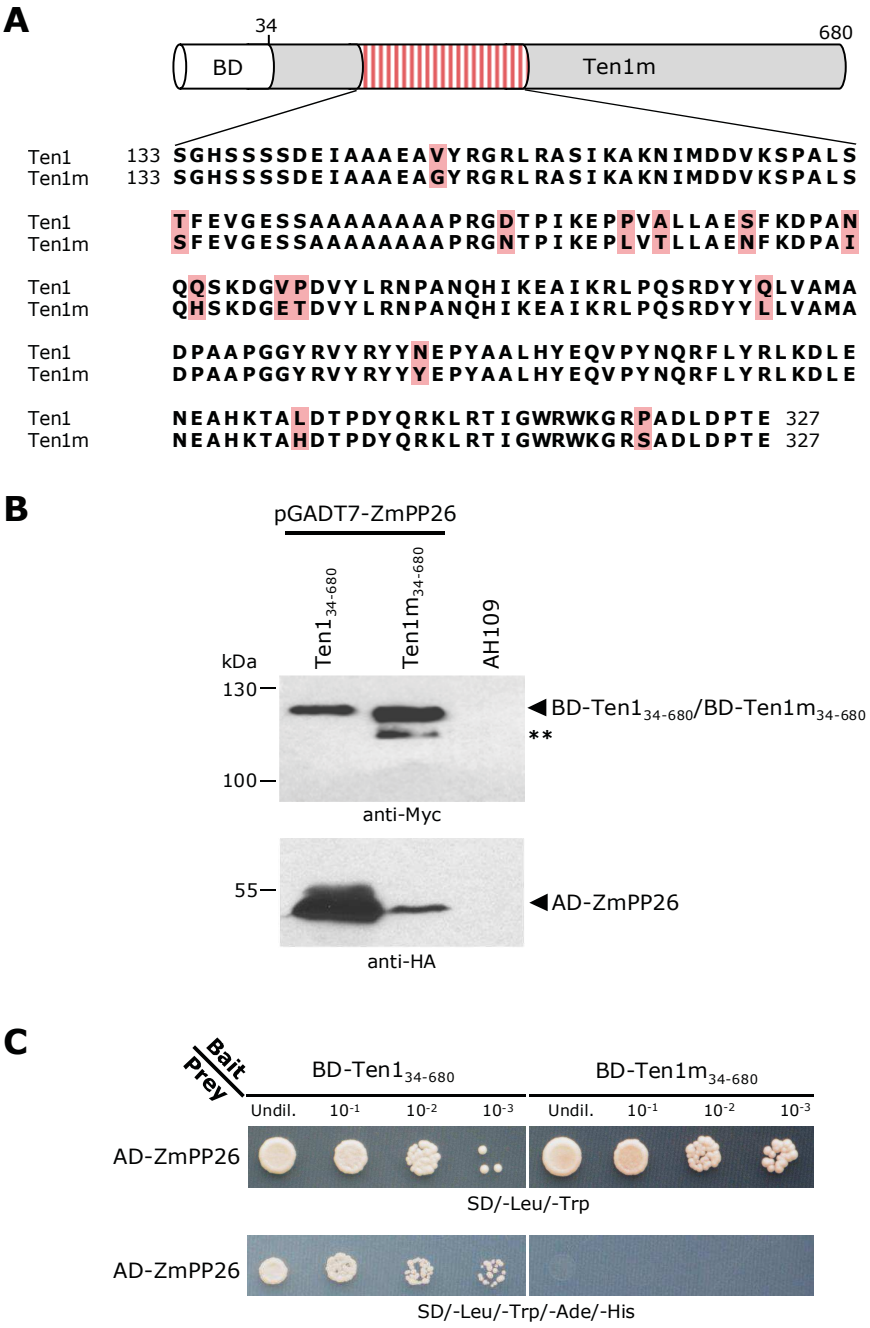

Fig. 20: Yeast two-hybrid assays with Ten1m$_{34-680}$ and ZmPP26. (A) Illustration of BD-Ten1m$_{34-680}$ harboring 14 amino acid substitutions (shaded in red) in the interacting domain (133-327). **(B)** SDS-PAGE followed by anti-Myc and anti-HA Western blots using yeast cell lysates. AH109 was co-transformed with pGADT7-ZmPP26 and pGBKT7 constructs harboring *ten1*$_{34-680}$ and *ten1m*$_{34-680}$, respectively. **, product of protein degradation. **(C)** Low stringency (SD/-Leu/-Trp) and high stringency (SD/-Leu/-Trp/-Ade/-His) plates showing serial dilutions of AH109 strains co-expressing the indicated bait and prey proteins. BD, GAL4 binding domain; AD, GAL4 activation domain.

To investigate whether these amino acid substitutions abolish interaction with AD-ZmPP26 also in the context of BD-Ten1$_{34-680}$, the mutated sequence was amplified from the isolated yeast plasmid DNA via PCR and inserted into the bait vector pGBKT7-ten1$_{34-680}$ in order to replace the native interacting domain. This allowed the expression of a mutated bait fusion protein, in the following referred to as BD-Ten1m$_{34-680}$ (Fig. 20A). After co-transformation of AH109 with pGBKT7-ten1m$_{34-680}$ and pGADT7-ZmPP26, epitope-tagged fusion proteins were detected in cell lysates via anti-Myc and anti-HA Western blot analyses (Fig. 20B). The Western signal for AD-ZmPP26 showed a strong intensity when BD-Ten1$_{34-680}$ was co-expressed, whereas the signal was weaker in the presence of BD-Ten1m$_{34-680}$ (Fig. 20B). This suggests that the interaction with BD-Ten1$_{34-680}$ has an effect on protein stability of AD-ZmPP26, as already observed earlier (Fig. 10). Subsequently, the generated yeast strain was tested for the interaction of fusion proteins as described in chapter 2.6.1. Co-expression of BD-Ten1$_{34-680}$ and AD-ZmPP26 allowed growth on high stringency medium, whereas co-expression of BD-Ten1m$_{34-680}$ and AD-ZmPP26 did not (Fig. 20C). These results make it likely that the domain necessary for interaction with ZmPP26 is located between residue 133 and 327 of Ten1. Furthermore, Ten1m, harboring 14 amino acid substitutions in the identified interacting domain, shows no interaction with ZmPP26 in yeast two-hybrid assays.

2.6.6. The interaction of Ten1 and ZmPP26 may be biologically relevant

To determine whether the interaction of Ten1 and ZmPP26 is biologically relevant for *U. maydis*, the mutated protein Ten1m was tested for its ability to rescue the virulence defect of SG200Δ10A after maize seedling infection. Although HA$_3$-Ten1 was detected after IP from infected leaf material (Fig. 16A), this experiment could not be repeated in the course of this study. To demonstrate the stability of Ten1m after plant infection, it was thus first and foremost necessary to produce a functional HA-tag fusion protein of Ten1 that can be immunodetected in infected leaf material. To this end, another *HA*-tag fusion construct of *ten1* was expressed under the *ten1* promoter in SG200Δ10A via single integration into the *ip* locus. The resulting fusion protein Ten1$_{132}$-HA$_3$ harbors a triple HA-affinity tag between amino acids 132 and 133 (Fig. 21A), directly adjacent to the defined ZmPP26-interacting domain, in a protein region where no secondary structure elements were predicted by Phyre^2 (Fig. 35, appendix).

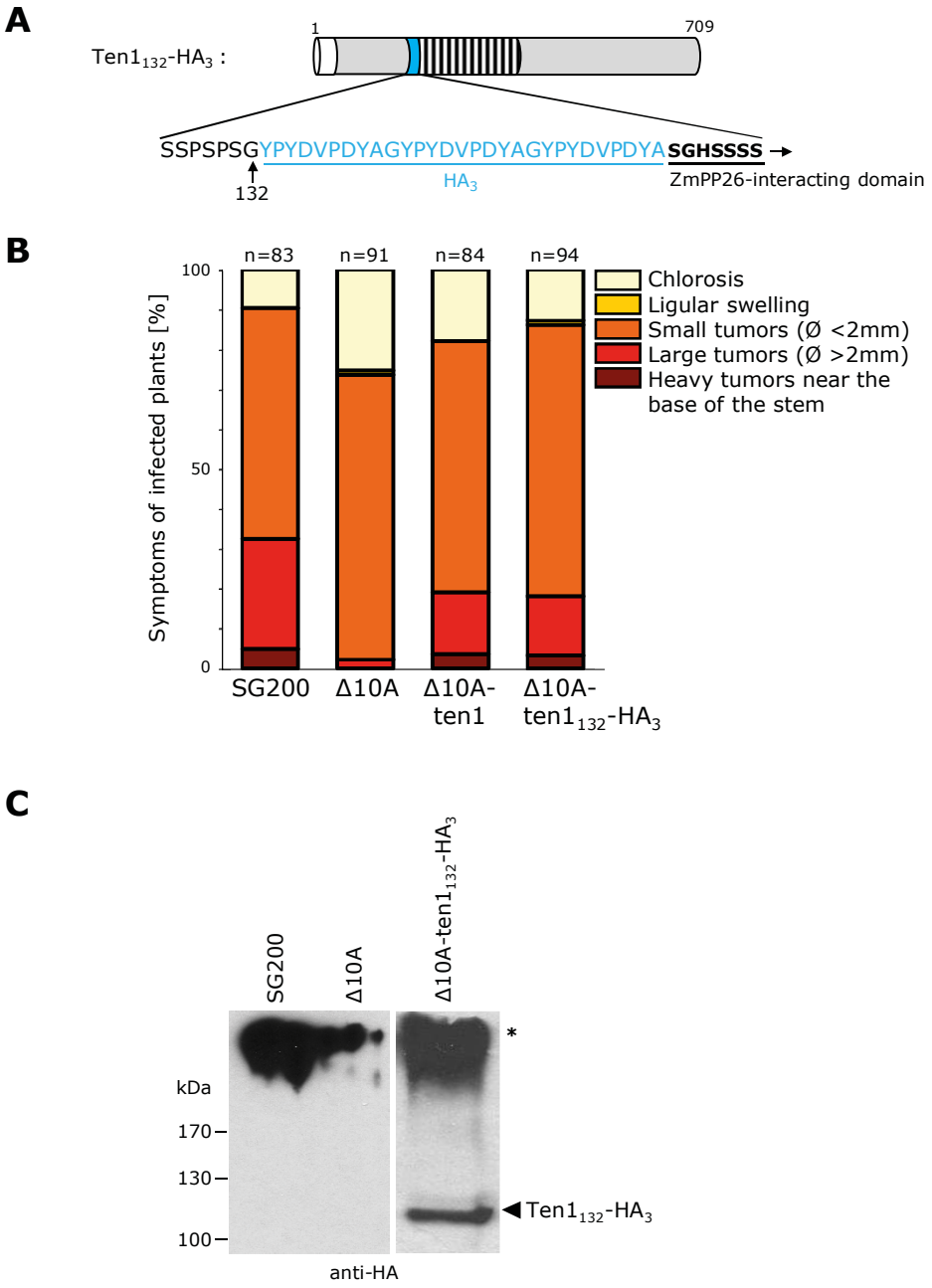

Fig. 21: Complementation of SG200Δ10A with Ten1$_{132}$-HA$_3$. (A) Illustration of the full-length fusion protein Ten1$_{132}$-HA$_3$ generated for complementation of SG200Δ10A. Numbers indicate amino acid positions. The white part indicates the N-terminal signal peptide of Ten1; the blue part indicates the triple HA affinity tag including linker amino acids (HA$_3$); the shaded part indicates the ZmPP26-interacting domain. **(B)** Infection symptoms on maize seedlings at 12 dpi caused by SG200, SG200Δ10A, SG200Δ10A-ten1, and SG200Δ10A-ten1$_{132}$-HA$_3$. Symptoms are classified into disease categories modified from Kämper *et al.* (2006). Shown are average values of three independent biological replicates. n, total number of infected plants. **(C)** SDS-PAGE followed by anti-HA Western blot using cell lysates from leaves infected with SG200, SG200Δ10A, and SG200Δ10A-ten1$_{132}$-HA$_3$ at 4 dpi. *, non-specific bands with high molecular weight due to treatment of infected plant material with 8 M urea buffer.

Seedling infections with SG200Δ10A-ten1$_{132}$-HA$_3$ revealed a partial rescue of the SG200Δ10A virulence defect at 12 dpi, similar to SG200Δ10A-ten1 (Fig. 21B). Moreover, at 4 dpi Ten1$_{132}$-HA$_3$ was detected in lysates of infected leaf material via anti-HA Western blot analysis at around 110 kDa (Fig. 21C). These results show that Ten1$_{132}$-HA$_3$ is a biologically active protein which can be detected in infected leaf material at 4 dpi.

To investigate the contribution of the mutated Ten1m to virulence of *U. maydis*, *ten1m$_{132}$-HA$_3$* was expressed under the *ten1* promoter via single integration into the *ip* locus of SG200Δ10A. The resulting fusion protein Ten1m$_{132}$-HA$_3$ harbors a triple HA-affinity tag between amino acids 132 and 133 (Fig. 22A), directly adjacent to the mutated ZmPP26-interacting domain. Seedling infections with SG200Δ10A-ten1$_{132}$-HA$_3$ revealed a partial rescue of the SG200Δ10A virulence defect at 12 dpi (Fig. 22B). In contrast, SG200Δ10A-ten1m$_{132}$-HA$_3$ phenocopied SG200Δ10A (Fig. 22B). Moreover, at 4 dpi both Ten1$_{132}$-HA$_3$ and Ten1m$_{132}$-HA$_3$ were detected at around 110 kDa in lysates of infected leaf material via anti-HA Western blot (Fig. 22C). These results indicate that the interaction of Ten1 and ZmPP26 is necessary to partially rescue the virulence defect of SG200Δ10A.

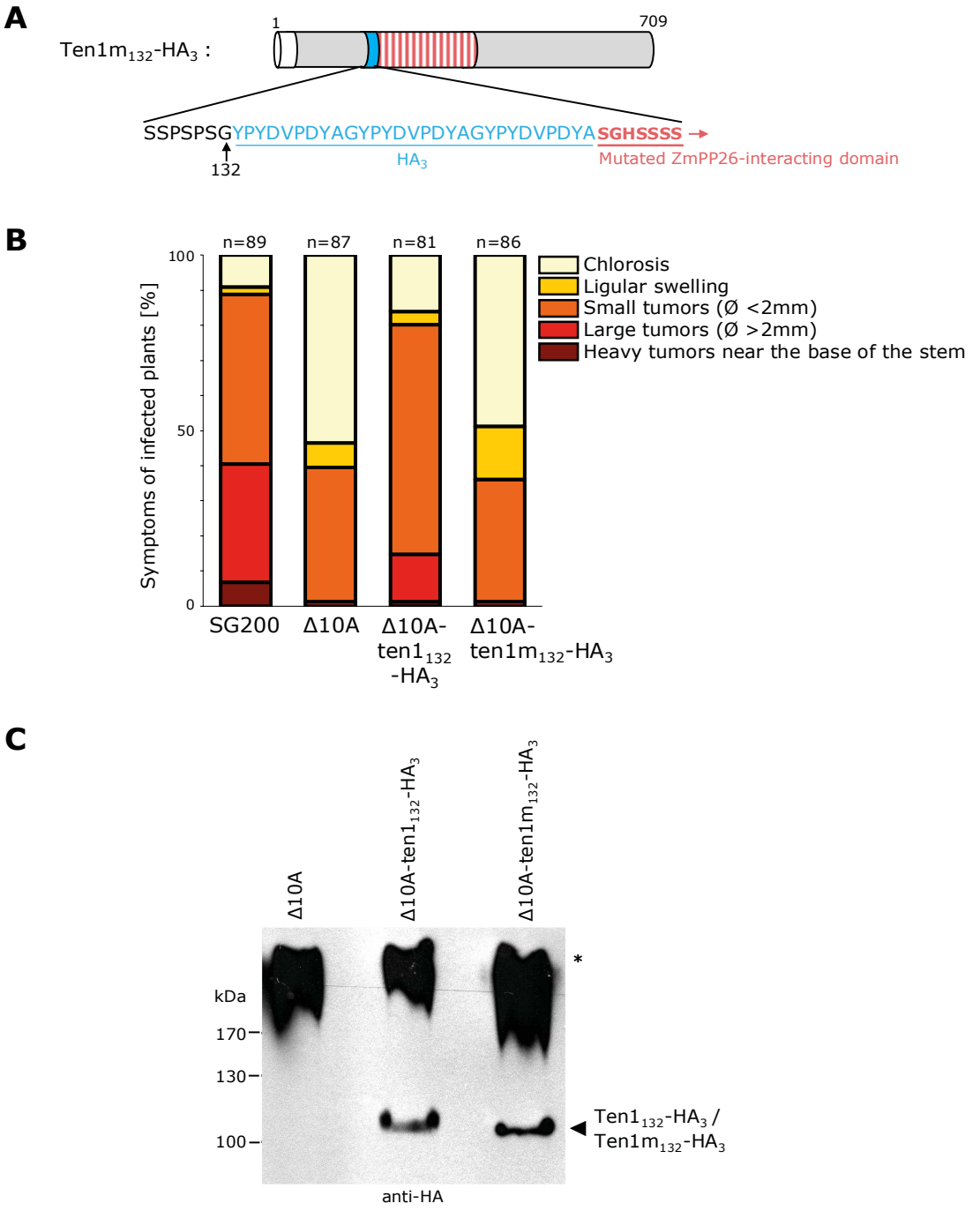

Fig. 22: Complementation of SG200Δ10A with mutated Ten1m$_{132}$-HA$_3$. (A) Illustration of the full-length fusion protein Ten1m$_{132}$-HA$_3$ generated for complementation of SG200Δ10A. Numbers indicate amino acid positions. The white part indicates the N-terminal signal peptide of Ten1; the blue part indicates the triple HA affinity tag including linker amino acids (HA$_3$); the red shaded part indicates the mutated ZmPP26-interacting domain. **(B)** Infection symptoms on maize seedlings at 12 dpi caused by SG200, SG200Δ10A, SG200Δ10A-ten1$_{132}$-HA$_3$, and SG200Δ10A-ten1m$_{132}$-HA$_3$. Symptoms are classified into disease categories modified from Kämper *et al.* (2006). Shown are average values of three independent biological replicates. n, total number of infected plants. **(C)** SDS-PAGE followed by anti-HA Western blot using cell lysates from leaves infected with SG200Δ10A, SG200Δ10A-ten1$_{132}$-HA$_3$, and SG200Δ10A-ten1m$_{132}$-HA$_3$ at 4 dpi. *, non-specific bands with high molecular weight due to treatment of infected plant material with 8 M urea buffer.

2.6.7. Heterologously expressed ZmPP26 shows strong PP2C-specific activity *in vitro*

To show that ZmPP26 has phosphatase activity, the protein was overexpressed in *E. coli*, affinity purified and tested for its activity *in vitro*. To this end, *ZmPP26* was amplified from maize cDNA via PCR and cloned into the plasmid pRSET-GST-PP. In *E. coli* strain BL21(DE3)pLysS this plasmid allows the expression of a GST (glutathione S-transferase) fusion protein via the IPTG-inducible production of the T7 RNA polymerase. Moreover, the produced fusion protein contains a PreScission Protease cleavage site (LEVLFQ/GP), allowing the removal of the GST tag. As a control, a catalytically dead mutant allele of *ZmPP26* was generated. The catalytic domain of almost all eukaryotic PP2Cs is formed by a binuclear metal binding site located in the cleft of a β-sandwich. This site consists of four conserved aspartic acid residues which coordinate the binding of Mg^{2+} or Mn^{2+} ions (Das *et al.*, 1996). An amino acid sequence alignment with human PP2C alpha (Mann *et al.*, 1992), ABI1 from *A. thaliana* (Leung *et al.*, 1994), and PTC1 from *S. cerevisiae* (Maeda *et al.*, 1993) revealed that in ZmPP26 these residues are D44, D65, D226, and D265 (Fig. 23).

Fig. 23: Multiple amino acid sequence alignment (ClustalW) of ZmPP26 and PP2Cs from human, *A. thaliana*, and *S. cerevisiae*. Conserved residues are highlighted in green. Red arrows indicate metal-coordinating residues determined by Das *et al.* (1996).

In the *A. thaliana* PP2C ABI1, three amino acid substitutions (DGH177-179KLN) were shown to abolish enzymatic activity (Sheen 1998). As these amino acids are conserved in ZmPP26 (Fig. 23), *ZmPP26*$_{DGH65\text{-}67KLN}$ was generated and also cloned into the background plasmid pRSET-GST-PP. After the introduction of the generated plasmids into BL21(DE3)pLysS, protein synthesis was induced by IPTG. Subsequently, GST-ZmPP26 as well as GST-ZmPP26$_{DGH65\text{-}67KLN}$ were affinity purified via glutathione sepharose. The fusion proteins were on-column cleaved using PreScission Protease and eluted without GST tag (Fig. 24A).

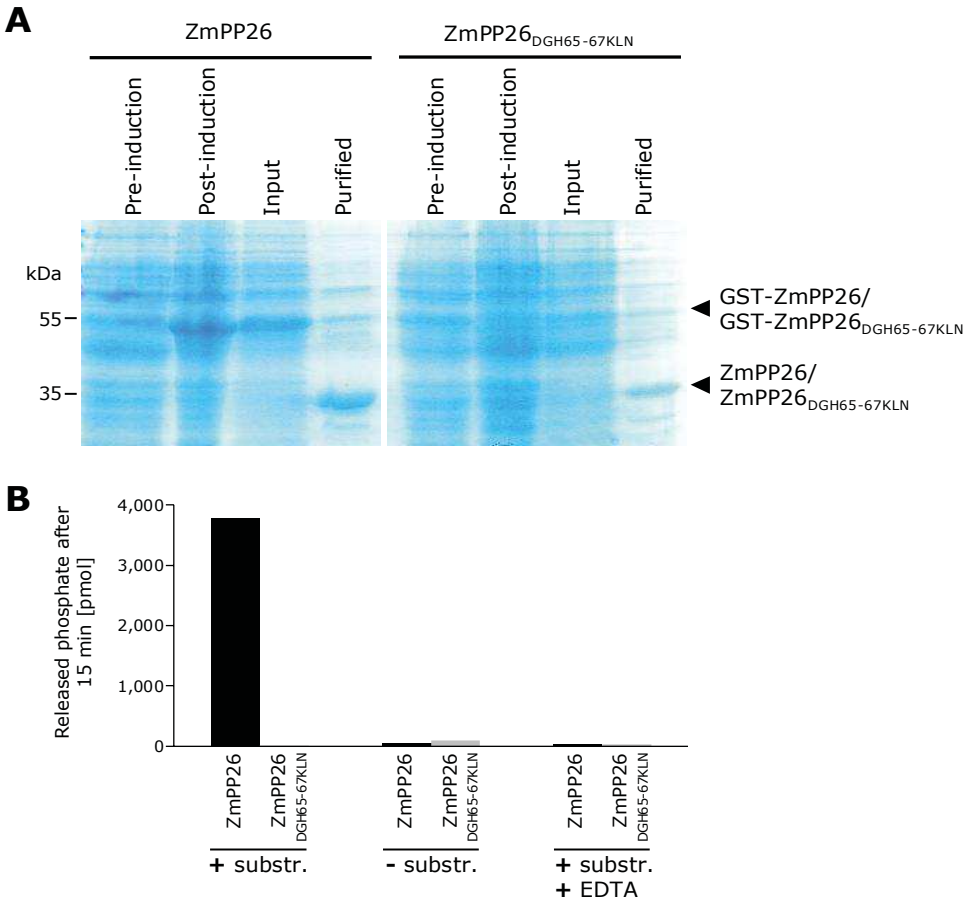

Fig. 24: Purification and *in vitro* phosphatase activity of ZmPP26 and the catalytic-dead mutant ZmPP26$_{DGH65\text{-}67KLN}$. (A) InstantBlue-stained polyacrylamide gel for visualization of purified proteins after overexpression in *E. coli*. Pre-induction, bacterial cell lysates prior to IPTG induction; post-induction, bacterial cell lysates 4 hours after IPTG induction; input, soluble fraction of bacterial cell lysates after induction (used for affinity purification); purified, proteins eluted without GST tag after on-column cleavage with PreScission protease. **(B)** *In vitro* phosphatase activity of purified ZmPP26 and ZmPP26$_{DGH65\text{-}67KLN}$. Shown is the amount of released phosphate from 100 µM of a synthetic phosphopeptide substrate after 15 minutes. Per reaction 0.7 nM ZmPP26 and ZmPP26$_{DGH65\text{-}67KLN}$ was used, respectively. The assay was performed in two biological replicates showing similar results.

The concentration of the purified proteins was determined via a target-specific and fluorescence-based quantitation method using the Qubit fluorometer (Invitrogen, Karlsruhe). Accordingly, the concentrations of ZmPP26 and ZmPP26$_{DGH65-67KLN}$ were 0.21 µg/µL and 0.12 µg/µL, respectively. Phosphatase activity of the enriched proteins was assessed via the Serine/Threonine Phosphatase Assay System (Promega, Mannheim) using a synthetic phosphopeptide (RRA(pT)VA) as substrate. In a reaction volume of 50 µL, 1 µg of ZmPP26/ZmPP26$_{DGH65-67KLN}$ was used, corresponding to a molar concentration of 0.7 nM (calculated molecular weight of both proteins: 30.7 kDa). In the presence of 0.7 nM ZmPP26 and 100 µM substrate, about 3,800 pmol released phosphate was detected over a reaction time of 15 minutes, whereas there was minimal released phosphate in the presence of ZmPP26 alone. After the addition of 10 mM EDTA, an inhibitor of PP2C activity under the assayed conditions (Irmler and Forchhammer, 2001), no released phosphate was measured despite the presence of both ZmPP26 and the substrate in the reaction. For 0.7 nM ZmPP26$_{DGH65-67KLN}$ no phosphatase activity could be detected under all tested conditions (Fig. 24B). This experiment shows that heterologously expressed ZmPP26 has phosphatase activity *in vitro* and that this activity likely is specific for the family of PP2C enzymes.

2.7. Ten1 is secreted to the axenic culture supernatant

The prediction of an N-terminal signal peptide within the first 33 amino acids raised the question as to whether Ten1 is indeed secreted by *U. maydis*. To test for secretion *in vitro*, *ten1$_{132}$-HA$_3$* was overexpressed under the constitutive *otef* promoter (Spellig *et al.*, 1996) in strain AB33 via *ip* locus integration of multiple copies of the construct. AB33 is a derivative of FB2 that contains the *bE1* and *bW2* genes under the control of the nitrate-inducible *nar* promoter. Exponentially growing sporidia of this strain can be shifted from saprophytic to filamentous growth after incubation in nitrate minimal medium (Brachmann *et al.*, 2001). As controls, the progenitor strain AB33 and AB33-GFP-HA were included in the experiment. The latter overexpressed cytoplasmic GFP-HA driven by the *otef* promoter and served as control for cell lysis. After the induction of hyphae in nitrate minimal medium, the cultures of AB33, AB33-ten1$_{132}$-HA$_3$, and AB33-GFP-HA were separated into pellet and supernatant fractions by centrifugation. Subsequently, proteins secreted to the supernatant were enriched by TCA

precipitation. Via anti-HA Western blot analyses Ten1 $_{132}$-HA$_3$ was detected in the cell lysate of the pellet fraction as well as in the supernatant fraction at around 100 kDa. In contrast, cytoplasmic GFP-HA was detected only in the cell lysate of the pellet fraction at around 35 kDa, but not in the supernatant fraction (Fig. 25A). As an internal control for cell lysis, the same samples were analyzed via anti-α tubulin Western blot. Two signals for α tubulin with sizes of about 55 kDa and 60 kDa were detected only in the cell lysate of pellet fractions and not in the supernatant samples, showing the absence of cell lysis (Fig. 25B). These results suggest that Ten1 $_{132}$-HA$_3$ is secreted in axenic culture by *U. maydis* hyphae.

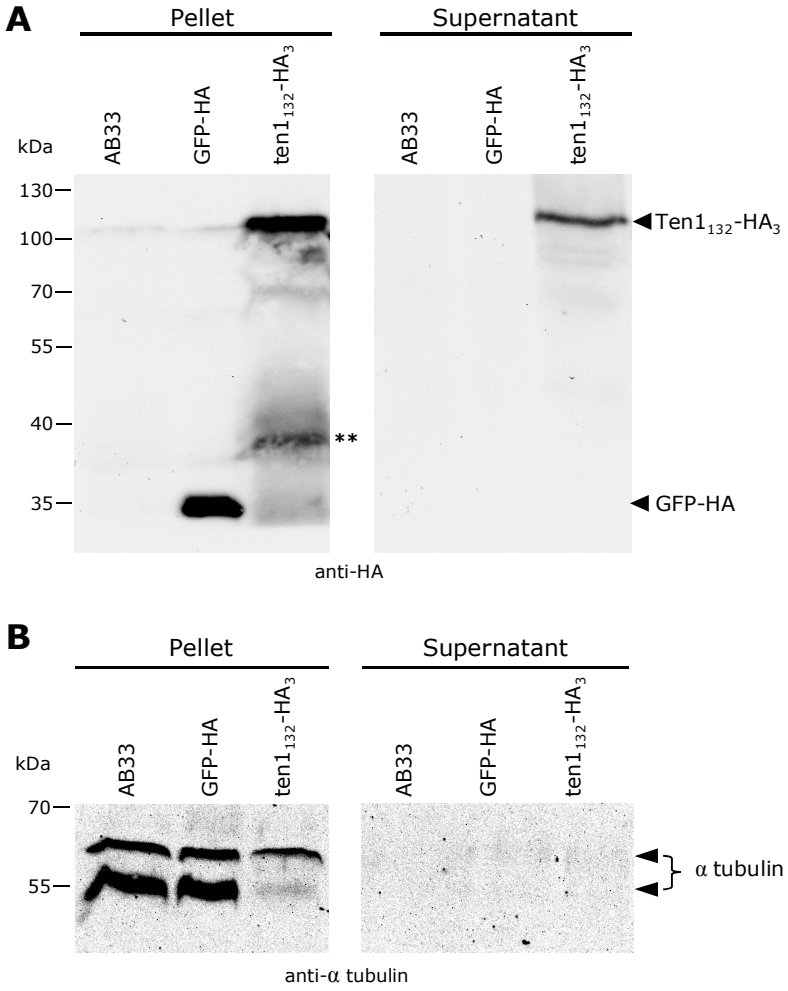

Fig. 25: Secretion of Ten1 $_{132}$-HA$_3$ to the axenic culture supernatant of AB33 hyphae. (A) SDS-PAGE followed by anti-HA Western blot using cell lysates from *U. maydis* hyphal cultures (pellet) and culture supernatants after TCA precipitation (supernatant). Samples were prepared from 50 mL hyphal culture of AB33, AB33-GFP-HA, and AB33-ten1 $_{132}$-HA$_3$ in nitrate minimal medium. **, product of protein degradation. **(B)** SDS-PAGE followed by anti-α tubulin Western blot using the same pellet and supernatant samples as in (A) for internal lysis control.

2.8. Immunoelectron microscopy shows translocation of Ten1 to plant cells

With the indication for secretion *in vitro*, the localization of Ten1 after secretion was investigated *in planta*. Live cell imaging of *U. maydis* effectors fused to the fluorescent protein mCherry proved to be useful to localize effectors in infected plant tissue (Djamei *et al.*, 2011; Tanaka *et al.*, 2014). Accordingly, translational fusions of *mCherry* and *ten1* (including an *HA*-tag for immunodetection) were expressed in SG200Δ10A via *ip* locus integration of a single copy of the construct. The fusion of mCherry-HA to the C-terminus of Ten1 resulted in a non-functional protein, *i.e.*, SG200Δ10A-ten1-mCherry-HA was not able to rescue the virulence defect of SG200Δ10A (not shown). In contrast, a strain expressing the N-terminal fusion protein HA-mCherry-Ten1 (with HA-mCherry fused to Ten1 after the predicted signal peptide) phenocopied SG200Δ10A-HA_3-ten1. Moreover, via confocal microscopy of leaves infected with SG200Δ10A-HA-mCherry-ten1, weak mCherry-specific fluorescence around hyphal tips was detected at 4 dpi (not shown). However, via anti-HA Western blot analysis using the same infected leaf samples only HA-mCherry was detected, indicating that the observed fluorescence stemmed from mCherry alone (not shown). Considering that the strain SG200Δ10A-HA-mCherry-ten1 was partially complementing the virulence defect of SG200Δ10A, the fluorescent fusion protein likely was cleaved after secretion, resulting in a retention of mCherry in the biotrophic interphase and in a release of Ten1. In the following, the question was addressed whether Ten1 is taken up by the plant or whether it remains in the apoplastic space after secretion.

To this end, immunoelectron microscopy (immuno-EM) using HA_3-Ten1 was carried out, considering that this fusion protein was shown to interact with the cytosolic ZmPP26 during infection of *U. maydis* (chapter 2.6.4). Leaf samples infected with SG200Δ10A-HA_3-ten1 and the control strain SG200 were collected at 4 dpi and chemically fixed. Using ultrathin sections of the fixed samples, immunogold labeling of HA_3-Ten1 and subsequent EM was performed (carried out by B. Zechmann, Baylor University, Texas, USA). Immunogold labeling can result in non-specific binding to cellular structures such as nuclei, cell walls, callose, or starch (U. Neumann, personal communication). To discriminate between labeling of HA_3-Ten1 and background labeling in the SG200 samples, the distribution of gold particles in different cell

compartments was quantified based on the obtained micrographs (carried out by B. Zechmann, Baylor University, Texas, USA). SG200-infected leaf samples showed occasional non-specific background labeling in the chloroplasts, in fungal hyphae, and particularly in plant nuclei (Fig. 26A). Leaves infected with SG200Δ10A-HA_3-ten1 exhibited labeling of HA_3-Ten1 in chloroplasts, in the plant cytosol, and predominantly in plant nuclei. However, no gold particles were detected at the biotrophic interface between fungal cell wall and plant plasma membrane (Fig. 26B). The quantification of gold particle distribution in samples infected with SG200Δ10A-HA_3-ten1 revealed a significantly increased labeling in the plant cytosol and in nuclei, in comparison to SG200. In contrast, gold labeling in fungal hyphae and chloroplasts was not significantly different from SG200 (Table 4). In conclusion, these experiments suggest that secreted Ten1 is taken up by the plant and that the protein mainly localizes to the nucleus of the plant cell.

Table 4: Quantification of immunogold particles in infected maize tissue[1].

	SG200 (n=9)	SG200Δ10A-HA_3-ten1 (n=14)
Fungal cytoplasm	0.8 ± 0.3	1.32 ± 0.4 ns
Biotrophic interface[2]	0.06 ± 0.06	0 ± 0 ns
Plant cytosol	0.18 ± 0.05	1.7 ± 0.4 ***
Plant nucleus	0.9 ± 0.2	6.6 ± 1.5 ***
Chloroplast	0.23 ± 0.1	0.57 ± 0.18 ns

[1] All data in this table represent the mean number of gold particles bound to HA per µm² in different cell compartments of (n) analyzed micrographs ± standard errors. ***, significant differences between SG200 and SG200Δ10A-HA_3-ten1 based on a Mann-Whitney U test at the confidence level of 0.001. ns, not significantly different.

[2] The biotrophic interface was defined as the region between fungal cell wall and plant plasma membrane.

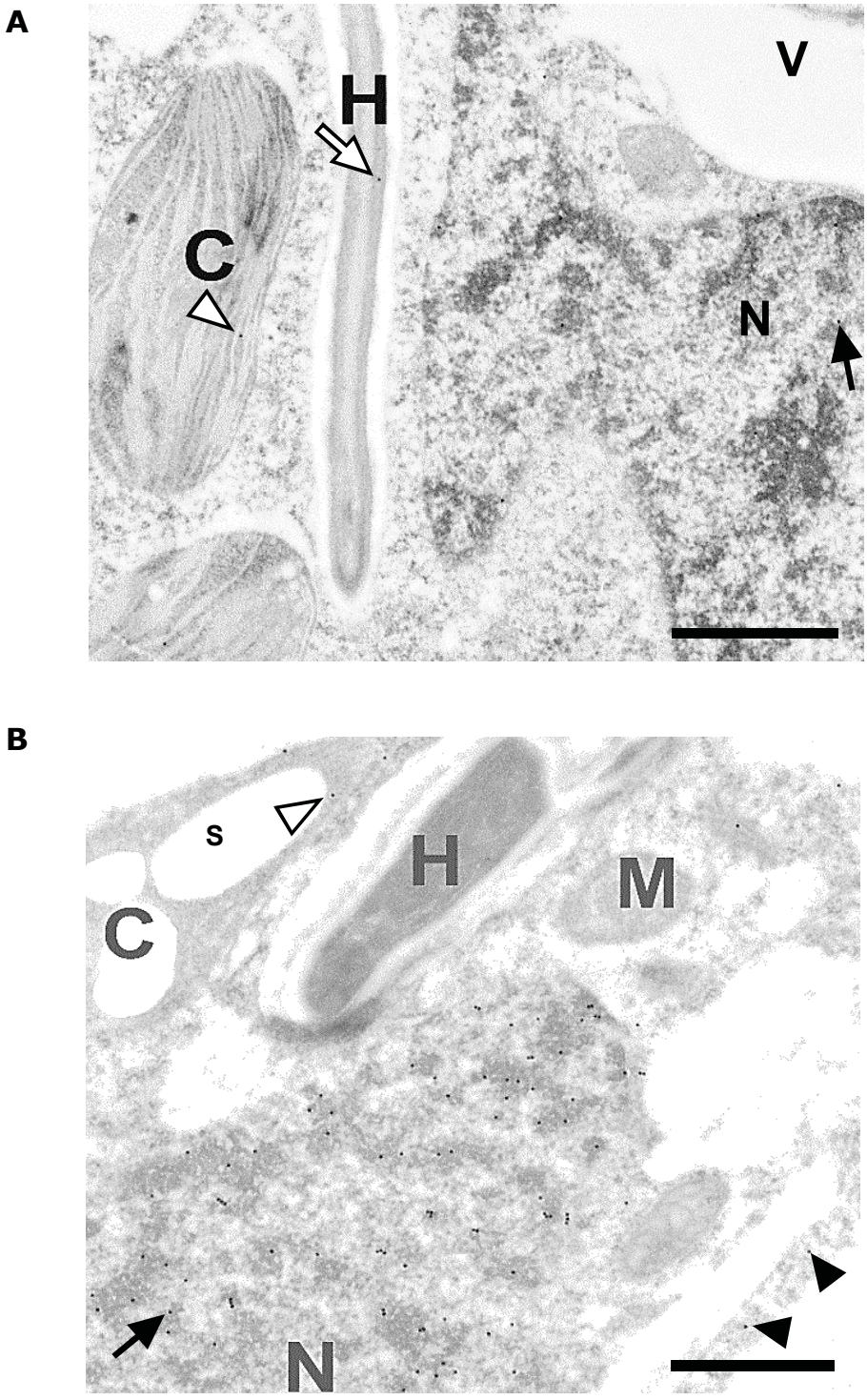

Fig. 26: Immunogold detection of HA_3-Ten1 in infected maize leaves. (A) Transmission electron micrographs showing unspecific immunogold labeling in ultrathin sections of SG200-infected maize leaves at 4 dpi. **(B)** Transmission electron micrographs showing immunogold labeling of HA_3-Ten1 in ultrathin sections of leaves infected with SG200Δ10A-HA_3-ten1 at 4 dpi. Filled arrows, detection of gold particles in plant nuclei; empty arrow, detection of gold particle in the fungal hypha; filled arrowheads, detection of gold particles in the plant cytosol; empty arrowheads, detection of gold particles in chloroplasts. V, vacuole; N, nucleus; H, hypha; M, mitochondrion; C, chloroplast; S, starch granule. Scale bars equal 1 µm.

To substantiate the translocation of Ten1, a recently established uptake assay was deployed which is based on the biotinylation of Avitagged effectors in the host cytoplasm (Lo Presti *et al.*, 2017). For this purpose, an *Avitag-HA* fusion construct of *ten1* was generated and expressed in a SG200 strain secreting HA_3-avitagged Suc2. Using a gene replacement approach *ten1*$_{132}$-*Avitag-HA* was expressed from the native *ten1* locus. The uptake assay relies in the first place on the detection of HA-Avitagged proteins via IP from infected maize leaf material. Therefore, seedlings were infected with SG200-Suc2-Avitag-HA_3-Ten1$_{132}$-Avitag-HA. At 4 dpi, infected leaf material was harvested and cell lysates were used for an IP via anti-HA magnetic beads. However, Ten1$_{132}$-Avitag-HA could not be detected after IP in three biological replicates (not shown). This result shows that the generated HA-tag fusion protein of Ten1 cannot be used for the uptake assay according to Lo Presti *et al*. (2017).

2.9. Ten1 and the *A. thaliana* PP2C WIN2 interact in yeast two-hybrid assays

ZmPP26 is a ortholog of WIN2, a group F PP2C from *A. thaliana* which is involved in the regulation of biotic stress responses (Lee *et al.*, 2008). WIN2 displays 71.2% amino acid identity with ZmPP26 (Fig. 27).

```
ZmPP26  MGYLSSVIGHP----TDGSSVSGGGLSQNGRFSYGYASSPGKRASMEDFYETKIDCVDGQIVGLFGVFDGHGGAKVAEYV  76
WIN2    MGYLNSVLSSSSQVHSDDGPVSGGGLSQNGKFSYGYASSPGKRSSMEDFYETRIDGVEGEIVGLFGVFDGHGGARAAEYV  80

ZmPP26  KENLFNNLVSHPKFISDTKVAIDDAYKSTDSEFLESDSSQNQ-CGSTASTAVLVGDRLFVANVGDSRAICREGNAIAVS  155
WIN2    KQNLFSNLIRHPKFISDTTAAIADAYNQTDSEFLKSENSQNRDAGSTASTAILVGDRLLVANVGDSRAVICRGGNAIAVS  160

ZmPP26  KDHKPDQTDERQRIEDAGGFVMWAGTWRVGGVLAVSRAFGDKLLKQYVVVDPEIREEVVDDTLEFLILASDGLWDVVSNE  235
WIN2    RDHKPDQSDERQRIEDAGGFVMWAGTWRVGGVLAVSRAFGDRLLKQYVVADPEIQEEKVDSSLEFLILASDGLWDVVSNE  240

ZmPP26  EAVAMTRSIKDPEEAAKMLLQEAYKRESSDNITCVVVHFLHGQ----GSSGYA------------------  284
WIN2    EAVGMIKAIEDPEEGAKRLMMEAYQRGSADNITCVVVRFFSDQAGGIGSSSTNIPIDHGIVPDRISGDSST  311
```

Fig. 27: Global sequence alignment of ZmPP26 and WIN2 from *A. thaliana*. Conserved residues are highlighted in green.

WIN2 was tested for interaction with Ten1 via yeast two-hybrid assays. *WIN2* was amplified in full-length from *A. thaliana* cDNA (kindly provided by M. Hilbert) via PCR and cloned into the prey plasmid pGADT7. Strains AH109-pGBKT7-ten1$_{34-680}$#1 as well as AH109-pGBKT7 were transformed with pGADT7-WIN2 to test for protein interaction and autoactivation of the GAL4 transcription factor by AD-WIN2, respectively. Via anti-Myc and anti-HA Western blot analyses using cell lysates of transformed AH109-pGBKT7-ten1$_{34-680}$#1, BD-Ten1$_{34-680}$ and

AD-WIN2 were detected at approx. 120 kDa and 55 kDa, respectively (Fig. 28A). In cell lysates of transformed AH109-pGBKT7, AD-WIN2 was detected via anti-HA Western blot (Fig. 28A), whereas the BD alone could not be detected via anti-Myc Western blot (not shown). The Western signal for AD-WIN2 showed enhanced intensity when BD-Ten1$_{34-680}$ was co-expressed (Fig. 28A). This suggests that the interaction with BD-Ten1$_{34-680}$ has an effect on protein stability of AD-ZmPP26. The generated yeast strains were streaked out on low stringency and high stringency media to verify the integration of bait and prey plasmids and to test for interaction of fusion proteins, as described in chapter 2.6.1. The strain co-expressing BD-Ten1$_{34-680}$ and AD-WIN2 allowed growth on high stringency medium, whereas autoactivation of the GAL4 transcription factor by AD-WIN2 was not observed (Fig. 28B). This shows an interaction of Ten1 and WIN2 in yeast two-hybrid assays.

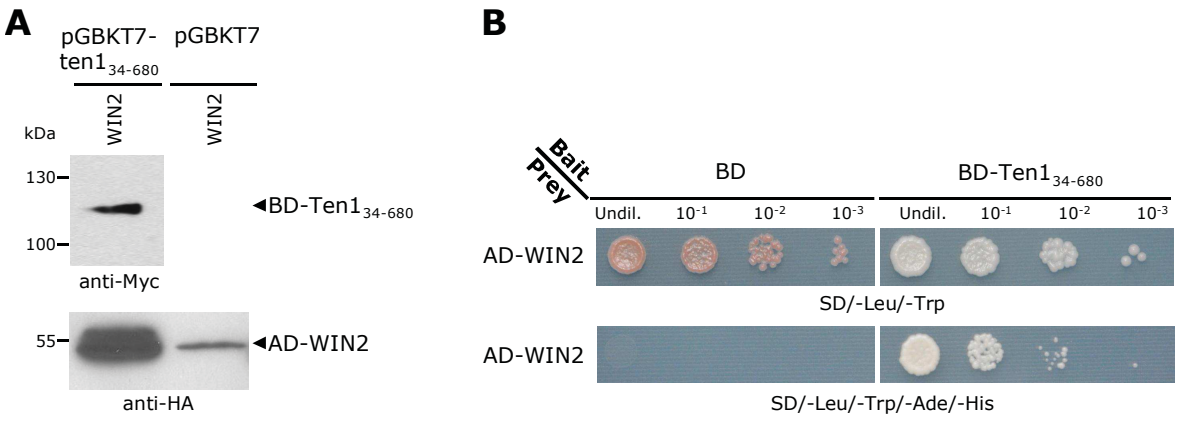

Fig. 28: Yeast two-hybrid assays with Ten1$_{34-680}$ and WIN2. (A) SDS-PAGE followed by anti-Myc and anti-HA Western blots using cell lysates. AH109-pGBKT7-ten1$_{34-680}$#1 and AH109-pGBKT7 were transformed with pGADT7-WIN2. **(B)** Low stringency (SD/-Leu/-Trp) and high stringency (SD/-Leu/-Trp/-Ade/-His) plates showing serial dilutions of AH109 strains co-expressing the indicated bait and prey proteins. AD, GAL4 activation domain; BD, GAL4 binding domain.

3. Discussion

In the present study Ten1 was characterized as a major virulence factor encoded by *U. maydis* effector gene cluster 10A. Ten1 was shown to be secreted in axenic culture and immunoelectron microscopy suggests a translocation of the protein to plant cells after secretion. Via yeast two-hybrid assays ZmPP26, a cytosolic maize type 2C protein phosphatase (PP2C), was identified as interaction partner of Ten1. This interaction was also shown during the biotrophic development of *U. maydis* and maize. Furthermore, evidence was obtained that the interaction of Ten1 and ZmPP26 is biologically relevant for the fungus. However, the outcome of this interaction could not be determined in the course of this study. In the following, the presented results will be discussed.

3.1. The conservation of Ten1 among related fungi

Comparative analyses of proteomes revealed a weak conservation of Ten1 in the three sequenced grass-infecting smut fungi *S. reilianum* f. sp. *zeae*, *S. scitamineum*, and *U. bromivora*. Related proteins from these species display only between 28.8% and 29.8% amino acid identity with Ten1. Interestingly, two related proteins were found both in *S. reilianum* f. sp. *zeae* (sr11226 and sr11227) and in *S. scitamineum* (SPSC_05103 and SPSC_05104). In *S. reilianum* f. sp. *zeae*, *sr11226* and *sr11227* are adjacent in the genome and are part of the previously described divergence cluster 10-15, which is homologous to gene cluster 10A in *U. maydis* (Schirawski *et al.*, 2010). A similar gene arrangement is found in *S. scitamineum*, where the adjacent genes *SPSC_05103* and *SPSC_05104* are part of the effector gene cluster Ss-scaf36-1, which is also homologous to *U. maydis* cluster 10A (Dutheil *et al.*, 2016). These findings suggest that gene duplications of *ten1* homologs occurred in the ancestor of *Sporisorium* species. The two gene copies might then have been retained to function in the respective host maize and sugarcane. To test for the ability of sr11226 to rescue the virulence defect of the cluster 10A deletion strain, a single copy of *sr11226* was expressed under the *ten1* promoter in SG200Δ10A via *ip* locus integration. However, seedling infections using five independent transformants of SG200Δ10A-sr11226 did not provide clear evidence for a contribution of sr11226 to virulence of *U. maydis* (not shown). The genome of *Ustilago*

hordei, another related smut fungus causing covered smut in barley (Laurie *et al.*, 2012), is also likely to encode a protein related to Ten1. A nucleotide sequence containing a stop codon was found in a *U. hordei* genomic region which is syntenic to the locus of *UMAG_03743* in *U. maydis*. This is a neighboring gene of *ten1* which is not part of gene cluster 10A (Kämper *et al.*, 2006). After *in silico* translation of the identified sequence from *U. hordei*, a stretch of amino acids was determined showing 34.8% identity with the C-terminus of Ten1 (residues 338-680). However, the anticipated coding sequence for the N-terminus of this Ten1-related protein is part of an unannotated region of the genome, the amplification of which was unsuccessful. This might be due to the low quality of the *U. hordei* genome assembly, compared to the genomes of related smuts (Dutheil *et al.* 2016). In *M. pennsylvanicum* the related protein mp06537 is detected, which shows only 20.7% amino acid identity with Ten1. This reduced conservation could reflect an adaptation to the dicot host of this species (Sharma *et al.*, 2014). Ten1 is weakly conserved also in *Pseudozyma hubeiensis*, *P. antarctica*, and *P. aphidis*. *Pseudozyma* spp. belong to the order *Ustilaginales* and are mostly used in biotechnology as they are able to produce biosurfactants such as mannosylerythritol lipids (MELs; Yoshida *et al.*, 2014). However, *P. antarctica* and *P. aphidis* are also associated with grasses (Allen *et al.*, 2004). Interestingly, *P. antarctica* has a secretome comparable in size and composition to the grass-infecting smuts and it was hypothesized that this species may have originated from a grass-colonizing ancestor (Schuster *et al.*, 2017). Taken together, the weak conservation of Ten1 among related smuts or smut-related species suggests an accelerated evolution of the effector Ten1 in order to adapt to its host target ZmPP26, or to evade recognition by host immunity (Lanver *et al.*, 2017).

3.2. The biotrophic development of *ten1* deletion strains

The observed phenotype of SG200Δten1 at 12 dpi is not characterized by a decreased tumor rate (*i.e.*, the overall occurrence of heavy, large, and small tumors), but rather by a reduction of tumor size (*i.e.*, fewer large, but more small tumors), relative to SG200. This indicates that the *ten1* deletion strain is able to induce tumorigenesis and that the observed virulence phenotype is established after the onset of tumor formation at 5 dpi (Skibbe *et al.*, 2010). Accordingly, confocal microscopy analyses of infected leaves at 4 dpi showed an intracellular

proliferation of SG200Δten1 comparable to SG200. Unfortunately, attempts to visualize differences in fungal proliferation at later time points by confocal microscopy failed. With the maturation of large tumors, plant biomass is rapidly converted to fungal biomass (Snetselaar and McCann, 2017). Quantitative PCR (qPCR) using genomic DNA extracted from infected leaves was previously used to determine fungal biomass in relation to plant biomass at a given time point after infection (Brefort *et al.*, 2014; van der Linde *et al.*, 2011; Neidig, 2013; Tanaka *et al.*, 2014). However, the implementation of this method using SG200Δten1-infected leaf material led to inconclusive results.

3.3. Is Ten1 *the* major virulence factor encoded by cluster 10A?

The complementation strain SG200Δ10A-ten1 partially rescued the virulence defect of the cluster 10A deletion strain. This indicates that *ten1* is a major virulence factor of the cluster. The observed virulence phenotype of SG200Δ10A-ten1 further shows that the residual nine genes of cluster 10A are required for full virulence of *U. maydis*. Effector gene clusters of *U. maydis* likely arose through tandem gene duplication events followed by rapid evolution (Dutheil *et al.*, 2016). Effector genes of one cluster thus may encode proteins that target different host molecules to promote virulence. Interestingly, RNAseq analyses of FB1 and FB2 strains during biotrophic development revealed a nearly identical expression pattern of *ten1* and three other cluster genes, namely *UMAG_03745*, *UMAG_03748*, and *UMAG_03750* (D. Lanver, personal communication). Moreover, these RNAseq data showed a strong induction of *UMAG_03749*, *UMAG_03751*, and *UMAG_03753* at 4 dpi. It would be rewarding to investigate the contribution of these cluster genes to virulence by testing single gene deletion mutants or by complementing SG200Δ10A with individual genes.

3.4. Is Ten1 post-translationally modified?

In Western blot analyses involving SDS-PAGE, epitope-tagged Ten1 proteins were continuously detected at a molecular weight which was approx. 30 kDa to 35 kDa higher than expected (*e.g.*, $Ten1_{132}$-HA_3 has an expected molecular weight of 75.3 kDa, but was detected at approx. 110 kDa). This aberrant migration behavior raises the question whether Ten1 is post-

translationally modified. In fungi, glycosylation is the most universal form of post-translational modification and it is important for stability, secretion, and localization of proteins (Deshpande *et al.*, 2008). Moreover, *N*- and *O*-glycosylation of proteins is proposed to play an important role for virulence of *U. maydis* (Fernandez-Alvarez *et al.*, 2009, 2013). Whereas a prediction of *N*-glycosylation sites in Ten1 via the NetNGlyc 1.0 server was negative, 53 residues of Ten1 are predicted to be *O*-glycosylated according to the NetOGlyc 4.0 server (Steentoft *et al.*, 2013). Although designed for mammalian proteins, González *et al.* (2012) could show that predictions using the NetOGlyc tool are also reliable for secreted fungal proteins. The authors further revealed that of all *U. maydis* proteins predicted to be secreted, 72% are also predicted to be *O*-glycosylated. Interestingly, serine/threonine-rich regions predicted to be highly *O*-glycosylated tend to be located at protein ends, especially at the C-terminus (González *et al.*, 2012). Indeed, the amino acid sequence of Ten1 shows a high abundance of serine and threonine residues towards the N- and C-termini of the protein (Fig. 29). In the course of this study, an enzymatic deglycosylation of immunoprecipitated HA_3-Ten1 failed because the protein could not be detected via Western blot after IP in the first place (not shown). Future experiments could involve other methods for the detection of glycosylation such as staining or affinity-based binding of sugars (*e.g.* by lectins) after the separation of proteins via SDS-PAGE (Roth *et al.*, 2012). Moreover, the *pmt4* mutant strain could be used as background for the expression of epitope-tagged Ten1. This mutant is affected in *O*-mannosylation, a type of *O*-glycosylation important for pathogenic development of *U. maydis* (Fernandez-Alvarez *et al.*, 2009).

Another explanation for an anomalous migration behavior of a protein in SDS-PAGE is a high content of positively charged amino acids (Serdyuk *et al.*, 2007). The intrinsic positive charge of the protein is thus not dominated by negatively charged SDS molecules, resulting in a slower gel migration of the protein-SDS complex towards the anode (Righetti *et al.*, 2001; Serdyuk *et al.*, 2007). Ten1 has a predicted isoelectric point of 9.81, resulting in an estimated net charge of 19.6 under SDS-PAGE conditions (considering that the separating gel has a pH of 8.8). This positive charge of Ten1 is caused by a high content of lysine and arginine residues, together making up 100 of the 680 amino acids of Ten1 (Fig. 29). The aberrant migration behavior of Ten1 in SDS-PAGE is thus likely attributed to the intrinsic charge of the protein.

Fig. 29: Amino acid sequence of Ten1. Lysine and arginine residues are highlighted in blue; serine and threonine residues are highlighted in red. Black box indicates the predicted signal peptide.

3.5. The localization of Ten1 after secretion

Immuno-EM detected Ten1 in plant cells, manifested by a significant accumulation of the protein in the plant cytoplasm and especially in plant nuclei. Other translocated effectors of *U. maydis* such as Tin2, Tin3, and See1 were also detected in plant nuclei via immuno-EM (Lo Presti *et al.*, 2017; Redkar *et al.*, 2015). It is generally accepted that only small proteins (with a molecular weight below approx. 30 kDa) can freely diffuse through the central channel of the nuclear pore complex (NPC), whereas larger proteins depend on a nuclear localization signal (NLS) for nuclear import (Beck and Hurt, 2016). Indeed, Tin2, Tin3, and See1 are relatively small proteins, having an expected molecular weight of 23.3 kDa, 30.4 kDa, and 17.7 kDa, respectively. These molecules thus may diffuse into nuclei after uptake by the plant cell. In contrast, the fusion protein HA_3-Ten1, which was detected in plant nuclei by immunogold labeling, has a calculated molecular weight of 75.5 kDa (without the predicted signal peptide). This makes it unlikely that Ten1 is imported in the nucleus by diffusion. A prediction of subcellular protein localization via WoLF PSORT (Horton *et al.*, 2005) suggests a nuclear localization of Ten1. Moreover, Ten1 contains six tandem arginine residues at the very C-terminus (Fig. 29), which are predicted to serve as an NLS by three different prediction programs: NucPred, NLSpred, and NLStradamus (Brameier *et al.*, 2007; Cokol *et al.*, 2000; Nair *et al.*, 2003; Nguyen Ba *et al.*, 2009). Fusions of an HA-tag or mCherry to the C-terminus of Ten1 resulted in non-functional fusion proteins, indicating that a free C-terminus is essential for the virulence function of Ten1. It would be interesting to investigate whether a mutated

Ten1 protein lacking these C-terminal arginines is able to complement the virulence defect of SG200Δ10A. Furthermore, to corroborate that these residues serve as an NLS, the mutated protein could be tested for plant uptake and nuclear localization via immuno-EM.

3.6. Type 2C protein phosphatases (PP2Cs) in plants

Reversible phosphorylation, mediated by protein kinases and protein phosphatases, is an essential posttranslational modification of proteins and represents a major mechanism of signal transduction (Kyriakis, 2014). Compared to all other organisms, plants possess the largest number of kinases, with *A. thaliana* expressing more than 1,000 kinase genes (Schweighofer *et al.*, 2004). In contrast to the large number of kinases, only about 150 protein phosphatases have been identified in *A. thaliana*. Therefore, phosphatases are often considered housekeeping enzymes with low specificity that balance the signaling system of the cell by counteracting protein kinases (Schweighofer and Meskiene, 2015). Nevertheless, phosphatases can exhibit a high specificity in substrate recognition and they can play important roles in different signaling pathways of the plant. These involve plant growth, metabolism, cell differentiation, light and hormonal signaling, and stress regulation (Schweighofer and Meskiene, 2015). Phosphatases can be classified according to the target residues they dephosphorylate: serine/threonine-specific phosphatases, tyrosine-specific phosphatases, and aspartic acid-specific phosphatases (Kerk *et al.*, 2007). The majority of plant phosphatases belong to the serine/threonine-specific group which is subdivided into phosphoprotein phosphatases (PPPs) and metal-dependent type 2C phosphatases (PP2Cs; Schweighofer and Meskiene, 2015). With 80 members PP2Cs represent the largest phosphatase family in *A. thaliana* (Fuchs *et al.*, 2013). These enzymes are Mn^{2+}/Mg^{2+}-dependent and resistant to known chemical inhibitors of phosphatase activity (Moorhead *et al.*, 2009). Moreover, unlike most members of the PPP family, PP2Cs lack regulatory subunits and are considered to be active as monomers (Schweighofer *et al.*, 2004). According to phylogenetic analyses, the PP2Cs of *A. thaliana* are classified into groups of related proteins (Kerk *et al.*, 2002; Schweighofer *et al.*, 2004). To some of these groups, functions in stress signaling and plant development are attributed.

A. thaliana PP2Cs from group A, such as ABI1 (Leung *et al.*, 1994), ABI2 (Leung, 1997), and HAB1 (Rodriguez *et al.*, 1998) are major regulators of abscisic acid (ABA) signaling and are by far the best-characterized PP2Cs in plants (Fuchs *et al.*, 2013). The plant hormone ABA is an endogenous messenger in biotic and abiotic stress responses, but is also required to regulate growth and development under non-stress conditions (Raghavendra *et al.*, 2010). Members of group B PP2Cs have been described as regulators of MAPK activity. The best-studied proteins of these so-called AP2Cs are AP2C1 and AP2C3, which are involved in the MAPK-dependent regulation of plant innate immunity and stomatal development, respectively (Schweighofer *et al.*, 2007; Umbrasaite *et al.*, 2010). Recently, AP2C1 was shown to act as a negative regulator of basal resistance and defense responses to *Pseudomonas syringae* by controlling MAPK activation (Shubchynskyy *et al.*, 2017). Group C of *A. thaliana* PP2Cs contain important regulators of plant development (Fuchs *et al.*, 2013). Among these, the phosphatases POL and PLL were characterized by several studies and described as regulators of stem cell identity (Song *et al.*, 2006, 2008). Phosphatases from group D are known to antagonize SAUR proteins (encoded by *SMALL AUXIN UP-RNA* genes), which control plant cell expansion by activating plasma membrane H^+-ATPase activity (Spartz *et al.*, 2014). Recently, another group D enzyme, PP2C38 was described as a negative regulator of the PRR-BIK complex, providing a fine-tuning of immune responses upon PAMP perception (Couto *et al.*, 2016). Group F harbors two phosphatases which are implicated in plant defense against *P. syringae*: WIN2 (Lee *et al.*, 2008) and PIA1 (Widjaja *et al.*, 2009).

According to the classification of phosphatases from *A. thaliana* (Kerk *et al.*, 2002) and rice (Singh *et al.*, 2010), Wei and Pan (2014) defined the maize phosphatome. This comprises a total of 104 PP2Cs which also branch into phylogenetically distinct groups of related proteins (Fig. 30). ZmPP26, the interactor of Ten1, is part of group F2 containing eight related proteins (Wei and Pan, 2014; Fig. 30).

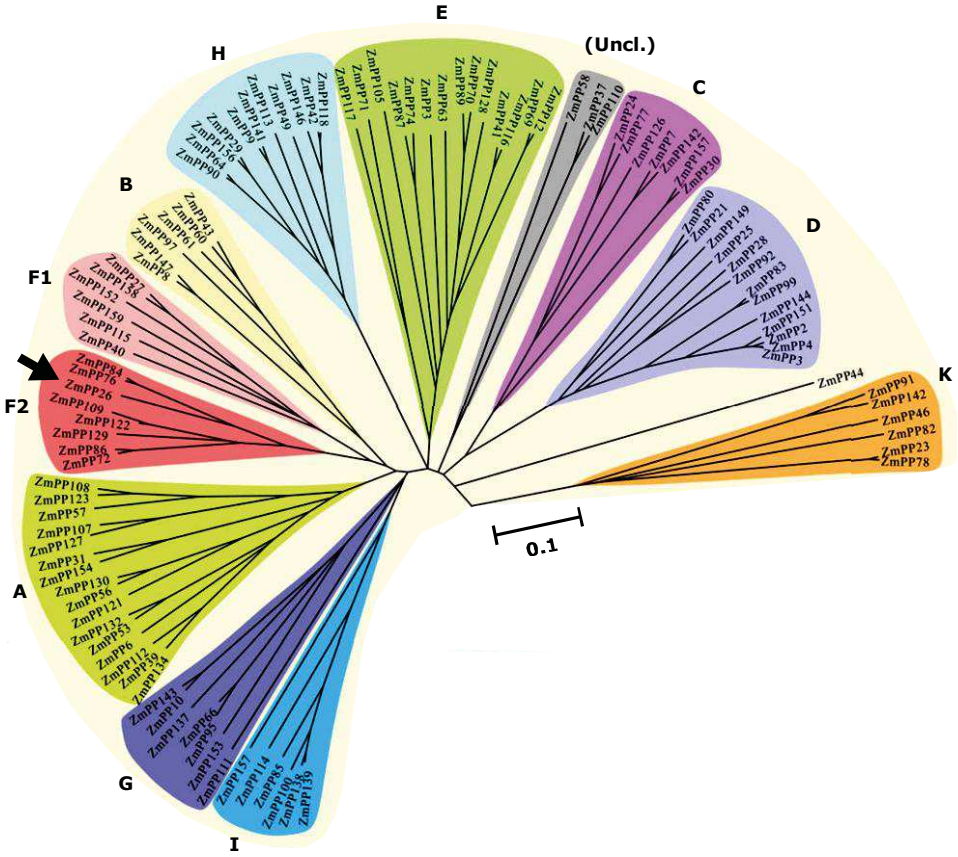

Fig. 30: Phylogenetic analysis of all 104 PP2Cs from maize. Un-rooted neighbor joining tree based on the catalytic domain sequences of all analyzed proteins. PP2Cs fall into 11 groups (A to K) with the exception of ZmPP44 and three other proteins with unknown classification (Uncl.). Arrow highlights the position of ZmPP26 within group F2. Scale bar represents 0.1 amino acid substitutions per site (modified from Wei and Pan, 2014).

3.7. The interaction of Ten1 and ZmPP26

3.7.1. How do Ten1 and ZmPP26 interact?

Yeast two-hybrid assays showed that any truncation of Ten1$_{133\text{-}327}$ abolishes interaction with ZmPP26. Furthermore, as many as 14 amino acid substitutions in this domain are necessary to eliminate the interaction of Ten1 and ZmPP26. These results indicate that binding of ZmPP26 is not mediated by specific residues, but rather that the entire interacting domain Ten1$_{133\text{-}327}$ functions as a binding surface for ZmPP26. Computational analyses of known protein-protein interactions revealed putative “hot spot” residues, which mainly contribute to binding at protein interfaces: the aromatic residues phenylalanine, tryptophan, and tyrosine, as well as arginine (Bogan and Thorn, 1998; Clackson and Wells, 1995; Moreira *et al.*, 2007; Watkins *et*

al., 2016). Whereas Ten1$_{133-327}$ does not display an increased frequency of phenylalanine, tryptophan, and arginine compared to the rest of the protein, 13 of the 19 tyrosines of Ten1 reside between position 133 and 327. Nevertheless, none of these presumed "hot spot" residues were affected by the 14 amino acid substitutions in Ten1m, which eliminated interaction. Beside crucial residues contributing to binding, a protein-protein interface is shaped by the secondary structure and physicochemical properties of all involved amino acids. This usually results in a high degree of geometric and chemical complementarity between the surfaces of two proteins (Yan *et al.*, 2008). This complementarity between Ten1 and ZmPP26 may disappear due to the amino acid substitutions in Ten1$_{133-327}$. Interestingly, in Western blot analyses, epitope-tagged Ten1m proteins were detected at a slightly lower molecular weight than epitope-tagged native Ten1 proteins (Fig. 20B; Fig. 22C). This could indicate that the introduced amino acid substitutions cause an altered protein conformation which is reflected by the migration behavior of Ten1m in SDS-PAGE. Indeed, the exchange even of single amino acids was reported to influence the mobility of several proteins in denaturing SDS gel electrophoresis (de Jong *et al.*, 1978; Panayotatos *et al.*, 1993; Rae and Elliott, 1986; Shi *et al.*, 2012). Alternatively, the altered mobility may be also explained by the estimated charge of Ten1m under SDS-PAGE conditions, which slightly decreases due to introduced amino acid substitutions (19.5 compared to 19.6 for the native Ten1 protein).

3.7.2. Does the interaction with Ten1 influence phosphatase activity of ZmPP26?

In the course of this study, the question was addressed whether and how the phosphatase activity of ZmPP26 is influenced by the interaction with Ten1. Since epitope-tagged Ten1 was most strongly detected after overexpression in *U. maydis*, overexpressed Ten1$_{132}$-HA$_3$ was enriched via anti-HA magnetic beads from the cytoplasm of SG200. After the elution of proteins from the beads via HA peptide, Ten1$_{132}$-HA$_3$ could be detected via anti-HA Western blot (not shown). However, as the amount of Ten1$_{132}$-HA$_3$ protein in the eluate could not be quantified, convincing *in vitro* phosphatase activity assays using both ZmPP26 and Ten1 could not be performed. In addition, it has to be considered that an assay involving cytoplasmically expressed Ten1 may not be conclusive as post-translational modifications could be essential for the functionality of Ten1. Future approaches for the purification of Ten1 could hence

include heterologous protein expression and secretion in *Pichia pastoris*. One possible effect of the interaction with Ten1 could be an inhibition of ZmPP26 phosphatase activity. In this case, the association with Ten1 might change the conformation of ZmPP26 or prevent the binding of the substrate to the catalytically active site of ZmPP26. However, Ten1 may as well stabilize ZmPP26 or prevent its inhibition by an upstream regulatory protein.

3.7.3. To what extent is the interaction with ZmPP26 biologically relevant?

Ten1m$_{132}$-HA$_3$ did not allow complementation of the SG200Δ10A virulence defect, indicating that the interaction of Ten1 and ZmPP26 may be biologically relevant for *U. maydis*. However, it remains to be shown that the absence of complementation actually resulted from the non-interaction of Ten1m and ZmPP26. Although Ten1m$_{132}$-HA$_3$ was detected via Western blot analysis in infected leaf material, secretion by the fungus was not experimentally shown. Moreover, the introduced amino acid substitutions in the interacting domain may negatively influence the translocation of Ten1m$_{132}$-HA$_3$ to plant cells. In order to address these issues, immuno-EM using leaves infected with SG200Δ10A-ten1m$_{132}$-HA$_3$ could be performed to test for the secretion and translocation of Ten1m$_{132}$-HA$_3$ protein. Furthermore, it is possible that in the *U. maydis*-maize pathosystem Ten1$_{132}$-HA$_3$ does not interact with ZmPP26 in the first place: in infected leaf material the interaction with ZmPP26 could be shown by mass spectrometry only after IP of HA$_3$-Ten1, but not after IP of Ten1$_{132}$-HA$_3$. Analogously, the non-interaction of Ten1m$_{132}$-HA$_3$ and ZmPP26 was not experimentally shown in infected leaves. In future studies, it will be necessary to demonstrate via mass spectrometry that HA-tagged Ten1m protein does not interact with ZmPP26 after IP from *U. maydis*-infected leaf material. For this to work, it may be necessary to move the mutated interacting domain into HA$_3$-Ten1.

3.7.4. What may be the biological function of the interaction during biotrophic development of *U. maydis*?

In the following, a possible biological function of ZmPP26 will be discussed, based on what is known from related PP2Cs from maize, wheat, and *A. thaliana*. Subsequently, a putative model will be proposed which describes the effector function of Ten1.

The only characterized member of maize group F2 PP2Cs is ZmPP76, the closest paralog of ZmPP26 (Fig. 30). *A. thaliana* plants overexpressing *ZmPP76* (in the publication designated as *ZmPP2C*) show ABA insensitivity and a downregulation of ABA-dependent genes, suggesting that ZmPP76 acts as a negative regulator of ABA signaling (Liu *et al.*, 2009). The ZmPP26 ortholog from wheat is TaPP2C1. This group F2 PP2C displays 89.2% amino acid identity with ZmPP26 and was described by Hu *et al.* (2015). Tobacco plants overexpressing *TaPP2C1* show ABA insensitivity and a downregulation of ABA-dependent genes. TaPP2C1 is thus also proposed to be a negative regulator of ABA signaling. The interaction of Ten1 with WIN2, the *A. thaliana* ortholog of ZmPP26, was demonstrated via yeast two-hybrid assays. In *A. thaliana*, this group F PP2C was shown to be involved in the stress response upon infection with the *P. syringae* strain *Pto*DC3000 (Lee *et al.*, 2008). The overexpression of *WIN2* in *A. thaliana* results in an enhanced resistance to *Pto*DC3000, accompanied by a slightly elevated free SA level in the plants. WIN2 is thus proposed to regulate pathogen-induced defense responses of *A. thaliana* by affecting the accumulation of SA. However, Lee *et al.* (2008) could not demonstrate how WIN2 is involved in SA signaling. It is widely accepted that ABA and SA-dependent defense responses antagonize each other (Denancé *et al.*, 2013; Mauch-Mani and Mauch, 2005; Moeder *et al.*, 2010; Robert-Seilaniantz *et al.*, 2011; Ton *et al.*, 2009). Yasuda *et al.* (2008) showed that the SA-induced systemic acquired resistance (SAR) of *A. thaliana* against *P. syringae* strain *Pto*DC3000 can be perturbed by the exogenous application of ABA. Conversely, the activation of SAR suppresses the expression of ABA biosynthesis and ABA-responsive genes. In light of these data, it is possible that WIN2 also acts as a negative regulator of ABA in *A. thaliana*. Accordingly, *WIN2* overexpression plants would actually show a downregulation of ABA signaling upon *P. syringae* infection. The slight accumulation of SA detected in these plants may thus be explained by antagonistic effects of SA and ABA.

In *A. thaliana*, the mechanism of ABA signaling by group A PP2Cs is well-understood. In the absence of ABA, these phosphatases repress hormonal signaling by dephosphorylation of SNF1-related kinases 2 (SnRK2s). The autophosphorylation of SnRK2s is required for kinase activity towards downstream targets. In the presence of ABA, a stable complex formed by ABA and PYR/PYL/RCAR receptor proteins binds to the active site of PP2Cs. By this, repression of SnRK2s is relieved and downstream transcription factors are activated, resulting

in the expression of ABA-responsive genes (Sheard and Zheng, 2009). Structural analyses revealed a gate-latch-lock mechanism by which the ABA-bound PYL2 receptor binds the group A PP2C HAB1 (Melcher *et al.*, 2009). This study further showed that a conserved tryptophan of HAB1 (W385; Fig. 31) docks into a cavity of PYL2, thereby locking the receptor for the inhibition of the PP2C active site. Later, the same tryptophan of HAB1 was shown to insert into the kinase catalytic cleft of SnRK2.6. This finding suggests a mechanism that directly couples the binding of ABA to SnRK2 kinase activation by a molecular mimicry of the PYL2-HAB1 interaction (Soon *et al.*, 2012; West *et al.*, 2013). Recently, Han *et al.* (2017) showed that residues adjacent to the key tryptophan residue are important for the binding of group A PP2Cs to ABA receptors. Accordingly, a conserved VxGΦL motif is able to modulate the binding affinity of PP2Cs to PYR/PYL/RCAR receptors, whereas "x" indicates any residue and "Φ" indicates a hydrophobic residue.

To investigate whether ZmPP26, ZmPP76, TaPP2C1, and WIN2 may share the described structural features with group A PP2Cs, a multiple amino acid sequence alignment with the *A. thaliana* PP2Cs HAB1 (Rodriguez *et al.*, 1998), ABI1 (Leung *et al.*, 1994), and ABI2 (Leung, 1997) was performed. Furthermore, ZmPP28 was included in the analysis, which is a group D PP2C distantly related to ZmPP26 (Fig. 30; Wei and Pan, 2014). In ZmPP26 and its homologs, the alignment revealed the presence of two tryptophan residues, which may be functionally conserved to mediate the binding of ABA receptors and SnRK2 kinases (Fig. 31). Moreover, the conserved VxGΦL motif is present in all analyzed PP2Cs, except for ZmPP28 (Fig. 31). These results indicate, that PP2Cs from group F or F2 may be also involved in ABA signaling.

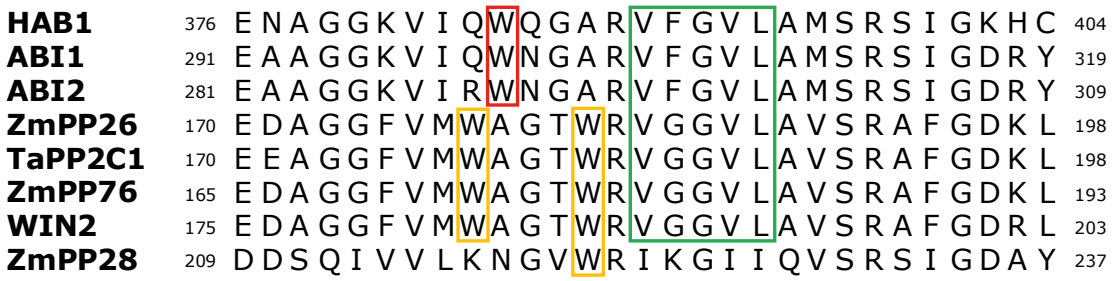

Fig. 31: Multiple sequence alignment (Clustal W) of ZmPP26, ZmPP76, ZmPP28, TaPP2C1, WIN2, and group A PP2Cs from *A. thaliana*. Red box indicates conserved tryptophan residues necessary for the binding of ABA receptors and SnRK2 kinases. Orange boxes indicate possibly conserved key tryptophan residues. Green box indicates VxGΦL motif modulating the binding affinity of PP2Cs to ABA receptors. Numbers indicate amino acid positions of the full-length proteins.

Assuming that ZmPP26 acts as a negative regulator of ABA signaling in maize, the protein may bind to and dephosphorylate SnRK2 kinases, which are located in the nucleus (Yoshida *et al.*, 2014b; Fig. 32A).

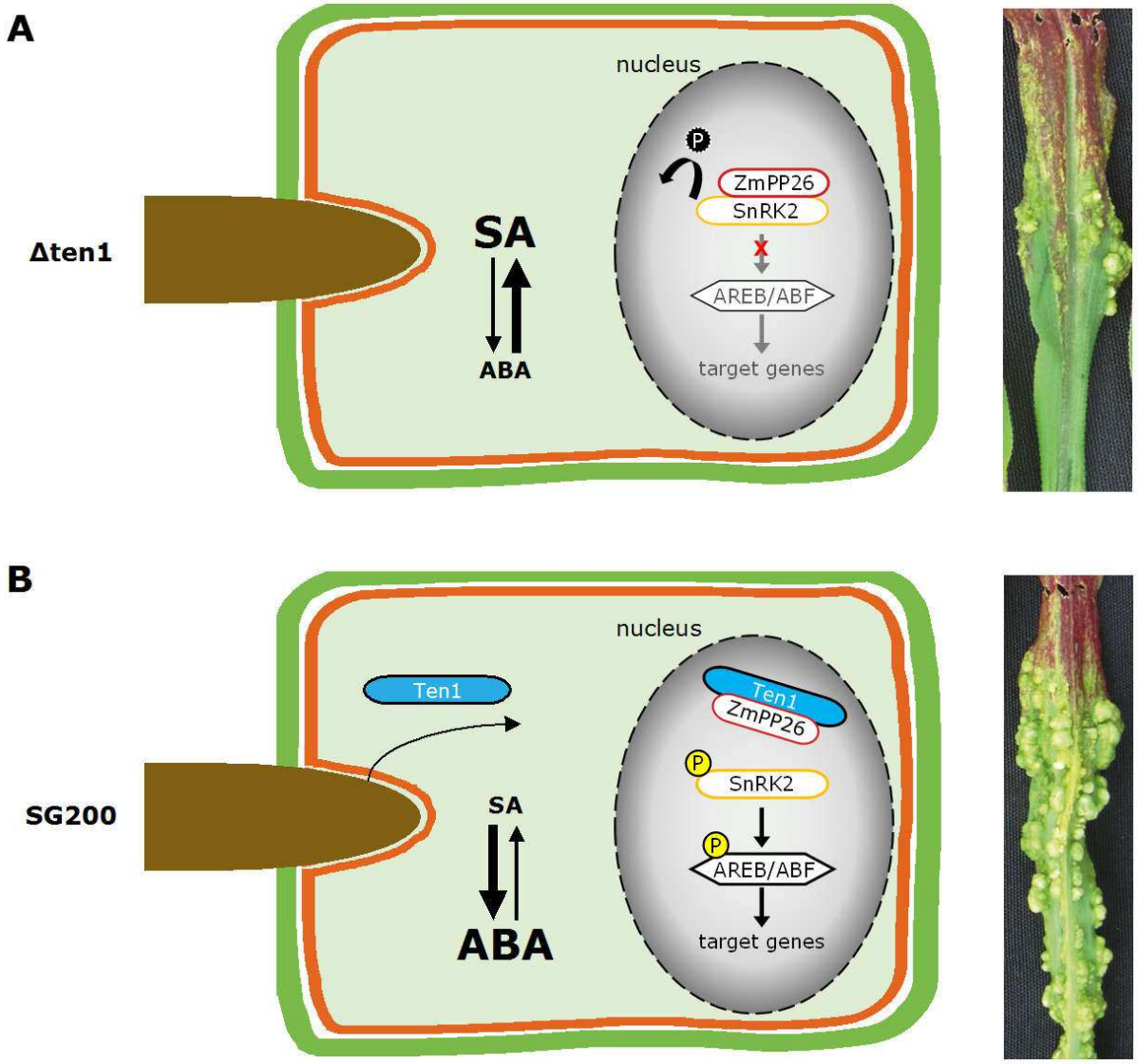

Fig. 32: Hypothetic model of the Ten1 effector function. (A) In the absence of Ten1, ZmPP26 binds to and dephosphorylates nuclear-localized SnRK2 kinases, resulting in a suppression of the downstream ABA signaling pathway. Due to antagonistic effects of SA and ABA, elevated cellular SA levels enhance SA-induced defense responses resulting in an adverse environment for SG200Δten1. **(B)** In SG200, secreted Ten1 is targeted to the plant nucleus where it binds ZmPP26. This results in a release of SnRK2 kinases from PP2C-dependent regulation. Following autophosphorylation of SnRK2, AREB/ABF transcription factors are activated, triggering the expression of ABA target genes. Due to antagonistic effects of SA and ABA, an enhanced accumulation of cellular ABA decreases SA-induced defense responses resulting in an advantageous environment for *U. maydis*. Green and orange structures depict the plant cell wall and the plant plasma membrane, respectively.

It is generally accepted that effective plant defense responses against biotrophic pathogens are SA-dependent (Glazebrook, 2005). The induction of *ZmPP26* four days after *U. maydis* infection (Fig. 12), may thus result in a downregulation of ABA signaling and, due to antagonistic effects, in an enhanced SA response (Fig. 32A). This time point of SA induction would be in accordance with the detected upregulation of *PR1* at 4 dpi, which is one of the prime marker genes of maize SA signaling (Doehlemann *et al.*, 2008). Moreover, RNAseq analyses of FB1 and FB2 strains during biotrophic development revealed an induction of the *U. maydis* gene *shy1* also at 4 dpi (D. Lanver, personal communication). *shy1* encodes for a salicylate hydroxylase which is needed for the degradation of SA (Rabe *et al.*, 2013).

Bruce *et al.* (2011) reported that maize seedling infections with the compatible wild type *U. maydis* strains 518 and 521 result in an accumulation of ABA in infected leaves and stems by the time of tumor appearance. Later, Morrison *et al.* (2015) could demonstrate that ABA accumulates also in cobs infected with either SG200 or with mixtures of FB1 and FB2 strains. These results suggest that the accumulation of ABA in the plant is linked to the pathogenic development of *U. maydis*. Moreover, Morrison *et al.* (2015) speculate that elevated ABA levels are needed to suppress host defenses, possibly by affecting the phytohormone crosstalk. In a hypothetic model for Ten1 effector function (Fig. 32B), secreted Ten1 protein is targeted to the nucleus of the maize cell where it binds to ZmPP26. This interaction results in a derepression of SnRK2 kinases and by this in an activation of ABA target gene expression, governed by AREB/ABF transcription factors (Yoshida *et al.*, 2014b). An enhanced ABA response may counteract plant SA signaling, resulting in a suppression of SA-mediated defense responses.

3.7.5. Perspectives

The proposed model for the function of Ten1 suggests that *U. maydis* may manipulate plant defense responses by exploiting antagonistic effects of SA and ABA signaling. Based on this hypothesis, future experiments should address the question whether SnRK2 kinases indeed serve as substrate for ZmPP26. In addition, structural comparative analyses of Ten1 and PYR/PYL/RCAR receptor proteins may elucidate whether Ten1 acts as a competitive inhibitor of PP2C activity by mimicking an ABA receptor. Furthermore, it has to be pointed out that the

interaction of Ten1 and ZmPP26 in infected maize leaf material was determined using SG200Δ10A-HA_3-ten1, a strain which does not express the other nine putative effector proteins of cluster 10A. It is possible that these proteins target additional host molecules, which may be also involved in the regulation of the plant hormonal balance.

4. Materials and methods

4.1. Materials and suppliers

4.1.1. Chemicals

Unless otherwise specified, all chemicals used in this study were obtained from BD (Heidelberg), Merck (Darmstadt), Roth (Karlsruhe), Sigma-Aldrich (Munich), Fluka (Buchs, Switzerland), Roche (Mannheim), and Clontech/Takara (Saint-Germain-en-Laye, France).

4.1.2. Enzymes and antibodies

All restriction enzymes and corresponding buffers were purchased from New England Biolabs (NEB, Frankfurt/Main). The following DNA polymerases were used: Phusion High-Fidelity DNA Polymerase and Taq DNA Polymerase (both from Thermo Scientific, Schwerte), KOD Xtreme Hot Start DNA Polymerase (Merck, Darmstadt), MyTaq Red Mix (Bioline, Luckenwalde). Ligation of DNA was performed with T4 DNA ligase (Thermo Scientific, Schwerte). Enzymatic degradation of RNA was carried out by RNase A (Serva, Heidelberg). For the enzymatic degradation of fungal cell walls, Novozym 234 (Novo Nordisk, Copenhagen, Denmark) was used. Antibodies were purchased from Sigma-Aldrich (Munich), Cell Signaling Technology (Danvers, USA), Qiagen (Hilden), Merck (Darmstadt), Roche (Mannheim), and BioVision (Milpitas, USA). A detailed list of used antibodies is given in Table 6. Dephosphorylation of DNA phosphomonoesters was carried out using Antarctic Phosphatase (NEB, Frankfurt/Main). For the cleavage of GST fusion proteins PreScission Protease (GE Healthcare, Munich) was used.

4.1.3. Buffers and solutions

Standard buffers and solutions were prepared according to Ausubel *et al.* (2002) and Sambrook *et al.* (1989). Special buffers and solutions are listed with the corresponding methods. When necessary, buffers, solutions and media were autoclaved for 5 min at 121°C before usage. Heat sensitive buffers and solutions were filter sterilized (pore size 0.2 µm; Whatman, Dassel or pore size 0.22 µm; Thermo Scientific, Schwerte).

4.1.4. Commercial kits

For the purification of linearized plasmids, PCR products and DNA fragments from agarose gels, the Wizard SV Gel and PCR Clean-Up System (Promega, Mannheim) was used. The isolation of plasmid DNA from bacteria and yeast was carried out with the QIAprep Spin Miniprep Kit and the isolation of RNA from plant material was

done with the RNeasy Plant Mini Kit (both kits from Qiagen, Hilden). For the assembly of multiple DNA fragments the Gibson Assembly Cloning Kit (NEB, Frankfurt/Main) was used. The *in vitro* measurement of protein phosphatase activity was carried out with the Serine/Threonine Phosphatase Assay System (Promega, Mannheim). For synthesis of complementary DNA (cDNA) from RNA the SuperScript III First-Strand Synthesis SuperMix (Thermo Scientific, Schwerte) was used. Removal of contaminating DNA from RNA preparations was carried out by the TURBO DNA-*free* Kit (Thermo Scientific, Schwerte).

4.2. Cell culture

4.2.1. Cultivation of *U. maydis*

Liquid *U. maydis* cultures were grown at 28°C and 200 rpm mainly in $YEPS_{light}$ medium in baffled flasks. For the cultivation on solid medium, potato dextrose (PD) agar plates (supplemented with 4 µg/mL carboxin or 400 µg/mL hygromycin as selective antibiotics when it was necessary) were used and incubated at 28°C. To test for filamentous growth on plate, cell suspensions were dropped on PD-charcoal agar and incubated at room temperature for 24 h. Hyphal growth of the modified strain AB33 (Brachmann *et al.*, 2001) in axenic culture was induced in liquid nitrate minimal medium with glucose (NM-glc). The permanent preservation of strains was realized by adding 50% NSY-glycerol to a densely grown overnight culture and by storing at -80°C.

$YEPS_{light}$ (modified from Tsukuda *et al.*, 1988)	1% (w/v) Yeast extract 1% (w/v) Peptone 1% (w/v) Sucrose In ddH_2O
PD agar	2.4% (w/v) Potato dextrose broth 2% (w/v) Bacto agar In ddH_2O [PD-charcoal agar: 1% (w/v) charcoal (Sigma C-9157)]
NM-glc (modified from Banks *et al.*, 1993)	0.3% (w/v) Potassium nitrate 6.25% (v/v) Salt solution (Holliday, 1974) 2% (v/v) Glucose In ddH_2O
NSY-glycerol	0.8% (w/v) Nutrient broth 0.1% (w/v) Yeast extract 0.5% (w/v) Sucrose 69.6% (v/v) Glycerol In ddH_2O

4.2.2. Cultivation of *S. cerevisiae*

Liquid *S. cerevisiae* cultures were grown at 28°C and 200 rpm in YEPD or SD medium. For the cultivation on solid medium, YEPD and SD agar plates were incubated at 30°C. The permanent preservation of strains was realized by adding 50% NSY-glycerol to a densely grown overnight culture and by storing at -80°C.

YEPD	1% (w/v) Yeast extract
	2% (w/v) Peptone
	In ddH_2O
	[Solid medium: 2% (w/v) bacto agar]
SD	0.67% (w/v) Yeast nitrogen base w/o amino acids
	2% (v/v) Glucose
	In ddH_2O
	[Solid medium: 2% (w/v) bacto agar]

SD medium for nutritional selection contained 0.16% Dropout Supplement -Ade/-His/-Leu/ -Trp and, where needed, individually added amino acids. Stock solutions of adenine, histidine, leucine, and tryptophan were prepared according to the Yeast Protocols Handbook PT3024-1, version no. PR742227 (Clontech/Takara, Saint-Germain-en-Laye, France).

4.2.3. Cultivation of *E. coli* and *A. tumefaciens*

E.coli cultures were grown at 200 rpm in liquid dYT medium or on dYT agar plates at 37°C. Where needed, the following selective antibiotics were added: ampicillin (100 µg/mL), kanamycin (40 µg/mL), and chloramphenicol (liquid medium 25 µg/mL, solid medium 170 µg/mL). *A. tumefaciens* cultures were grown at 200 rpm in liquid dYT medium or on dYT agar plates at 28°C. Where needed, the following selective antibiotics were added: kanamycin (50 µg/mL), rifampicin (100 µg/mL), and gentamicin (30 µg/mL). The permanent preservation of strains was realized by adding 25% (v/v) glycerol and by storing at -80°C.

dYT (Sambrook *et al.*, 1989)	1.6% (w/v) Tryptone
	1% (w/v) Yeast extract
	0.5% (w/v) Sodium chloride
	In ddH_2O
	[Solid medium: 2% (w/v) bacto agar]

4.2.4. Cell density measurement

The cell density of liquid cultures was determined in an Ultrospec 3000 *pro* photometer (GE Healthcare, Munich) at 600 nm (OD_{600}). To assure a linear dependency of the measured ODs, cultures were always appropriately diluted to values below 0.8. As blank the corresponding culture medium was used. For *S. cerevisiae* cultures an OD_{600} of 0.1 roughly corresponds to 1 x 10^6 cells/mL (Gietz and Schiestl, 2007), which was also assumed for *U. maydis* cultures.

4.3. Strains, plasmids, and oligonucleotides

4.3.1. *U. maydis* strains

In this chapter all used *U. maydis* strains are listed, including those created in the course of this study (Table 5). For the generation of deletion mutants the respective genes were replaced by hygromycin resistance gene cassettes as described by Brachmann *et al.* (2004) and Kämper (2004). For the integration of genes into the *ip* locus (gene *sdh2*) SspI-linearized plasmids carrying a carboxin resistance allele (ip^r; Broomfield and Hargreaves, 1992) were used. These plasmids were introduced into the genome via homologous recombination with the endogenous, carboxin sensitive *ip* allele (ip^s). All strains were verified by Southern analysis and, where needed, by PCR. The strains AB33-GFP-HA and AB33-ten1$_{132}$-HA$_3$ harbored a multiple copy insertion of the respective construct. All other strains with an *ip* locus integration harbored a single copy insertion. Plasmids used for the generation of strains are listed separately in chapter 4.3.5.

Table 5: *U. maydis* strains used in this study

Strain (running no.)	Genotype	Resistance(s)[1]	Reference
AB33	*a2 Pnar-bW2 Pnar-bE1, ble*	P	Brachmann *et al.* (2001)
AB33-GFP-HA (SR256)	*a2 Pnar-bW2 Pnar-bE1, ble* $ip^r[P_{otef}$*:egfp:HA:strep]*ip^s	P, C	S. Reissmann
FB1	*a1 b1*	-	Banuett and Herskowitz (1989)
FB2	*a2 b2*	-	Banuett and Herskowitz (1989)
SG200	*a1mfa2 bW2bE1, ble*	P	Kämper *et al.* (2006)
SG200AM1	*a1mfa2 bW2bE1, ble,* $ip^r[P_{UMAG\_01779}$*:(3xegfp)]*ip^s	P, C	Mendoza-Mendoza *et al.* (2009)
SG200Δ10A (#19)	*a1mfa2 bW2bE1, ble, UMAG_03744-UMAG_03753::hyg*	P, H	Kämper *et al.* (2006)
SG200-SP-mCherry-HA (ULL106)	*a1mfa2 bW2bE1, ble,* $ip^r[P_{UMAG\_05731}$*:*SP_{UMAG_05731}*:mCherry:Avitag:HA]*ip^s	P, C	L. Lo Presti

(Table 5, continued)

AB33-ten1$_{132}$-HA$_3$ (PE197)	*a2 Pnar-bW2 Pnar-bE1, ble ip^r[P$_{otef}$:UMAG_03744$_{132}$:(3xHA)]ip^s*	P, C	This study
FB1Δten1 (PE46)	*a1 b1, UMAG_03744::hyg*	H	This study
FB2Δten1 (PE50)	*a2 b2, UMAG_03744::hyg*	H	This study
SG200AM1Δten1 (PE52)	*a1mfa2 bW2bE1, ble, ip^r[P$_{UMAG_01779}$:(3xegfp)]ip^s, UMAG_03744::hyg*	P, C	This study
SG200Δ10A-HA$_3$-ten1 (PE145)	*a1mfa2 bW2bE1, ble, UMAG_03744-UMAG_03753::hyg, ip^r[P$_{UMAG_03744}$:(3xHA):UMAG_03744]ip^s*	P, H, C	This study
SG200Δ10A-HA-mCherry-ten1 (PE182)	*a1mfa2 bW2bE1, ble, UMAG_03744-UMAG_03753::hyg, ip^r[P$_{UMAG_03744}$:HA:mCherry]ip^s*	P, H, C	This study
SG200Δ10A-sr11226 (PE221)	*a1mfa2 bW2bE1, ble, UMAG_03744-UMAG_03753::hyg, ip^r[P$_{UMAG_03744}$:sr11226]ip^s*	P, H, C	This study
SG200Δ10A-ten1 (PE95)	*a1mfa2 bW2bE1, ble, UMAG_03744-UMAG_03753::hyg, ip^r[P$_{UMAG_03744}$:UMAG_03744]ip^s*	P, H, C	This study
SG200Δ10A-ten1$_{132}$-HA$_3$ (PE159)	*a1mfa2 bW2bE1, ble, UMAG_03744-UMAG_03753::hyg, ip^r[P$_{UMAG_03744}$:UMAG_03744$_{132}$:(3xHA)]ip^s*	P, H, C	This study
SG200Δ10A-ten1-HA (PE105)	*a1mfa2 bW2bE1, ble, UMAG_03744-UMAG_03753::hyg, ip^r[P$_{UMAG_03744}$:UMAG_03744:HA]ip^s*	P, H, C	This study
SG200Δ10A-ten1m$_{132}$-HA$_3$ (PE227)	*a1mfa2 bW2bE1, ble, UMAG_03744-UMAG_03753::hyg, ip^r[P$_{UMAG_03744}$:UMAG_03744m$_{132}$:(3xHA)]ip^s*	P, H, C	This study
SG200Δten1 (PE75)	*a1mfa2 bW2bE1, ble, UMAG_03744::hyg*	P, H	This study
SG200Δten1-ten1$_{132}$-HA$_3$ (PE234)	*a1mfa2 bW2bE1, ble, UMAG_03744::hyg, ip^r[P$_{UMAG_03744}$:UMAG_03744$_{132}$: (3xHA)]ip^s*	P, H, C	This study
SG200-ten1$_{(34-680)132}$-HA$_3$ (PE232)	*a1mfa2 bW2bE1, ble, ip^r[P$_{otef}$:UMAG_03744$_{(34-680)132}$:(3xHA)]ip^s*	P, C	This study

[1] Phleomycin (P), carboxin (C), hygromycin (H)

4.3.2. *S. cerevisiae* strains

For yeast two-hybrid analyses the strain AH109 was used [*MATa, trp1-901, leu2-3, ura3-52, his3-200, gal4Δ, gal80Δ, LYS2::GAL1$_{UAS}$-GAL1$_{TATA}$-HIS3, GAL2$_{UAS}$-GAL2$_{TATA}$-ADE2, URA3::MEL1$_{UAS}$-MEL1$_{TATA}$-lacZ*]. This strain harbors the *ADE2* and *HIS3* markers and is auxotrophic for adenine, histidine, leucine, tryptophan, and uracil (Clontech/Takara, Saint-Germain-en-Laye, France). All generated strains carry the name of the respective plasmid they harbor (see chapter 4.3.5.) and are therefore not listed separately here.

4.3.3. *E. coli* strains

For all cloning purposes and for the generation of plasmids the *E. coli* K12 derivative TOP10 (Invitrogen, Karlsruhe) was used [F-, *mcr*A, Δ(*mrr-hsd*RMS-*mcr*BC), Φ80*lac*ZΔM15, Δ*lac*X74, *deo*R, *rec*A1, *ara*D139,

Δ(*ara-leu*)7697, *gal*U, *gal*K, *rps*L(StrR), *end*A1, *nup*G]. For the heterologous expression of both ZmPP26 and ZmPP26$_{DGH65\text{-}67KLN}$ the strain BL21(DE3)pLysS (Merck, Darmstadt) was used [F–, *omp*T, *hsd*S_B(r_B^-, m_B^-), *gal*, *dcm*, λ(DE3), pLysS(Cam^R)].

4.3.4. *A. tumefaciens* strains

For the transient expression of proteins in *N. benthamiana*, the strain GV3101 (Koncz and Schell, 1986) was used [C58, (rif^R), Ti pMP90, (pTiC58DT-DNA), ($gent^R$/$strep^R$), Nopaline]. This strain is resistant to rifampicin and gentamicin and harbors the disarmed Ti plasmid pMP90 that contains the *vir* genes but not a functional T-DNA region. All generated strains carry the name of the respective plasmid they harbor (see chapter 4.3.5.) and are therefore not listed separately here.

4.3.5. Plasmids and oligonucleotides

In this chapter all used plasmids as well as the oligonucleotides necessary for their construction are listed. All plasmids were checked by restriction analyses and, where needed, by sequencing (carried out by Eurofins Genomics, Ebersberg). Unless otherwise denoted, all plasmids were generated in the course of this study. The running number of plasmids is given in parentheses. The plasmids pGBKT7, pEZRK, and all their derivatives conferred kanamycin resistance, all residual plasmids ampicillin resistance.

All oligonucleotides used in this study were purchased from and synthesized by Eurofins Genomics (Ebersberg). In the following, oligonucleotide sequences are always given from 5' to 3'. Restriction enzyme recognition sites are underlined; sequences serving as Gibson Assembly overhangs to other fragments are written in lowercase. Primers either hybridize with the sense strand (reverse, marked with [R]) or with the antisense strand (forward, marked with [F]) of the respective DNA template.

Plasmid for cloning of PCR products

pJET-Stuffer (K. O. Schink and M. Bölker, personal communication)
This plasmid is a derivative of pJET1.2 (Thermo Scientific, Schwerte) and was used as a linearized backbone for cloning of blunt-end DNA fragments. Re-circularized pJET1.2 normally expresses a lethal restriction enzyme (Eco47IR) after transformation of *E. coli*. This derivative harbors a 0.6 kb fragment in the ORF of *eco47IR* and can be thus amplified in *E. coli*. Prior to cloning of DNA, the 0.6 kb fragment can be cut out via EcoRV.

Plasmids for the generation of stable *U. maydis* mutants

p123 (Aichinger *et al.*, 2003)
Harbors *gfp* under the control of the constitutive *otef* promoter (Spellig *et al.*, 1996) and the *nos* terminator. It can be linearized via SspI and inserted into the *ip* locus of *U. maydis*. This plasmid was used as starting plasmid for the cloning of all complementation constructs.

p123-Potef-mCherry-HA (pLL49 from L. Lo Presti, personal communication)
Harbors *mCherry* with a C-terminal HA-tag under the control of the *otef* promoter and the *nos* terminator. This plasmid was used both as template for the amplification of *mCherry* and as backbone for mCherry constructs (plasmid pLL49 from L. Lo Presti).

p123-Potef-ten1$_{132}$-HA$_3$ (p84)
The *otef* promoter sequence and the first 96 nucleotides of the coding sequence of *ten1* were amplified from p123-Potef-ten1-HA-JW by s6/s182. The resulting 1.1 kb fragment contained an overhang to NdeI/PvuII-cut p123-Pten1-ten1 at its 5' end. The coding sequence for ten1$_{132}$-HA$_3$ was amplified from p123-Pten1-ten1$_{132}$-HA$_3$ by s181/s253. The resulting 0.5 kb fragment contained overhangs to NdeI/PvuII-cut p123-Pten1-ten1 at its 3' end as well as to the PCR product [s6/s182] at the 5' end. The two fragments were combined with NdeI/PvuII-cut p123-Pten1-ten1 by Gibson Assembly. This plasmid was used for overexpression of *ten1* in axenic culture for secretion analyses.

s6 [R] caacaaacaacaagagtagcag
s182 [F] cagattgtactgagagtgcacc
s181 [R] acggtagaccgcttctgcag
s253 [F] acctttctgctactcttgttgtttg

p123-Potef-ten1$_{(34-680)132}$-HA$_3$ (p111)
The coding sequence of *ten1* without the predicted secretion signal sequence was amplified from p123-Potef-ten1$_{132}$-HA$_3$ by s42/s302. The resulting 1 kb fragment contained overhangs to BstBI/NcoI-cut p123-Potef-ten1$_{132}$-HA$_3$. The two fragments were combined by Gibson Assembly. This plasmid was used for overexpression of *ten1* in axenic culture for an enrichment of the protein for the phosphatase activity assay.

s42 [R] ATCTTCCACTGCTGATCGGC
s302 [F] cccccgggctgcaggaattcgatccATGGCTGAAGGCGAAGCAGATTCC

p123-Potef-ten1-HA-JW (no. 221 from J. Wu, personal communication)
Harbors *ten1* with a C-terminal HA-tag sequence under the control of the constitutive *otef* promoter and the *nos* terminator. This plasmid was used as template for the amplification of the coding sequence of *ten1* together with the *otef* promoter sequence (plasmid no. 227 from J. Wu).

p123-Pten1-HA-mCherry-ten1 (p80)
The promoter sequence of *ten1* and the first 99 nucleotides of its coding sequence (predicted signal peptide sequence) were amplified from p123-Pten1-ten1 by s183/s182. The resulting 1.1 kb fragment contained overhangs to NdeI/PvuII-cut p123-Pten1-ten1 as well as to the 5' end of a HA$_3$ fragment. A 0.3 kb fragment of the coding sequence of *ten1* was amplified from p123-Pten1-ten1 by s181/s180, containing an overhang to NdeI/PvuII-cut p123-Pten1-ten1. The coding sequence of *mCherry*

was amplified from pEZRK-mCherry-ZmPP26 by s240/s239. The resulting 0.7 kb fragment contained an HA-tag at the 5' end and a $(G)_4$-S linker at the 3' end as well as overhangs to the PCR products [s183/s182] and [s181/s180], respectively. The three fragments were combined with NdeI/PvuII-cut p123-Pten1-ten1 by Gibson Assembly. Following SspI linearization, this complementation construct was inserted into the *ip* locus of *U. maydis*. This plasmid was used for complementation of Δ10A and *in planta* localization studies of Ten1.

s183 [R] ggggtaGCAAAAAACAGACGAGCTGGC
s182 [F] cagattgtactgagagtgcacc
s181 [R] acggtagaccgcttctgcag
s180 [F] GCTGAAGGCGAAGCAGATTCC
s240 [R] gaatctgcttcgccttcagcGGATCCTCCGCCACCTCTAG
s239 [F] ccagctcgtctgttttttgcTACCCCTACGATGTTCCAGATTACGCTGGAGCGGTGAGCAAGGGCGAGGAG

p123-Pten1-HA_3-ten1 (p55)
The promoter sequence of *ten1* and the first 99 nucleotides of its coding sequence (predicted signal peptide sequence) were amplified from p123-Pten1-ten1 by s183/s182. The resulting 1.1 kb fragment contained overhangs to NdeI/PvuII-cut p123-Pten1-ten1 as well as to the 5' end of a HA_3 fragment. A 0.3 kb fragment of the coding sequence of *ten1* was amplified from p123-Pten1-ten1 by s181/s180, containing an overhang to NdeI/PvuII-cut p123-Pten1-ten1. The HA_3 fragment was synthesized as an Ultramer Oligonucleotide (IDT, Coralville, USA) and contained 3 successive HA-tag sequences each separated by a single glycine as linker, a $(G)_4$-S linker at the very 3' end, and overhangs to the PCR products [s183/s182] and [s181/s180], respectively. The three fragments were combined with NdeI/PvuII-cut p123-Pten1-ten1 by Gibson Assembly. This plasmid was used for complementation of SG200Δ10A.

s183 [R] ggggtaGCAAAAAACAGACGAGCTGGC
s182 [F] cagattgtactgagagtgcacc
s181 [R] acggtagaccgcttctgcag
s180 [F] GCTGAAGGCGAAGCAGATTCC
HA_3 cgtctgtttttgcTACCCCTACGATGTTCCAGATTACGCTGGCTATCCCTATGACGTCCCGGACTATGCAGGAT
ATCCATATGACGTTCCAGATTACGCTGGTGGCGGAGGATCCgctgaaggcgaagcagattc

p123-Pten1-mCherry-HA (p8)
The promoter sequence (0.9 kb of the 5' UTR) of *ten1* was amplified from p123-Pten1-ten1-JW by s10/s8 and cloned into p123-Potef-mCherry-HA via KpnI and XmaI. This plasmid was used for localization of mCherry *in planta* to analyze *ten1* promoter activity after infection.

s10 [R] CGCCCCGGGGTCGTGTCTTTTAGTACAAC
s8 [F] CGGGGTACCTCATGCAAGGCCGGTACTTG

p123-Pten1-sr11226 (p37)
The 0.3 kb *nos* terminator sequence was amplified from p123-Potef-mCherry-HA by s84/s104, creating overhangs to XbaI/EcoRV-cut p123-Pten1-sr11226-HA. The two fragments were combined by Gibson Assembly. This plasmid was used for complementation of SG200Δ10A.

s84 [R] gggagaccggcagatctgatCTCATGTTTGACAGCTTATCATCGG
s104 [F] gcaccgtcgtcatcgtctgtGACCGGCTGCAGATCGTTCAAAC

p123-Pten1-sr11226-HA (p28)

The coding sequence of *sr11226* was amplified from *S. reilianum* f. sp. *zeae* genomic DNA by s13/s12 and cloned into p123-Pten1-mCherry-HA via NheI and XbaI. This plasmid was used for complementation of SG200Δ10A.

s13 [R] ACGTCTAGACAGACGATGACGACGGTG
s12 [F] CTAGCTAGCATGAATCCGTTTCGCGCT

p123-Pten1-ten1 (p34)

The promoter sequence and the ORF of *ten1* were amplified from p123-Pten1-ten1-mCherry-HA by s89/s81, resulting in a 3 kb fragment with overhangs to EcoRV/PvuII-cut p123 as well as to the 5' end of the *nos* terminator sequence. The 0.3 kb *nos* terminator sequence was amplified from p123-Potef-mCherry-HA by s84/s90, creating overhangs to the 3' end of *ten1* as well as to EcoRV/PvuII-cut p123. The two fragments were combined with EcoRV/PvuII-cut p123-Potef-mchery-HA by Gibson Assembly. This plasmid was used for complementation of SG200Δ10A.

s89 [R] tttgaacgatctgcagccggTCAACGACGACGACGACGACG
s81 [F] acactatagaactcgagcagTCATGCAAGGCCGGTAC
s84 [R] gggagaccggcagatctgatCTCATGTTTGACAGCTTATCATCGG
s90 [F] gtcgtcgtcgtcgtcgTGACCGGCTGCAGATCGTTCAAAC

p123-Pten1-ten1$_{132}$-HA$_3$ (p65)

The promoter sequence of *ten1* and the first 396 nucleotides of its coding sequence were amplified from p123-Pten1-ten1 by s190/s182. The resulting 1.5 kb fragment contained overhangs to NdeI/PvuII-cut p123-Pten1-ten1 as well as to the 5' end of a HA$_3$ fragment. The latter was amplified from p123-Pten1-HA$_3$-ten1 by s192/s191 and contained overhangs to NdeI/PvuII-cut p123-Pten1-ten1 as well as to the PCR product [s190/s182]. The two fragments were combined with NdeI/PvuII-cut p123-Pten1-ten1 by Gibson Assembly. This plasmid was used for complementation of SG200Δ10A.

s190 [R] ggggtaGCCACTCGGCGAAGGC
s182 [F] cagattgtactgagagtgcacc
s192 [R] gcttctgcagctgctatttcgtcgctgctcgagctatgaccactAGCGTAATCTGGAACGTCATATGG
s191 [F] ccttcgccgagtggcTACCCCTACGATGTTCCAGATTACG

p123-Pten1-ten1-HA (p38)

The promoter sequence of *ten1* and its ORF were amplified from p123-Pten1-ten1-mCherry-HA by s105/s81. The resulting 3 kb fragment contained an HA-tag at its 3' end and overhangs to EcoRV/PvuII-cut p123-Potef-mCherry-HA as well as to the 5' end of the *nos* terminator sequence. The 0.3 kb *nos* terminator sequence was amplified from p123-Potef-mCherry-HA by s84/s106, creating overhangs to the 3' end of *ten1* (including HA-tag) as well as to EcoRV/PvuII-cut p123-Potef-mCherry-HA. The two fragments were combined with EcoRV/PvuII-cut p123-Potef-mCherry-HA by Gibson Assembly. This plasmid was used for complementation of SG200Δ10A.

s105 [R] ggcatagtccgggacatcatacgggtaACGACGACGACGACGACG
s81 [F] acactatagaactcgagcagTCATGCAAGGCCGGTAC
s84 [R] gggagaccggcagatctgatCTCATGTTTGACAGCTTATCATCGG
s106 [F] atgatgtcccggactatgccTGAccggctgcagatcgttcaaac

p123-Pten1-ten1-JW (no. 165 from J. Wu, personal communication)
Harbors *ten1* under the control of the native promoter and the *nos* terminator. This plasmid was used as template for the amplification of the coding sequence of *ten1* together with its native promoter sequence (plasmid no. 165 from J. Wu).

p123-Pten1-ten1m$_{132}$-HA$_3$ (p110)
The coding sequence that included the mutated part of Ten1 (residues 133-327 harboring 14 amino acid substitutions) was amplified from plasmid pGBKT7-ten1#67 by s42/s301 and cloned into p123-Pten1-ten1$_{132}$-HA$_3$ via BstBI and PvuII. pGBKT7-ten1#67 was previously generated by random mutagenesis via error-prone PCR. This plasmid was used for complementation of SG200Δ10A.

s42	[R]	ATCTTCCACTGCTGATCGGC
s301	[F]	TCGAGCAGCGACGAAATAGCA

p123-Pten1-ten1-mCherry-HA (p9)
The promoter sequence and the ORF of *ten1* were amplified from p123-Pten1-ten1-JW by s11/s8 and cloned into p123-Potef-mCherry-HA via KpnI and XmaI. This plasmid was used for complementation of Δ10A and *in planta* localization studies of Ten1.

s11	[R]	TTCCCGGGACGACGACGACGACGACG
s8	[F]	CGGGGTACCTCATGCAAGGCCGGTACTTG

pJETΔten1-hyg (p27)
One kb of the 3' flanking sequence of *ten1* was amplified from *U. maydis* genomic DNA by the primers s58 and s57, resulting in a fragment suitable for Gibson Assembly with overhangs of complementary nucleotides to EcoRV-cut pJET-Stuffer as well as to the 5' end of the hygromycin resistance cassette. This 2.7 kb cassette was cut out from pMF1-h by SfiI. One kb of the 5' flanking sequence of *ten1* was amplified by s60/s59, containing overhangs to the 3' end of the hygromycin resistance cassette as well as to EcoRV-cut pJET-Stuffer. The three fragments were combined with EcoRV-cut pJET-Stuffer by Gibson Assembly. The deletion construct was cut out via SspI from the pJET-Stuffer backbone and used for *U. maydis* transformation.

s58	[R]	ttgtcacgccatggtggccaTCTAGGCCGTCGTGTCTTTTAGTACAACCG
s57	[F]	ctcgagtttttcagcaagatAATATTTCATGCAAGGCCGGTAC
s60	[R]	aggagatcttctagaaagatAATATTTGCCACTACTACCACAGCC
s59	[F]	gccgcattaataggcctgagTGGCCGACTGCTTGTATTAGAAACGCTG

pJET-Pten1-ten1$_{132}$-Avitag-HA-hyg (pLL265 from L. Lo Presti, personal communication)
Harbors *ten1* with an Avitag-HA-tag after residue 132 of Ten1 under the control of the *ten1* promoter and the *nos* terminator.

pMF1-h (Brachmann *et al.*, 2004)
Harbors a 2.7 kb hygromycin resistance cassette flanked by SfiI restriction sites. The *hph* gene is expressed under the control of the *hsp70* promoter and the *nos* terminator. This plasmid was used as template for the amplification of the hygromycin resistance cassette for gene deletion constructs.

Plasmids for yeast two-hybrid analyses

pGBKT7 (Clontech/Takara, Saint-Germain-en-Laye, France)

This plasmid allows the constitutive expression of proteins fused to the GAL4 DNA binding domain (BD) via the *ADH1* promoter in yeast. Transcription is terminated by the T7 and *ADH1* terminator sequences. Moreover, pGBKT7 contains a multiple cloning site, the T7 promoter and a c-Myc epitope tag. In *E. coli* and *S. cerevisiae* the plasmid replicates autonomously from the pUC and 2µ ori, respectively. It carries a kanamycin resistance gene for selection in *E. coli* as well as a *TRP1* nutritional marker for selection in yeast. This plasmid was used as starting plasmid for the cloning of all bait constructs for yeast two-hybrid analyses.

pGBKT7-sr11226$_{37\text{-}1138}$ (p36)

The coding sequence of *sr11226* without the predicted secretion signal sequence (first 108 nucleotides) was amplified from p123-Pten1-sr11226-HA by s88/s87. The resulting 3.4 kb fragment contained overhangs to SmaI-cut pGBKT7. Both fragments were combined by Gibson Assembly.

s88 [R] ctgcaggtcgacggatccccTCACAGACGATGACGACGGTG
s87 [F] gccatggaggccgaattcccTATGCTGGAACCTGTCTCGCGGAT

pGBKT7-ten1$_{34\text{-}680}$ (p7)

The coding sequence of *ten1* without the predicted secretion signal sequence was amplified from *U. maydis* genomic DNA by s2/s5 and cloned into pGBKT7 via NotI and NdeI.

s2 [R] ATAAGAATGCGGCCGCTCAACGACGACGACGACGACGCAT
s5 [F] GGAATTCCATATGGCTGAAGGCGAAGCAGATTC

pGBKT7 plasmids for the expression of truncated Ten1 proteins

Truncated sequences of *ten1* were amplified from p123-Pten1-ten1 with the primers listed below. All PCR products contained overhangs to SmaI-cut pGBKT7 with which they were combined by Gibson Assembly.

ten1$_{133\text{-}680}$ (1,667 bp)	(p60)	s194	[R]	ctgcaggtcgacggatccccTCAACGACGACGACGACGAC
		s193	[F]	gccatggaggccgaattcccTAGTGGTCATAGCTCGAGCAGC
ten1$_{328\text{-}680}$ (1,082 bp)	(p61)	s194	[R]	ctgcaggtcgacggatccccTCAACGACGACGACGACGAC
		s195	[F]	gccatggaggccgaattcccTCCGTTGCCGCCGCG
ten1$_{133\text{-}327}$ (585 bp)	(p67)	s200	[R]	ctgcaggtcgacggatccccTCACTCCGTAGGATCCAGATCAGCC
		s193	[F]	gccatggaggccgaattcccTAGTGGTCATAGCTCGAGCAGC
ten1$_{133\text{-}170}$ (158 bp)	(p72)	s219	[R]	ctgcaggtcgacggatccccTCACGCAGGAGATTTGACATCATCCATG
		s193	[F]	gccatggaggccgaattcccTAGTGGTCATAGCTCGAGCAGC
ten1$_{133\text{-}256}$ (375 bp)	(p86)	s254	[R]	ctgcaggtcgacggatccccTCAAGCGGCCGGGTCCG
		s193	[F]	gccatggaggccgaattcccTAGTGGTCATAGCTCGAGCAGC
ten1$_{171\text{-}256}$ (261 bp)	(p88)	s254	[R]	ctgcaggtcgacggatccccTCAAGCGGCCGGGTCCG
		s220	[F]	gccatggaggccgaattcccTCTTTCAACATTTGAAGTCGGCGAG
ten1$_{257\text{-}327}$ (216 bp)	(p87)	s200	[R]	ctgcaggtcgacggatccccTCACTCCGTAGGATCCAGATCAGCC
		s255	[F]	gccatggaggccgaattcccTCCTGGTGGCTATCGAGTGTATC
ten1$_{279\text{-}327}$ (180 bp)	(p74)	s200	[R]	ctgcaggtcgacggatccccTCACTCCGTAGGATCCAGATCAGCC
		s222	[F]	gccatggaggccgaattcccTCCATACAACCAACGATTTCTCTATCG

pGBKT7-ten1m$_{34-680}$ (p107)
The coding sequence that included the mutated part of Ten1 (residues 133-327 harboring 14 amino acid substitutions) was excised from plasmid pGBKT7-ten1#67 and cloned into pGBKT7 via BamHI and PspXI. pGBKT7-ten1#67 was previously generated by random mutagenesis via error-prone PCR.

pGADT7 (Clontech/Takara, Saint-Germain-en-Laye, France)
This plasmid allows the constitutive expression of proteins fused to the GAL4 activation domain (AD) via the *ADH1* promoter and its terminator sequence in yeast. The GAL4 AD fusion contains an N-terminal SV40 nuclear localization signal and an HA-tag located between the AD and the protein of interest. In *E. coli* and *S. cerevisiae* the plasmid replicates autonomously from the pUC and 2µ ori, respectively. It carries an ampicillin resistance gene for selection in *E. coli* as well as a *LEU2* nutritional marker for selection in yeast. This plasmid was used as starting plasmid for the cloning of all prey constructs for yeast two-hybrid analyses.

pGADT7-PVA12 (p23)
The coding sequence of *PVA12* was amplified from pAD-GAL4-2.1-PVA12 by s52/51 and cloned into pGADT7 via XmaI and NdeI. Plasmid pAD-GAL4-2.1-PVA12 was isolated from yeast cells that showed protein interaction of Ten1 and PVA12 in yeast two-hybrid analysis.

s52 [R] TTCCCGGGTCATCTCTTCATGAGGAA
s51 [F] GGAATTCCATATGAGCACCGAGTCAGGA

pGADT7-VAP27-2 (p24)
The coding sequence of *VAP27-2* was amplified from pAD-GAL4-2.1-VAP27-2 by s54/53 and cloned into pGADT7 via XmaI and NdeI. Plasmid pAD-GAL4-2.1-VAP27-2 was isolated from yeast cells that showed protein interaction of Ten1 and VAP27-2 in yeast two-hybrid analysis.

s54 [R] TTCCCGGGTCATAGGTGTAGAAGGTA
s53 [F] GGAATTCCATATGGGCAGCGAGGACATG

pGADT7-WIN2 (p43)
The coding sequence of *WIN2* was amplified from *A. thaliana* cDNA by s110/109. The resulting 936 bp fragment contained overhangs to SmaI-cut pGADT7. Both fragments were combined by Gibson Assembly.

s110 [R] tcccgtatcgatgcccacccCTAGGTTGATGAGTCACCGGAG
s109 [F] gaggccagtgaattccacccTATGGGATATCTGAATTCTGTTTTGTCATC

pGADT7-ZmPP26 (p25)
The coding sequence of *ZmPP26* was amplified from pAD-GAL4-2.1-ZmPP26 by s56/55 and cloned into pGADT7 via XmaI and ClaI. Plasmid pAD-GAL4-2.1-ZmPP26 (p19) was isolated from yeast cells that showed protein interaction of Ten1 and ZmPP26 in yeast two-hybrid analysis.

s56 [R] TAGTATCGATTTAAGCGTATCCGCTGCT
s55 [F] TCCCGGGTATGGGGTACTTGAGCT

pGADT7-ZmPP76 (p44)
The coding sequence of *ZmPP76* was amplified from maize cDNA by s132/131. The resulting 873 bp fragment contained overhangs to SmaI-cut pGADT7. Both fragments were combined by Gibson Assembly.

s132 [R] tcccgtatcgatgcccacccCTAGGAGTGTTGGTCGTTGGTG
s131 [F] gaggccagtgaattccacccTATGGGGCTCGCCGGG

pGADT7-ZmPP84 (p45)
The coding sequence of *ZmPP84* was amplified from maize cDNA by s134/133. The resulting 768 bp fragment contained overhangs to SmaI-cut pGADT7. Both fragments were combined by Gibson Assembly.

s134 [R] TcccgtatcgatgcccacccTTAGGAGTTTTGGTCATTGGTGG
s133 [F] gaggccagtgaattccacccTATGGAGGACTTCTATGAGGCAAG

Plasmids for gene expression in *N. benthamiana*

pEZRK-LCY (D. Lanver, pers. communication; courtesy of D. Ehrhardt, Stanford, USA)
This binary vector allows the *A. tumefaciens*-mediated constitutive expression of proteins under the control of the cauliflower mosaic virus (CaMV) 35S promoter and the octopine synthase (*ocs*) terminator. Moreover it contains a multiple cloning site, the pBR322 origin of replication, and a kanamycin resistance gene for cloning in *E. coli*. This plasmid was used as starting plasmid for the cloning of all transient protein expression constructs.

pEZRK-HA$_3$-ten1$_{34\text{-}680}$ (p77)
The coding sequence of *ten1* without the predicted secretion signal sequence but with a HA$_3$ tag at the 5' end was amplified from p123-Pten1-HA$_3$-ten1 by s233/s232 and cloned into pEZRK-LCY via KpnI and XmaI.

s233 [R] TCCCGGGTCAACGACGACGACGACG
s232 [F] TTGGTACCATGTACCCCTACGATGTTCCAGATTACG

pEZRK-ZmPP26-His$_6$ (p79)
The coding sequence of *ZmPP26* was amplified from pGADT7-ZmPP26 by s234/s70 and cloned into pEZRK-LCY via KpnI and XmaI.

s234 [R] TCCCGGGTTAATGGTGATGGTGATGGTGACCTCCGCCAGCGTATCCGCTGCTACCTTG
s70 [F] TTGGTACCATGGGGTACTTGAGCTCCGTG

Plasmids for gene expression in *E. coli*

pRSET-GST-PP (A. Müller, personal communication; Schreiner *et al.*, 2008)
This derivative of pRSET (Thermo Scientific, Schwerte) harbors a glutathione S-transferase (GST) tag with a downstream PreScission Protease cleavage site.

pRSET-GST-PP-ZmPP26 (p53)

The coding sequence of *ZmPP26* was amplified from pGADT7-ZmPP26 by s169/s168. The resulting 0.9 kb fragment contained overhangs to PvuII-cut pRSET-GST-PP. Both fragments were combined by Gibson Assembly.

s169 [R] ttcgaattccatggtaccagTTAAGCGTATCCGCTGCTACC
s168 [F] tccgagctcgagatctgcagTATGGGGTACTTGAGCTCCGTG

pRSET-GST-PP-ZmPP26$_{DGH65-67KLN}$ (p76)

The coding sequence of mutated *ZmPP26* was amplified from pGADT7-ZmPP26$_{DGH65-67KLN}$ by s229/s228. The resulting 0.7 kb fragment contained overhangs to NcoI-cut pRSET-GST-PP-ZmPP26. Both fragments were combined by Gibson Assembly.

s229 [R] atcaagcttcgaattccatgTTAAGCGTATCCGCTGCTACCTT
s228 [F] cctggtaaaagggcatccatgg

Oligonucleotides used for sequencing

In the following, all additional sequencing primers are listed which were not already mentioned above.

s4	TTTCTCTATCGACTCAAGGATCTG
s7	AAAGCCGTAACGTCAACTTC
s26	CGCGTTTGGAATCACTAC
s33	GCAGGGCTAGATGAGCAGAC
s34	CGCTGTCTTCTGTTCCCATT
s40	TGAGACAGGCAATGAGGCTG
s41	ACGTGAACCTGACCCAGTTC
s48	CTATAGATCAGAGGTTACATGG
s61	AGGAGATCTTCTAGAAAGATAA
	TATTTGCCACTACTACCACAGCC
s63	GGAAGGCAACCCAGCATCAC
s64	TGTAGCACACGACTCACATC
s91	TGCTATTTCGTCGCTGCTCG
s92	TTAGCACCACCATGACCATC
s94	AATTAGCTTGGCTGCAAGCG
s188	ACTTGCTGTTTCGCGTGCTT
s189	CCACATCCCACAGCCCATCA
s292	CACTCCGTCTTTGCTTTGTTGGT
Gal4 AD (Eurofins)	TACCACTACAATGGATG
Gal4 BD (Eurofins)	TCATCGGAAGAGAGTAG
M13 rev -29 (Eurofins)	CAGGAAACAGCTATGACC
pESC_MCS1u (Eurofins)	TGACCAAACCTCTGGCGAAG
T7 (Eurofins)	TAATACGACTCACTATAGGG
T7 term (Eurofins)	CTAGTTATTGCTCAGCGGT

Oligonucleotides used for qPCR

For the amplification of *tenI*	s42	[R]	ATCTTCCACTGCTGATCGGC
	s37	[F]	TCGGATGGAGATGGAAGGGT
For the amplification of *ppi*	s45	[R]	ACATCGTCAAGGCTATCG
	s44	[F]	AAAGAACACCGGACTTGG

4.4. Methods of microbiology

4.4.1. Transformation of *U. maydis*

U. maydis was transformed according to a protocol modified from (Schulz *et al.*, 1990) and (Gillissen *et al.*, 1992). A 50 mL $YEPS_{light}$ culture was grown to an OD_{600} of 1.0. The cells were harvested in a 50 mL Falcon tube (3,500 rpm, 5 min, room temperature) and washed in 25 mL SCS solution. For protoplastation, the cells were resuspended in 2 mL Novozym solution (2.5 mg/mL Novozym 234 in SCS, filter sterilized). Protoplastation was checked microscopically after 4 to 5 min and 20 mL SCS was carefully added as soon as about 50% of the cells showed protoplastation. The protoplasts were pelleted (2,300 rpm, 10 min, 4°C) and washed by slowly pipetting as follows: 1X with 20 mL SCS, 1X with 10 mL SCS, 1X with 20 mL STC solution. Eventually the protoplasts were resuspended in 0.5 mL ice cold STC, aliquoted in 70 µL per tube and stored at -80°C.

SCS solution	1 M Sorbitol 20 mM Sodium acetate In ddH_2O, final pH adjusted to 5.9
STC solution	1 M Sorbitol 100 mM Calcium chloride ($CaCl_2 \cdot 2H_2O$) 10 mM Tris-HCl with pH 7.5 In ddH_2O

Prior to transformation of protoplasts, double agar plates were prepared: 12 mL bottom regeneration agar light ($Reg\text{-}Agar_{light}$) containing 2-fold concentrated antibiotic (carboxin or hygromycin) were overlaid with 12 mL top $Reg\text{-}Agar_{light}$ without antibiotic. One aliquot of protoplasts was incubated with linearized DNA (up to 5 µg) and 1 µL of a heparin solution (10 mg/mL) for 15 min on ice. After adding 0.5 mL ice cold STC/PEG solution, the protoplasts were incubated again for 15 min on ice and subsequently spread on the double agar plate. After incubation for 3 to 5 days at 28°C, colonies were picked with pipette tips and single-colony purified on PD plates containing antibiotic. Putative transformants were verified by Southern analysis.

STC/PEG solution	40% PEG4000 In STC solution
$Reg\text{-}Agar_{light}$	1 M Sorbitol 1% (w/v) Yeast extract 0.4% (w/v) Bacto peptone 0.4% (w/v) Sucrose 1.5% (w/v) Bacto agar In ddH_2O

4.4.2. *U. maydis* infection of maize

To assess virulence of *U. maydis* strains, cultures were grown overnight in $YEPS_{light}$ to an OD_{600} of about 0.8 to 1.0. The cells were harvested in 50 mL Falcon tubes (3,500 rpm, 5 min, room temperature), resuspended in ddH_2O and adjusted to an OD_{600} of 1.0. Seven-days-old maize seedlings were syringe-inoculated with each at least 1 mL of *U. maydis* cell suspension at about 1 cm above the stem base, providing that the tip of the needle was directed towards the center of the leaf whirl. Compatible strains were mixed at a 1:1 ratio prior to inoculation of 10-days-old seedlings in this case. Four plants per pot were grown in a greenhouse with a daylight temperature of 28°C and a night temperature of 20°C. Light intensity during the daylight phase was at least 28,000 lux (up to 90,000 lux in bright sunshine). Relative humidity was maintained constant between 40% and 60%. For all plant infections done in this study the maize variety Early Golden Bantam (UrbanFarmers, New York City, USA) was used.

The symptoms of *U. maydis* infection were checked 12 days post-inoculation (dpi) and classified into disease categories as described by Kämper *et al.* (2006). Per strain to be tested at least 2 independent infections with each 25 to 40 plants were done. The overall disease ratings were expressed in relation to the total number of infected plants.

4.4.3. *In vitro* induction of *U. maydis* filaments and appressoria

For the induction of *b*-filaments *in vitro*, AB33 strains were grown in $YEPS_{light}$ to an OD_{600} of 1.0. The cells were harvested in 50 mL Falcon tubes (3,500 rpm, 5 min, room temperature) and washed twice with ddH_2O. Eventually the cells were resuspended in NM-glc medium, transferred to flasks and incubated at 28°C. Filamentous growth was usually observed after approx. 6 to 8 h of incubation.

In vitro appressoria formation was induced according to a protocol modified from (Mendoza-Mendoza *et al.*, 2009). SG200AM strains were grown in $YEPS_{light}$ to an OD_{600} of 0.8. Cells were harvested in 2 mL microcentrifuge tubes (3,500 rpm, 5 min, room temperature) and resuspended in 2% $YEPS_{light}$ (in ddH_2O) to yield an OD_{600} of 0.1. To the cell suspension 100 µM 16-hydroxyhexadecanoic acid was added (HFA, Sigma-Aldrich, Munich). A 10 mM stock solution of HFA was prepared with 100% ethanol. Via a micro sprayer (ECOSPRAY, BLUESTAR FORENSIC, Monaco, France) the cell suspension was sprayed on Parafilm M (Bemis, Neenah, USA) which was attached to a microscope slide. The latter was transferred to a petri dish containing moist tissue paper and eventually the petri dish was sealed with Parafilm M and incubated at 28°C for 16 h. In preparation for the microscopic analysis sporidia not attached to the artificial hydrophobic surface were washed off with water.

4.4.4. Transformation of *S. cerevisiae*

Competent yeast cells were prepared and transformed according to a protocol modified from (Knop *et al.*, 1999). Cells were grown in 50 mL YEPD (or where needed, in SD for nutritional selection) to an OD_{600} of 0.6, harvested in a 50 mL Falcon tube (2,000 rpm, 3 min, room temperature) and washed 1X with 15 mL ddH_2O and 1X with 10 mL SORB. Eventually the cells were resuspended in 360 µL SORB, aliquoted in 50 µL per 1.5 mL microcentrifuge tube and stored at -80°C.

SORB	100 mM Lithium acetate
	10 mM Tris-HCl with pH 8.0
	1 mM EDTA
	1 M Sorbitol
	In ddH_2O, final pH adjusted to 8.0

One aliquot of competent cells was supplemented with up to 4 µg plasmid DNA (*e.g.* 10 µL), a 6-fold volume of PEG (*e.g.* 360 µL) and mixed by inversion and flicking. The cells were incubated for 30 min at 30°C and subsequently heat shocked at 42°C for 15 min. After harvesting (2,000 rpm, 3 min, room temperature), the cells were washed once with 1 mL YEPD and then incubated for 3 h to 4 h at 30°C in 1 mL fresh YEPD. During the incubation the samples were constantly mixed by flicking every 30 min. A serial dilution (0, 10^{-1}, 10^{-2}, 10^{-3}) of the culture was prepared and 100 µL of each sample was spread on SD plates for nutritional selection. After incubation for 3 to 4 days at 30°C, colonies were picked with pipette tips and single-colony purified on fresh SD plates.

4.4.5. Yeast two-hybrid analyses

For the identification of plant interactors a cDNA library was screened, that was generated from *U. maydis*-infected leaf material using the phagemid vector pAD-GAL4-2.1 (Farfsing, 2004). The screen was carried out according to a protocol modified from the Matchmaker GAL4 Two-Hybrid System 3 & Libraries User Manual PT3247-1, version no. PR742219 (Clontech/Takara, Saint-Germain-en-Laye, France). A sequential transformation was done where yeast strain AH109 was at first transformed with the bait plasmid pGBKT7-ten1$_{34\text{-}680}$. After confirming expression of the bait fusion protein by anti-Myc Western blot analysis, competent cells of positive transformants were generated (see chapter 4.4.4) and 500 µg plasmid DNA of the cDNA library was introduced via a library-scale transformation. Such co-transformed cells were spread both on low stringency SD medium (-Leu/-Trp) to determine the transformation efficiency, and on high stringency SD medium (-Ade/-His/-Leu/-Trp) to detect protein-protein interaction. A transformation efficiency of about 3.72 x 10^4 cfu/µg DNA was determined. Colonies indicating interaction were picked with pipette tips and single-colony purified on SD plates (-Leu/-Trp). Single colonies were grown for 48 h in 4 mL SD medium (-Leu/-Trp) at 28°C for subsequent plasmid preparation (see chapter 4.5.2). To increase the concentration of plasmid DNA, the isolated plasmids from yeast were further introduced into TOP10 *E. coli* for plasmid preparation and subsequent sequencing of prey

plasmids. For the preparation of yeast drop plates, strains were grown overnight at 28°C in SD (-Leu/ -Trp) and adjusted to an OD_{600} of 0.3 in 10 mL SD (-Leu/-Trp) the next day. In order to obtain mid-log phase, cultures were then grown for 5 h at 30°C to a final OD_{600} of approx. 0.5 (as described in Yeast Protocols Handbook, p. 10). Serial dilutions (0, 10^{-1}, 10^{-2}, 10^{-3}) of the cultures with a volume of 200 µL, respectively, were prepared in PCR tubes and 4 µL of each sample was dropped on low stringency and on high stringency SD plates. The residual volume of each culture was centrifuged in a 15 mL Falcon tube (3,000 rpm, 2 min, room temperature) and the cells were subjected to protein extraction for expression analysis via Western (see chapter 4.6.1). After 4 days of incubation at 30°C colony growth on drop plates was assessed.

4.4.6. Transformation of *E. coli*

Chemically competent *E. coli* cells were prepared and transformed according to a protocol modified from (Cohen *et al.*, 1972). TOP10 *E. coli* cells were grown overnight in 20 mL dYT at 37°C. Two mL of the culture was transferred to 100 mL fresh dYT supplemented with $MgCl_2$ and $MgSO_4$ to a final concentration of 10 mM, respectively. Cells were then grown for 2.5 h to an OD_{600} of about 0.6 and cooled on ice for 30 min. After harvesting the cells in a 250 mL centrifuge bottle (Sorvall SLA-3000 rotor, 3,000 rpm, 8 min, 4°C) the pellet was resuspended in 33 mL ice cold RF1 solution by pipetting. The suspension was incubated on ice for 30 min and the cells were again harvested. The cells were resuspended in 5 mL ice cold RF2 solution and transferred to a 50 mL Falcon tube. After incubation on ice for 1 h, 50 µL aliquots were prepared in pre-cooled 1.5 mL microcentrifuge tubes, frozen in liquid nitrogen and stored at -80°C.

RF1 solution	100 mM Rubidium chloride
	50 mM Manganese chloride ($MnCl_2 \cdot 4H_2O$)
	30 mM Potassium acetate
	10 mM Calcium chloride ($CaCl_2 \cdot 2H_2O$)
	15% (w/v) Glycerol
	In ddH_2O, final pH adjusted to 5.8
RF2 solution	10 mM MOPS
	10 mM Rubidium chloride
	75 mM Calcium chloride ($CaCl_2 \cdot 2H_2O$)
	15% (w/v) Glycerol
	In ddH_2O, final pH adjusted to 5.8

One aliquot of competent cells was thawed on ice for 2 min and 1 µL to 5 µL DNA (plasmid DNA or ligation product) was added. After incubation on ice for 30 min, the cells were heat shocked at 42°C for 1 min and then immediately cooled on ice for at least 2 min. For the recovery of the cells, dYT (without antibiotics) was added to a total volume of 1 mL and the sample was incubated at 37°C and 500 rpm for 1 h. The cells were harvested (5,000 rpm, 5 min, room temperature) and the supernatant was discarded by pouring. The cells were resuspended

in the residual medium of the tube and spread on a dYT agar plate containing selective antibiotic. After incubation overnight at 37°C, single colonies were picked from the plate with pipette tips for subsequent analyses.

4.4.7. Transformation of *A. tumefaciens*

Freeze/thaw-competent *A. tumefaciens* cells were prepared and transformed according to a protocol modified from (Wise *et al.*, 2006). GV3101 *A. tumefaciens* cells were grown at 28°C in 50 mL dYT medium containing rifampicin (100 µg/mL) and gentamicin (30 µg/mL) to an OD_{600} of 0.5 to 0.7. After incubation on ice for 30 min, the cells were harvested in a 50 mL Falcon tube (8,000 rpm, 5 min, 4°C) and resuspended in 1 mL ice cold 20 mM $CaCl_2$. With this suspension, aliquots of 100 µL were prepared in pre-cooled 1.5 mL microcentrifuge tubes, frozen in liquid nitrogen and stored at -80°C.

For transformation, 1 µg DNA (*e.g.* 4 µL of a plasmid miniprep) was added to one aliquot of frozen competent cells. After thawing the cells at 37°C for 5 min, the tube was plunged for 5 s into liquid nitrogen and subsequently re-thawed at room temperature. For the recovery of the cells, dYT (without antibiotics) was added to a total volume of 1 mL and the sample was incubated at 28°C and 500 rpm for 2 h. The cells were harvested (5,000 rpm, 5 min, room temperature) and the supernatant was discarded by pouring. The cells were resuspended in the residual medium of the tube and spread on a dYT agar plate containing selective antibiotic. After incubation at 28°C for 48 h, colonies were picked with pipette tips and single-colony purified on fresh dYT plates for subsequent analyses.

4.4.8. *A. tumefaciens*-mediated transformation of *N. benthamiana*

The transient transformation of *N. benthamiana* plants via syringe infiltration was done according to a protocol modified from (Hotson *et al.*, 2003). *A. tumefaciens* strains were grown overnight at 28°C in 5 mL dYT containing selective antibiotics. The OD_{600} of this high density culture was determined and the volume needed for a new culture with an OD_{600} of 0.6 in a total volume of 5 mL was transferred to a 5 mL Eppendorf Tube. The cells were centrifuged (3,000 rpm, 5 min, room temperature) and washed with 2 mL agro induction medium. After harvesting the cells again, they were resuspended in 5 mL agro induction medium and incubated at room temperature for 2 h prior to plant infiltration.

Agro induction medium	10 mM MES (from 0.1 M MES solution with pH 5.6)
	10 mM $MgCl_2$
	150 µM Acetosyringone
	In ddH_2O

Leaves of 5-6 weeks old *N. benthamiana* plantlets were infiltrated with *A. tumefaciens* suspension at the abaxial side using a needleless 1 mL syringe. Depending on the experimental design either single spots on the leaf were

infiltrated or the whole leaf area was treated by repeated infiltrations. Typically no more than 2 leaves per plant were infiltrated. Leaves were harvested 3 days post-infiltration for all downstream analyses. *N. benthamiana* plantlets were grown in a plant growth chamber (Percival AR-95LX, purchased from CLF PlantClimatics, Wertingen) with a daylight temperature of 24°C and a night temperature of 20°C. Light intensity during the daylight phase (16 h) was 270 µmol m^{-2} s^{-1} (at a distance of about 183 cm from the lamps). Relative humidity was maintained constant between 40% and 60%.

4.5. Methods of molecular biology

4.5.1. *In vitro* modification of nucleic acids

Standard methods such as electrophoresis, purification, and precipitation of nucleic acids or molecular cloning techniques were performed as described in Ausubel *et al.* (2002) and Sambrook *et al.* (1989). Photometric measurements to determine the concentration of nucleic acids were done with a NanoDrop 2000 spectrophotometer (Thermo Scientific, Schwerte).

Restriction of DNA

The restriction of DNA was carried out by type II restriction endonucleases at enzyme specific temperatures for 2 h to 16 h. In cases where more than one enzyme was used, reactions were incubated for at least 3 h to 4 h. A typical restriction reaction with a total volume of 20 µL is described below.

0.5 µg to 5µg	DNA
2 µL	Enzyme specific NEB buffer 1-4/CutSmart buffer (10X)
2 µL	BSA (10X, needed for some enzymes)
0.5 U	Restriction endonuclease
X µL	ddH_2O

Dephosphorylation of linear DNA fragments

To prevent self-ligation of linearized fragments with compatible cohesive or blunt ends, phosphate groups were removed from the 5' end by Antarctic Phosphatase. Reactions were incubated at 37°C for 15 min and subsequently heat inactivated at 65°C for 5 min (or at conditions that inactivated the previously used restriction enzymes). In the following a typical dephosphorylation reaction with a total volume of 60 µL is described.

20 µL	Restriction reaction
6 µL	Antarctic Phosphatase Reaction Buffer (10X)
5 U	Antarctic Phosphatase
X µL	ddH_2O

Ligation of DNA fragments

For the ligation of a linearized vector and an insert with T4 DNA Ligase, the respective DNA was used in a molar ratio of 1:5. Reactions were incubated at room temperature for at least 2 h or at 16°C overnight. A typical ligation reaction with a total volume of 20 µL is described below.

X µL	Vector DNA
X µL	Insert DNA
2 µL	T4 DNA Ligase Reaction Buffer (10X)
1 U	T4 DNA Ligase
X µL	ddH_2O

Gibson Assembly™

The enzymatic assembly of multiple DNA fragments was carried out as described by (Gibson *et al.*, 2009). The Gibson Assembly Cloning Kit (NEB, Frankfurt/Main) was used following the manufacturer's protocol.

Polymerase chain reaction (PCR)

For the standard amplification of DNA fragments, PCR (Mullis *et al.*, 1986) was used. Depending on the experimental design, different polymerases were deployed. Fragments for cloning purposes were amplified via Phusion High-Fidelity DNA Polymerase or KOD Xtreme Hot Start DNA Polymerase (for long strand and GC-rich DNA templates). Typical PCR reactions for both polymerases with a total volume of 50 µL are described below.

40 ng (250 ng)	Plasmid DNA/cDNA (genomic DNA)	98°C – 30 s (3 min for genomic DNA)
0.5 µM	Forward primer	98°C – 10 s
0.5 µM	Reverse primer	60°C to 70°C – 30 s
200 µM	dNTPs (ratio 1:1:1:1)	72°C – 30 s per kb product
10 µL	Phusion HF Buffer (10X)	72°C – 10 min
0.5 U	Phusion High-Fidelity DNA Polymerase	10°C – hold
X µL	ddH_2O	Steps 2 to 4 performed for 30 cycles

40 ng (250 ng)	Plasmid DNA/cDNA (genomic DNA)	94°C – 2 min
0.3 µM	Forward primer	98°C – 10 s
0.3 µM	Reverse primer	58°C to 65°C – 30 s
400 µM	dNTPs (ratio 1:1:1:1)	68°C – 1 min per kb product
25 µL	Xtreme Buffer (2X)	10°C – hold
1 U	Xtreme Hot Start DNA Polymerase	Steps 2 to 4 performed for 40 cycles
X µL	ddH_2O	

For large-scale amplification of DNA (*e.g.* colony PCR) MyTaq Red Mix was used. A typical colony PCR reaction for both fungal and bacterial cells with a total volume of 15 µL is described below.

1 µL	Cell culture (or 1 colony picked from plate)	94°C – 2 min
0.5 µM	Forward primer	94°C – 30 s
0.5 µM	Reverse primer	52°C to 60°C – 30 s
7.5 µL	MyTaq Red Mix (2X)	72°C – 30 s per kb product
X µL	ddH_2O	72°C – 10 min
		10°C – hold
		Steps 2 to 4 performed for 30 cycles

For random mutagenesis of DNA, error-prone PCR was carried out using Taq DNA Polymerase (Thermo Scientific, Schwerte). A library of random mutations from one DNA template was generated according to (McCullum *et al.*, 2010).

All PCR reactions were performed in a TProfessional Standard Gradient Thermocycler (Biometra, Göttingen). Annealing and melting temperatures of oligonucleotides were calculated with PCR Primer Stats of the Sequence Manipulation Suite (Stothard, 2000).

4.5.2. Isolation of nucleic acids

Isolation of genomic DNA from *U. maydis*

U. maydis was grown overnight in 2.5 mL $YEPS_{light}$ and the cells were harvested in a 2 mL microcentrifuge tube (13,000 rpm, 1 min, room temperature) the next day. The pellet was stored at -20°C overnight or for at least 3 h. To the frozen pellet 500 µL TE-phenol/chloroform, 400 µL *Ustilago* lysis buffer and approx. 300 mg glass beads were added. The tube was vortexed on a Vibrax VXR basic (IKA, Staufen) at 1,600 rpm for 25 min. The homogenized sample was then centrifuged (13,000 rpm, 15 min, room temperature) and 400 µL of the aqueous phase was transferred to a fresh 1.5 mL microcentrifuge tube containing 1 mL 100% ethanol. The tubes were inverted 5 times and then centrifuged (13,000 rpm, 5 min, room temperature). The supernatant was discarded and the pellet was washed once with 1 mL 70% ethanol. After centrifugation again (13,000 rpm, 1 min, room temperature) residual ethanol was removed with a pipette. Eventually, the DNA pellet was resuspended in 80 µL TE buffer (containing 50 µg/mL RNase A) by incubating the tube at 50°C in a heating block with gentle shaking for 7 min. Genomic DNA was stored at -20°C.

Ustilago lysis buffer	2% (v/v) Triton X-100 1% (w/v) SDS 100 mM NaCl 10 mM Tris-HCl with pH 8.0 1 mM EDTA In ddH_2O
TE buffer	10 mM Trizma base 1 mM EDTA-Na_2 dihydrate In ddH_2O, final pH adjusted to 8.0
TE-phenol/chloroform	Mixture of phenol (in TE buffer) and chloroform at a 1:1 ratio

Isolation of plasmid DNA from *E. coli* and *S. cerevisiae*

Plasmid preparations from *E. coli* and *S. cerevisiae* cells were carried out with the QIAprep Spin Miniprep Kit (Qiagen, Hilden) according to the manufacturer's protocol. For *S. cerevisiae* cells the protocol was slightly modified. In addition to buffer P1, 300 mg glass beads were added to the cell pellet and the sample was vortexed on a Vibrax VXR basic (IKA, Staufen) at 1,600 rpm for 15 min. After centrifugation (2,000 rpm, 5 min, room temperature) to settle down the beads and cell debris, the supernatant was transferred to a fresh 1.5 mL microcentrifuge tube and the standard protocol was followed by adding buffer P2. Plasmid DNA was stored at -20°C.

Isolation of RNA from plant material

The isolation of total RNA from *N. benthamiana* leaves and infected maize leaves was carried out with the RNeasy Plant Mini Kit (Qiagen, Hilden) according to the manufacturer's protocol. As starting material 20 leaf discs per sample were punched out using a cork borer with a diameter of 4 mm, corresponding to about 100 mg to 150 mg plant material. After freezing the discs in a 1.5 mL microcentrifuge tube in liquid nitrogen, they were ground using an EPPI-pestle (schuett-biotec, Göttingen). For cell lysis 450 µL RLC buffer containing 1% β-mercaptoethanol was added to the plant powder and from then on the standard protocol was followed. To remove contaminating DNA from the RNA preparations, the TURBO DNA-*free* Kit (Thermo Scientific, Schwerte) was used according to the manufacturer's protocol. In order to increase the RNA concentration the samples were subjected to sodium acetate precipitation. To each RNA sample a 3-fold volume of ice cold ethanol and 10% ice cold 3 M sodium acetate were added. After gentle mixing by pipetting RNA was precipitated overnight at -20°C. The tubes were then centrifuged (13,000 rpm, 10 min, 4°C) and the pellet was washed 3X with 1 mL ice cold 70% ethanol. After removing residual ethanol, the pellet was dried for 2 min at room temperature and resuspended in 20 µL of RNase-free water. RNA was stored at -80°C.

4.5.3. Separation and detection of DNA

Agarose gel electrophoresis

Size-dependent separation was carried out by agarose gel electrophoresis where negatively charged DNA migrates towards the anode of an electric field. Concentrations of agarose varied between 0.8% and 2.5%, determined by the sizes of fragments to be separated. Agarose powder was mixed with TAE buffer and dissolved by boiling. After cooling down to 60°C the solution was supplemented with ethidium bromide to a final concentration of 0.5 µg/mL. The gel was poured into a casting tray containing an appropriate casting comb and cooled down for 20 min to 30 min. The tray with the solid gel was then placed into a running gel chamber, covered with TAE buffer and carefully freed from the comb. DNA samples were mixed with non-denaturing loading dye and the gel was loaded at the site of the cathode. Separation was carried out at a constant voltage of 90 V to 120 V. DNA was displayed at 254 nm on an UV table (2UV Transilluminator, UVP, Upland, USA) and documented using the UVsolo TS imaging system (Biometra, Göttingen).

TAE buffer	40 mM Trizma base 40 mM Acetic acid 1 mM EDTA In ddH_2O, final pH adjusted to 8.0
6X DNA loading dye	50% (w/v) Sucrose 0.1% (v/v) Bromophenol blue In TE buffer

Southern analysis

For Southern analysis (Southern, 1975) 20 µL genomic DNA of *U. maydis* (see chapter 4.5.2) was digested overnight with a suitable restriction endonuclease in a total volume of 40 µL. Such processed DNA was separated on a 0.8% agarose gel at 90 V for 3 h. Following this, the gel was incubated in 0.25 M HCl for 15 min for depurination of the DNA and then neutralized in 0.4 M NaOH for 15 min. To transfer the DNA to a nylon membrane (Hybond-N+, GE Healthcare, Munich) a capillary blot was set up with 0.4 M NaOH as transfer solution. Transfer was carried out overnight or for 72 h at the longest. The membrane was then placed into a hybridization tube and pre-hybridized with Southern hybridization buffer for 30 min at 65°C in a hybridization oven (Mini-Hybridisation Oven OV2, Biometra, Göttingen). The immobilized DNA fragments were detected by digoxigenin- (DIG) labelled probes which were generated either with the PCR DIG Labeling Mix or with DIG-High Prime (both by Roche, Mannheim) according to the manufacturer's protocols. Probes were mixed with 40 mL Southern hybridization buffer and denatured at 100°C for 10 min. After pre-hybridization of the membrane the hybridization buffer was discarded and the hot probe/buffer solution was directly added. Hybridization was performed at 65°C at least overnight or for 72 h at the longest. Following this, the membrane was washed twice with Southern wash buffer at 65°C for 15 min, respectively. For DIG detection, the membrane was first washed

with 20 mL DIG wash buffer for 5 min, then blocked with 50 mL DIG2 buffer for 30 min, and incubated with 50 mL Anti-DIG antibody solution for 1 h (all these incubation steps at room temperature). In preparation for the chemiluminescent reaction the membrane was equilibrated in 20 mL DIG3 buffer for 5 min at room temperature. After incubating with 40 mL CDP-Star solution for 5 min at room temperature, the membrane was exposed to blue/UV light-sensitive X-ray films (CEA, Hamburg) and DNA fragments were visualized using the AGFA CP 1000 film processor (AGFA HealthCare, Mortsel, Belgium).

Southern hybridization buffer	50% (v/v) 1 M Sodium phosphate buffer with pH 7.0 7% SDS (v/v, from a 20% solution) In ddH_2O
1 M Sodium phosphate buffer	Solution 1: 1 M Na_2HPO_4, in ddH_2O Solution 2: 1 M $Na_2HPO_4 \cdot 2H_2O$, in ddH_2O Solution 2 added to solution 1 until pH reached 7.0
Southern wash buffer	10% (v/v) 1 M Sodium phosphate buffer with pH 7.0 1% SDS (v/v, from a 20% solution) In ddH_2O
DIG1 buffer	0.1 M Maleic acid 0.15 M NaCl In ddH_2O, final pH adjusted to 5.8
DIG2 buffer	2% (w/v) Milk powder in DIG1 buffer
DIG wash buffer	0.3% (v/v) Tween 20 in DIG1 buffer
Anti-DIG antibody solution	1:10,000 diluted Anti-Digoxigenin-AP, Fab fragments (Roche, Mannheim) in DIG2 buffer
DIG3 buffer	0.1 M Tris-HCl with pH 9.5 0.1 M NaCl 50 mM $MgCl_2$ In ddH_2O, final pH adjusted to 9.5
CDP-Star solution	1:250 diluted CDP-*Star* (Roche, Mannheim) in DIG3 buffer

Quantitative reverse transcription PCR (qRT-PCR)

For gene expression analyses quantitative PCR (qPCR) was performed with cDNA transcripts generated from RNA. After total RNA isolation (see chapter 4.5.2) mRNA was transcribed into cDNA using the SuperScript III First-Strand Synthesis SuperMix according to the manufacturer's protocol. For the reverse transcription reaction 2 µg total RNA and oligo(dT)$_{20}$ primers were used. The synthesized cDNA was mixed at a 1:1 ratio with ultrapure water and stored at -20°C. For qRT-PCR the Platinum SYBR Green qPCR SuperMix-UDG (Invitrogen, Karlsruhe) and 1 µL of the diluted cDNA were used in a total volume of 25 µL:

1 µL	cDNA (1:2 diluted)	95°C – 3 min
12.5 µL	Platinum SYBR Green qPCR SuperMix-UDG	95°C – 15 s
1 µL	Primers (1:1 mixture of forward and reverse primers, each having a concentration of 10 µM)	60°C – 30 s 72°C – 30 s
10.5 µL	ddH_2O	Steps 2 to 4 performed for 40 cycles

All qRT-PCR reactions were performed with the CFX Connect™ Real-Time PCR Detection System (Bio-Rad, Munich). To confirm the specificity of product amplification a melting curve analysis was done: after a first denaturing step for 15 s at 95°C, fluorescence melting peaks were obtained over a temperature range from 65°C to 95°C (via steps of 0.5°C, 5 s per step). For the determination of threshold cycles (C_T) the CFX Manager™ Software was used. Relative gene expression was elaborated based on the $2^{-\Delta\Delta C}$T method (Livak and Schmittgen, 2001). Oligonucleotides used for qRT-PCR are listed in chapter 4.3.5.

4.6. Biochemical methods

4.6.1. Isolation of proteins

Total protein extraction from *U. maydis* axenic culture

For protein expression analyses a quick and dirty protocol for total protein extraction of *U. maydis* was followed. From a liquid culture (*e.g.* 50 mL YEPS$_{light}$ with an OD$_{600}$ of 1.0) 2 mL of cells were harvested (10,000 rpm, 2 min, room temperature) in a 2 mL screw cap microcentrifuge tube. To the cell pellet 100 µL 4X SDS sample buffer and approx. 200 mg of silica beads (Lysing Matrix B, MP Biomedicals, Irvine, USA) were added. The lid was screwed on tightly and the tube was agitated in a high-speed homogenizer (FastPrep-24, MP Biomedicals) at 6 m/s for 3X 1 min for mechanical disruption of the cells. Between homogenizing steps the sample was cooled on ice for 3 min. Eventually the proteins were denatured at 99°C for 15 min in preparation for SDS polyacrylamide gel electrophoresis (SDS-PAGE) and Western blot analysis.

4X SDS sample buffer	12% SDS (v/v, from a 20% solution) 6% (v/v) β-mercaptoethanol 30% (w/v) Glycerol 0.05% (w/v) Coomassie Brilliant Blue G 250 (Serva, Heidelberg) 150 mM Tris-HCl with pH 7.0 In ddH_2O

Total protein extraction from infected maize leaves

For protein expression analyses in *U. maydis*-infected maize tissue, 2 leaf discs per strain were punched out from a strongly infected area using a cork borer with a diameter of 7 mm. After freezing the discs in a 1.5 mL microcentrifuge tube in liquid nitrogen, they were ground using an EPPI-pestle (schuett-biotec, Göttingen) in 80 µL urea lysis buffer. The samples were boiled for 15 min at 99°C and subsequently centrifuged (13,000 rpm, 5 min, room temperature) to precipitate cell debris. The supernatant was loaded on a SDS gel for Western blot analysis.

Urea lysis buffer	8 M Urea 50 mM Tris-HCl with pH 6.8 5 mM EDTA 50 mM DTT 1 tablet/100 mL cOmplete, EDTA-free Protease Inhibitor Cocktail (Roche, Mannheim) In ddH_2O

Protein precipitation from axenic culture supernatant of *U. maydis*

HA-tagged proteins secreted to axenic culture supernatant by AB33 derivatives were precipitated using trichloroacetic acid (TCA). In preparation for this, filamentous hyphae were induced overnight (for approx. 15 h) in 50 mL NM-glc medium (see chapter 4.4.3), supplemented with 1 tablet cOmplete, EDTA-free Protease Inhibitor Cocktail (Roche, Mannheim) to prevent protein degradation. The hyphae were filtered through a cellulose filter (MN 615, 185 mm, Macherey-Nagel, Düren) and the flow-through was centrifuged in a 50 mL Falcon tube (7,000 rpm, 10 min, room temperature). The resulting supernatant of about 40 mL was transferred to a 50 mL Schott bottle on ice and 12 mL of ice cold 100% TCA was added. Moreover, 0.05% sodium deoxycholate (from a 10% stock solution) was added. Precipitation of proteins occurred overnight at 4°C on ice. The precipitate was harvested in a 50 mL Falcon tube (7,000 rpm, 1 h, 4°C), resuspended in 1.5 mL ice cold acetone and transferred to a 2 mL microcentrifuge tube. The precipitate was harvested (14,000 rpm, 5 min, 4°C) and washed 4X with 200 µL acetone. After the last washing step, the pellet was dried at 50°C for 5 min and resuspended in 70 µL 2X SDS sample buffer. Eventually the proteins were denatured at 99°C for 10 min in preparation for SDS-PAGE and Western blot analysis.

Immunoprecipitation (IP) of HA-tagged Ten1 from *U. maydis* axenic culture

For the purification of overexpressed cytoplasmic Ten1 to be used for the phosphatase activity assay, a non-denaturing protocol for gentle protein elution after IP was followed. SG200-ten1$_{(34\text{-}680)132}$-HA$_3$ and, as a control SG200, were grown overnight in 400 mL YEPS$_{light}$ to an OD$_{600}$ of 1.0. The cells were harvested (5,000 rpm, 15 min, room temperature) and the pellet was frozen overnight at -20°C. The next day, the cells were resuspended in 17 mL IP extraction buffer (see "Co-immunoprecipitation (co-IP) of Ten1 and ZmPP26 from *N. benthamiana*" later in this chapter), lysed for 10 min on ice and the sample was homogenized using a French press (SLM Aminco Spectronic Instruments) under a pressure of approx. 6.9 Mpa for 3 repetitions. The lysate was collected in a 50 mL centrifuge tube on ice and centrifuged at 20,000 rpm for 30 min at 4°C (Sorvall SS-34 rotor). From the resulting supernatant, 14 mL was transferred to a 15 mL Falcon tube. Per sample, 50 µL of Pierce Anti-HA Magnetic Beads (Thermo Scientific, Schwerte) were prepared according to the manufacturer's protocol and transferred to the 15 mL Falcon tube for IP of Ten1$_{(34\text{-}680)132}$-HA$_3$. After an incubation for 1.5 h at room temperature on a rotator, the beads were washed according to the manufacturer's protocol. Elution of proteins from the beads was carried out by adding 2X 80 µL HA Synthetic Peptide (Thermo Scientific, Schwerte; freshly solubilized with phosphate-free water to a concentration of 2 mg/mL) to the beads and by incubating the sample 2X at 37°C for 10 minutes with 1,000 rpm shaking. Protein elution was checked by anti-HA Western blot analysis.

IP of HA-tagged proteins from infected maize leaves for LC-MS/MS

To confirm the interaction of Ten1 and ZmPP26 by mass spectrometry (LC-MS/MS) analysis, HA-tag fusion proteins of Ten1 were enriched from *U. maydis*-infected maize leaves under non-denaturing conditions. Strongly infected leaf material was harvested from approx. 10 to 15 seedlings per strain and frozen in a 50 mL Falcon tube in liquid nitrogen. The leaves were ground by mortar and pestle, 2 mL of the powder was transferred to a 5 mL Eppendorf Tube on ice and 2 mL of HNN lysis buffer was added. After gentle vortexing cell lysis occurred for 30 min on ice. The lysate was centrifuged (14,000 rpm, 15 min, 4°C) and 2 mL of the supernatant was transferred to a fresh 2 mL microcentrifuge tube. Per sample, 12 µL of Pierce Anti-HA Magnetic Beads (Thermo Scientific, Schwerte) was added; 10 µL of beads were eventually used for the mass spectrometry analysis whereas 2 µL served as control for IP via Western blot analysis. After an incubation for 1.5 h at 4°C on a rotator, the beads were separated on a magnetic rack and the supernatant was discarded. The beads were washed 3X with 700 µL of 100 mM ammonium bicarbonate by shaking the tubes gently. After the last washing step the beads were resuspended in 240 µL of 100 mM ammonium bicarbonate and 40 µL of the beads sample was transferred to a fresh tube as IP control sample. After adding 100 µL elution buffer 1, the beads were vortexed and incubated at 27°C on a thermomixer for 30 min at 1,200 rpm in the dark to release the proteins via trypsin digest. The beads were subsequently separated and the flow-through was transferred to a fresh 2 mL microcentrifuge tube. The beads were resuspended in 40 µL elution buffer 2, gently shaken and again separated. The flow-through was transferred to the tube containing the trypsin digest eluate. This step was repeated with another 40 µL elution buffer 2 and the flow-through was combined with the other samples. For the complete trypsin digest of proteins, the sample was incubated overnight at room temperature in the dark. The next day, 40 µL iodoacetamide (5 mg/mL in HPLC

grade water) was added to the trypsin digest. The sample was gently vortexed and incubated at room temperature for 30 min in the dark. To acidify the sample 100 µL 5% trifluoroacetic acid (TFA) was added and the pH was determined via pH stripes to be below 2.

In preparation for the C18 purification, Micro SpinColumns (The Nest Group, Southborough, USA) were assembled with 2 mL conical microcentrifuge tubes and conditioned 2X with 150 µL acetonitrile under centrifugation (1,600 rpm, 30 s, room temperature). Next, the columns were equilibrated 3X with 150 µL 0.1% TFA under centrifugation (2,400 rpm, 30 s, room temperature). The column was transferred to a fresh conical 2 mL microcentrifuge tube and the acidified protein sample was loaded. After centrifugation (1,800 rpm, 2 min, room temperature) the flow-through was loaded again and the column centrifuged again. The column was washed 3X with 150 µL wash buffer under centrifugation (2,400 rpm, 30 s, room temperature). The columns were transferred to fresh 2 mL microcentrifuge tubes and the peptides were eluted by successively adding 3X 100 µL elution buffer 3 to the column under centrifugation (1,600 rpm, 30 s, room temperature). The eluted peptides were subsequently concentrated using the Savant SPD131DDA SpeedVac (Thermo Scientific, Schwerte) at high pressure and 15°C for 2 h and resuspended in 25 µL reconstitution buffer. After gentle vortexing, the samples were treated with 20 pulses of ultrasonication using the UP200St (Hielscher Ultrasonics, Teltow) with an amplitude of 20% and a pulse rate of 0.5 s. The whole sample was transferred into a chromatography vial (J.G. Finneran, Vineland, USA) and analyzed by LC-MS/MS (done by T. Glatter from the core facility for mass spectrometry and proteomics, Max Planck Institute for Terrestrial Microbiology, Marburg).

HNN lysis buffer	50 mM HEPES with pH 7.5 150 mM NaCl 50 mM NaF 5 mM EDTA 0.1% Nonidet P-40 1% Polyvinylpolypyrrolidone (PVPP) In ddH_2O, HPLC grade
Elution buffer 1	1.6 M Urea 1 mM TCEP 10 µg/mL Trypsin In 100 mM ammonium bicarbonate
Elution buffer 2	1.6 M Urea 1 mM TCEP In 100 mM ammonium bicarbonate
Wash buffer	5 % Acetonitrile 0.1% TFA In ddH_2O, HPLC grade

Elution buffer 3	50 % Acetonitrile 0.1% TFA In ddH_2O, HPLC grade
Reconstitution buffer	2 % Acetonitrile 0.15% Formic acid In ddH_2O, HPLC grade

Total protein extraction from *S. cerevisiae* cells

To check for protein expression in yeast two-hybrid strains a quick and dirty protocol for total protein preparation was followed. Cells from a liquid culture (*e.g.* 10 mL SD with an OD_{600} of 0.5 for drop plates) were harvested in a 15 mL Falcon tube (3,000 rpm, 2 min, room temperature) and transferred to a 2 mL microcentrifuge tube with residual supernatant. The sample was again centrifuged (13,000 rpm, 1 min, room temperature) and the supernatant was discarded. To the pellet 50 µL 4X SDS sample buffer, 50 µL ddH_2O and approx. 200 mg of glass beads were added. After boiling the mixture at 99°C for 10 min, the tube was vortexed on a Vibrax VXR basic (IKA, Staufen) at 1,600 rpm for 15 min and directly boiled again for 10 min. In preparation for Western blot analysis the beads and cell debris were pelleted (13,000 rpm, 3 min, room temperature) and the supernatant was loaded on a SDS gel.

Purification of ZmPP26 and ZmPP26$_{DGH65\text{-}67KLN}$ from *E. coli* via GST

BL21 *E. coli* strains expressing GST fusion proteins were grown overnight at 28°C in 10 mL selective dYT. The next day a main culture of 200 mL selective dYT was inoculated by adding 2 mL of the overnight culture (1:100 dilution) and grown at 37°C for approx. 2.5 h to an OD_{600} of 0.5 to 0.7. Two mL of the cells were harvested (10,000 rpm, 2 min, room temperature) and stored at -20°C as pre-induction control sample. The residual culture was supplemented with 200 µL 1 M IPTG (final conc. 1 mM) to induce target protein expression and grown at 28°C for 4 h. After harvesting 2 mL of the cells (10,000 rpm, 2 min, room temperature) as induction control sample, the residual culture was transferred to a 250 mL centrifuge bottle and centrifuged at 6,000 rpm for 30 min at 4°C (Sorvall SLA-3000 rotor). The resulting pellet was frozen overnight at -20°C and resuspended in 20 mL *E. coli* lysis buffer by pipetting the next day. The sample was homogenized using a French press (SLM Aminco Spectronic Instruments) under a pressure of approx. 6.9 Mpa for 3 repetitions. The lysate was collected in a 50 mL centrifuge tube on ice and centrifuged at 20,000 rpm for 30 min at 4°C (Sorvall SS-34 rotor). From the supernatant 20 µL were saved as input control sample for the affinity purification.

In preparation for affinity purification a 10 mL column (Pierce Centrifuge Column, Thermo Scientific, Schwerte) was loaded with 2.5 mL Glutathione Sepharose 4B (GE Healthcare, Munich) and washed once with 10 mL ice cold TBS. The supernatant of the bacterial cell lysate (approx. 15 mL) was loaded onto the column, collected in a 15 mL Falcon tube and loaded again. The column was washed 3X with 10 mL TBS and then 1X with 10 mL

PreScission cleavage buffer. For the on-column cleavage of the GST tag from the target protein, the column was tightly closed, loaded with 2 mL PreScission protease mix and incubated overnight at 4°C on a tube rotator. The purified protein was harvested in a 2 mL microcentrifuge tube, quantified by the Qubit 2.0 Fluorometer (Invitrogen, Karlsruhe) and stored at 4°C for downstream analyses. The pre-induction and the induction control samples were supplemented with 70 µL 2X SDS sample buffer, respectively and to the 20 µL input control sample 10 µL 4X SDS sample buffer was added. Moreover, 5 µL of the purified protein sample was supplemented with 10 µL 2X SDS sample buffer. All control samples were boiled at 99°C for 10 min in preparation for SDS-PAGE and Coomassie staining (see chapter 4.6.2).

E. coli lysis buffer	1% (w/v) Nonidet P-40 0.5 mM EGTA 1 tablet/100 mL cOmplete, EDTA-free Protease Inhibitor Cocktail In TBS
TBS	50 mM Tris-HCl with pH 7.5 150 mM NaCl In ddH_2O
PreScission cleavage buffer	50 mM Tris-HCl with pH 8.0 150 mM NaCl 1 mM EGTA In ddH_2O, final pH adjusted to 7.5
PreScission protease mix, 2 mL	2 µL 1 M DTT 7 µL PreScission Protease (GE Healthcare, Munich) 1.991 mL PreScission cleavage buffer

Co-immunoprecipitation (co-IP) of Ten1 and ZmPP26 from *N. benthamiana*

To confirm the interaction of Ten1 and ZmPP26, HA_3-$Ten1_{34-680}$ and ZmPP26-His_6 were transiently overexpressed in *N. benthamiana* via the CaMV 35S promoter and by *A. tumefaciens*-mediated infiltration. Whole infiltrated leaves were harvested 3 days post-infiltration and the primary vein as well as secondary veins were excised. The leaf material was frozen in a 50 mL Falcon tube in liquid nitrogen and subsequently ground by mortar and pestle. Two mL of the powder was transferred to a 5 mL Eppendorf Tube on ice and 2 mL of IP extraction buffer was added. After short vortexing the lysate was centrifuged (14,000 rpm, 30 min, 4°C).

In preparation for affinity purification 20 µL of magnetic Dynabeads Protein G (Thermo Scientific, Schwerte) per sample were aliquoted in a 2 mL low-binding surface tube (Thermo Scientific, Schwerte). All following buffers were added ice cold to the beads. The tube was placed on a magnetic rack, the supernatant was taken off from the beads and the beads were then washed 3X with 0.5 mL PBS. After the last washing step the beads were

resuspended in 0.7 mL PBS and 4 µL mouse anti-HA antibody was added. The tube was incubated at 4°C on a tube rotator for 2 h for binding the antibody to the beads. Following this, the beads were washed 1X with 0.5 mL PBS and 2X with 0.5 mL IP extraction buffer using the magnetic rack. After the last washing step the beads were resuspended in 50 µL IP extraction buffer. From the centrifuged plant lysate, 1.5 mL of the supernatant was added to the beads-antibody sample. The tube was incubated at 4°C on a tube rotator for 1.5 h to allow the binding of HA_3-$Ten1_{34-680}$ to the beads. After this, the beads were washed 5X with 1 mL IP extraction buffer and boiled at 99°C in 80 µL 4X SDS sample buffer for 10 min. The beads were separated using the magnetic rack and the supernatant was loaded on a SDS gel. Anti-HA and anti-His Western blot analyses were performed to test for IP of HA_3-$Ten1_{34-680}$ and for co-IP of ZmPP26-His_6.

PBS	7.9 mM Na_2HPO_4
	14.5 mM KH_2PO_4
	0.5 mM $MgCl_2 \cdot 6H_2O$
	2.7 mM KCl
	137 mM NaCl
	In ddH_2O, final pH adjusted to 7.2
IP extraction buffer	25 mM Tris-HCl with pH 8.0
	1 mM EDTA
	150 mM NaCl
	0.1% (w/v) Nonidet P-40
	0.2% Polyvinylpolypyrrolidone (PVPP)
	10% Glycerol
	1 tablet/100 mL cOmplete, EDTA-free Protease Inhibitor Cocktail

4.6.2. Separation and detection of proteins

SDS-PAGE

SDS polyacrylamide gel electrophoresis (SDS-PAGE) was performed according to (Laemmli, 1970). Protein samples denatured in SDS sample buffer were loaded on a vertical SDS polyacrylamide gel composed of stacking and separating gel (Mini-PROTEAN system, Bio-Rad, Munich). Depending on the concentration of the protein, between 2 µL and 20 µL of the sample was loaded per well. Whereas the stacking gel always contained 5% polyacrylamide (PAA), the separating gel varied between 8% and 15% in PAA content, depending on the sizes of the proteins to be separated. The composition for a standard SDS gel (10.5 cm X 11.5 cm X 1 cm) with a 5% stacking gel and a 10% separating gel is given below.

Stacking gel (5%), 2.5 mL	417 µL 30% Polyacrylamide (PAA) 625 µL 4X Stacking gel buffer 25 µL 10% Ammonium persulfate (APS) 3 µL Tetramethylethylenediamine (TEMED) 1.43 mL ddH_2O
Separating gel (10%), 5 mL	1.67 mL 30% Polyacrylamide (PAA) 1.25 mL 4X Separating gel buffer 50 µL 10% Ammonium persulfate (APS) 4 µL Tetramethylethylenediamine (TEMED) 2.026 mL ddH_2O
4X Stacking gel buffer	0.5 M Trizma base 0.4% SDS (v/v, from a 20% solution) In ddH_2O, final pH adjusted to 6.8
4X Separating gel buffer	1.5 M Trizma base 0.4% SDS (v/v, from a 20% solution) In ddH_2O, final pH adjusted to 8.8
SDS running buffer	25 mM Tris-HCl with pH 8.0 192 mM Glycine 4 mM SDS (v/v, from a 20% solution)

As a standard for molecular weight of the separated proteins the PageRuler Prestained Protein Ladder (Thermo Scientific, Schwerte) was used. The concentration of proteins in the stacking gel occurred at a constant voltage of 70 V for about 30 min; the separation was performed at a constant voltage between 120 V and 150 V until the desired resolution was achieved. For the visualization of proteins SDS gels were stained using the Coomassie-based InstantBlue stain (Expedeon, San Diego, USA) according to the manufacturer's protocol.

Western blot analysis

Proteins separated by SDS-PAGE were transferred either to a PVDF membrane using the Trans-Blot Turbo Blotting System or to a nitrocellulose membrane using the Trans-Blot SD Semi-Dry Transfer Cell (both systems from Bio-Rad, Munich). For the transfer to a PVDF membrane the manufacturer's protocol was followed and only original Turbo™ material was used. By default the preprogrammed protocol “HIGH MW” was chosen for all experiments. Accordingly, transfer was performed for 10 min at 1.3 A (up to 25 V) for one mini gel or at 2.5 A (up to 25 V) for two mini gels. For the transfer to nitrocellulose, Amersham Protran 0.45 NC membranes (GE Healthcare, Munich) and 2X 3 sheets of 0.35 mm filter paper BP002 (ALBET LabScience, Dassel) were wetted in transfer buffer according to (Bjerrum and Schafer-Nielsen, 1986). Transfer was performed for 2 h at 80 mA per mini gel. For the transfer of proteins with higher molecular weight (100 kDa to 200 kDa) nitrocellulose

membranes were preferentially used because transfer showed to be more efficient with the described protocol compared to the Turbo™ System.

After protein transfer with either method, the membrane was incubated first in blocking solution at room temperature for 1 h and then in antibody solution containing the primary antibody overnight (approx. 15 h) at 4°C. Following this, the membrane was washed 3X with TBS-T for 10 min and then incubated with antibody solution containing the secondary antibody at room temperature for 1 h. After washing 3X with TBS-T for 10 min, the membrane was incubated for 5 min with chemiluminescent detection reagent (Amersham ECL Prime, GE Healthcare, Munich or SuperSignal West Femto, Thermo Scientific, Schwerte). The membrane was exposed to blue/UV light-sensitive X-ray films (CEA, Hamburg) and proteins were visualized using the AGFA CP 1000 film processor (AGFA HealthCare, Mortsel, Belgium).

Bjerrum and Schafer-Nielsen transfer buffer	48 mM Trizma base 39 mM Glycine 1.3 mM SDS (v/v, from a 20% solution) 20% Methanol In ddH_2O
TBS-T	50 mM Tris-HCl with pH 7.5 150 mM NaCl 0.2% (v/v) Tween 20 In ddH_2O
Blocking solution	10% (w/v) Milk powder in TBS-T
Antibody solution	3% (w/v) Milk powder in TBS-T with diluted antibody

Antibodies

The primary and secondary antibodies used in this study are listed in Table 6.

Table 6: Used antibodies

Antibody	Usage	Manufacturer
Mouse anti-HA	Monoclonal primary antibody derived from mouse (1:10,000 dilution)	Sigma-Aldrich (Munich)
Rabbit anti-HA	Monoclonal primary antibody derived from rabbit (1:10,000 dilution)	Sigma-Aldrich (Munich)

(Table 6, continued)

Anti-mouse IgG	HRP-linked secondary antibody derived from horse (1:10,000 dilution)	Cell Signaling Technology (Danvers, USA)
Anti-rabbit IgG	HRP-linked secondary antibody derived from goat (1:10,000 dilution)	Cell Signaling Technology (Danvers, USA)
Mouse anti-α-tubulin	Monoclonal primary antibody derived from mouse (1:2,000 dilution)	Merck (Darmstadt)
Mouse anti-GFP	Monoclonal primary antibody derived from mouse (1:1,000 dilution)	Roche (Mannheim)
Rabbit anti-mCherry	Monoclonal primary antibody derived from rabbit (1:5,000 dilution)	BioVision (Milpitas, USA)
Penta His HRP Conjugate	HRP-linked antibody for the detection of His-tagged proteins, derived from mouse (1:8,000 dilution)	Qiagen (Hilden)

4.6.3. LC-MS/MS analysis

LC-MS/MS analysis of trypsin-digested protein lysates was performed on a Q Exactive Plus mass spectrometer (Thermo Scientific, Schwerte), which was connected to an electrospray Ion max ion source (Thermo Scientific, Schwerte). Peptide separation was carried out using the UltiMate 3000 RSLCnano system (Thermo Scientific, Schwerte) equipped with a RP-HPLC column (75 µm x 35 cm), packed in-house with C18 resin (ReproSil-Pur 120 C18-AQ, 2.4 µm, Dr. Maisch, Ammerbuch-Entringen). The following separating gradient was used: 98% solvent A (0.15% formic acid) and 2% solvent B (80% acetonitrile, 0.15% formic acid) to 25% solvent B over 105 min and to 40% solvent B for additional 35 min at a flow rate of 300 nl/min. The data acquisition mode was set to obtain one high resolution MS scan at a resolution of 70,000 full-width at half maximum (at m/z 200) followed by MS/MS scans of the 10 most intense ions. To increase the efficiency of MS/MS attempts, the charged state screening modus was enabled to exclude unassigned and singly charged ions. The dynamic exclusion duration was set to 30 s. The ion accumulation time was set to 30 ms (MS) and 50 ms at a resolution of 17,500 (MS/MS). The automatic gain control (AGC) was set to 3x106 for MS survey scan and 1x105 for MS/MS scans.

The protein databases for *U. maydis* and *Z. mays* were downloaded from the UniProt database (http://www.uniprot.org/; retrieved in October 2016). Search of the mass spectrometry raw data was performed using Mascot (Version 2.5, Matrix Science, Boston, USA). Search criteria were set as follows: full tryptic specificity was required (cleavage after lysine or arginine residues); two missed cleavages were allowed; carbamidomethylation (C) was set as fixed modification; oxidation (M) as variable modification. The mass tolerance was set to 10 ppm for precursor ions and 0.02 Da for fragment ions. The search results were then loaded into Scaffold 4 (Proteome Software, Portland, USA) and the protein false discovery rate was adjusted to 1%. All LC-MS/MS analyses were conducted by T. Glatter from the core facility for mass spectrometry and proteomics, Max Planck Institute for Terrestrial Microbiology, Marburg.

4.6.4. Chemical fixation of infected plant material and TEM

In preparation for transmission electron microscopy (TEM) maize tissue infected with SG200Δ10A-HA_3-ten1 and, as a control, SG200 was chemically fixated. Per strain to be analyzed 5 pots were infected and well-infected leaf material from 3 different plants was harvested 4 dpi. The samples were cut in totally 50 pieces of about 1 mm² and incubated in 2.5 mL of fixation mixture in a 5 mL Eppendorf Tube. Fixation was carried out for 90 min under mild vacuum conditions (500 hPa). The samples were then washed 4X with 0.06 M phosphate buffer for 15 min, respectively. Buffer was taken off from the samples using a 10 mL syringe (Ø 0. mm X 40 mm). The samples were dehydrated in 2.5 mL of the following percentages of acetone (in ddH_2O): 50%, 70% and 90%. For each step, the sample was incubated 2X for 10 min on a rotator. The leaf material was infiltrated with the acrylic resin LR White (Agar Scientific Ltd, Essex, UK) and 90% acetone at a 2:1 ratio overnight. The next day, the mixture was taken off and the samples were infiltrated first with LR White plus acetone at a 1:1 ratio for 3 h and then with LR White plus acetone in a 2:1 ratio overnight. The next day, the samples were eventually infiltrated in 50 mL 100% LR White for 4 h. For polymerization, 40 mL of the mixture was subsequently transferred to a 100 mL plastic cup (Article no. G332A, Plano, Wetzlar) and another cup was imposed on top of the first one so that the liquid was barred between the bottoms of both cups without air bubbles. Both cups were sealed with Parafilm M and incubated at 50°C for 48 h (all previous experimental steps were done at room temperature). After polymerization, samples were stored at room temperature until analysis by TEM.

Fixation mixture	2.5% Paraformaldehyde (Agar Scientific Ltd, Essex, UK) 0.5% Glutaraldehyde (Agar Scientific Ltd, Essex, UK) 0.06 M Phosphate buffer
Phosphate buffer (0.2 M stock)	Solution 1: 0.2 M Na_2HPO_4, in ddH_2O Solution 2: 0.2 M $NaH_2PO_4 \cdot 2H_2O$, in ddH_2O 61 mL solution 2 mixed with 39 mL solution 1 to obtain pH 7.0

The further preparation of samples, the immunogold labeling of HA_3-Ten1, and the TEM was performed by B. Zechmann (Baylor University, Waco, USA) as described in Redkar *et al.* (2015).

4.7. Cell staining and microscopy

4.7.1. WGA Alexa Fluor® 488/propidium iodide staining

Fungal hyphae were stained with Wheat Germ Agglutinin, Alexa Fluor 488 (WGA-AF488) Conjugate (Thermo Scientific, Schwerte) and plant cell walls were stained with propidium iodide (PI, Sigma-Aldrich, Munich). *U. maydis*-infected leaf material was harvested at 4 dpi and 12 dpi and discolored in ethanol overnight in a 2 mL microcentrifuge tube. The sample was washed 1X with ddH_2O and was then treated with 10% KOH at 85°C for

3 h to 4 h. The leaves were washed 2X with PBS and then incubated in WGA/PI solution for 30 min at room temperature. During the incubation the leaves were vacuum infiltrated 3X for 2 min with 2 min breaks in between. Eventually, the leaves were washed 1X with PBS and analyzed by confocal microscopy.

WGA/PI solution	20 µg/mL Propidium iodide 10 µg/mL WGA-AF488 0.02% Tween 20 In PBS
PI stock solution	10 mg/mL PI (81845 Sigma-Aldrich) in PBS
WGA-AF488 stock solution	1 mg/mL in ddH_2O

4.7.2. Confocal microscopy

The Leica TCS SP5 confocal microscope was used for microscopy and the Leica Application Suite Advanced Fluorescence (LAS AF) software was used for image processing (both from Leica Microsystems, Wetzlar). The excitation and emission spectra for all fluorophores used in this study are listed in Table 7.

Table 7: Wavelengths of excitation and emission spectra for confocal microscopy

Fluorophore	Excitation	Emission
GFP (eGFP)	488 nm (Argon laser)	497 nm to 517 nm
AF488	488 nm (Argon laser)	500 nm to 540 nm
mCherry	561 nm (DPSS laser)	600 nm to 620 nm
PI	561 nm (DPSS laser)	580 nm to 660 nm

4.8. Bioinformatic analyses

Gene and protein information of smut fungi and *Pseudozyma spec.* was acquired from the PEDANT 3 database (http://pedant.gsf.de). Maize gene and protein information was acquired from MaizeGDB (http://maizegdb.org/). The comparison of nucleotide and amino acid sequences was performed by BLAST (https://blast.ncbi.nlm.nih.gov). For pairwise sequence alignments EMBOSS Needle (http://www.ebi.ac.uk/ Tools/psa/ emboss_needle/) was used with a "Gap Open Penalty" of 1 and a "Gap Extend Penalty" of 0.0005. For multiple sequence alignments Clustal Omega (http://www.ebi.ac.uk/Tools/msa/ clustalo/) was used. The prediction of functional and structural domains of proteins was carried out with InterPro (https://www.ebi.ac.uk/interpro/). For the estimation of the isoelectric point (pI) and the charge of a protein PROTEIN CALCULATOR v3.4 (http://protcalc.sourceforge.net/) was used. Prediction of *N*- and *O*-glycosylation

sites were carried out via the NetNGlyc 1.0 Server (http://www.cbs.dtu.dk/services/NetNGlyc/) and the NetOGlyc 4.0 Server (http://www.cbs.dtu.dk/ services/NetOGlyc/), respectively. For the prediction of nuclear localization signals, NucPred (www.sbc.su.se/~maccallr/nucpred/), NLStradamus (http:// www.moseslab.csb.utoronto.ca/ NLStradamus/), and the PredictProtein server (https:// www.predictprotein.org/) were used. To check amino acid sequences for an N-terminal secretion signal SignalP 4.1 (http://www.cbs.dtu.dk/services/SignalP/) was used. Protein structure prediction was conducted with Phyre2 (www.sbg.bio.ic.ac.uk/~phyre/). For the graphical alignment of sequences BioEdit 7.0.5.3. (http://www.mbio.ncsu.edu/BioEdit/page2.html) was used. For molecular cloning Vector NTI (Thermo Scientific, Schwerte) as well as the Lasergene Molecular Biology Suite (DNASTAR, Madison, USA) were used.

5. References

Ahuja, I., Kissen, R., and Bones, A.M. (2012). Phytoalexins in defense against pathogens. Trends Plant Sci. *17*, 73–90.

Aichinger, C., Hansson, K., Eichhorn, H., Lessing, F., Mannhaupt, G., Mewes, W., and Kahmann, R. (2003). Identification of plant-regulated genes in *Ustilago maydis* by enhancer-trapping mutagenesis. Mol. Genet. Genomics *270*, 303–314.

Albert, I., Böhm, H., Albert, M., Feiler, C.E., Imkampe, J., Wallmeroth, N., Brancato, C., Raaymakers, T.M., Oome, S., Zhang, H., et al. (2015). An RLP23–SOBIR1–BAK1 complex mediates NLP-triggered immunity. Nat. Plants *1*, 15140.

Allen, T.W., Quayyum, H.A., Burpee, L.L., and Buck, J.W. (2004). Effect of foliar disease on the epiphytic yeast communities of creeping bentgrass and tall fescue. Can. J. Microbiol. *50*, 853–860.

Ausubel, F. (2002). Short protocols in molecular biology: a compendium of methods from current protocols in molecular biology (New York: Wiley; ISBN 9780471250920).

Banks, G.R., Shelton, P.A., Kanuga, N., Holden, D.W., and Spanos, A. (1993). The *Ustilago maydis* nar 1 gene encoding nitrate reductase activity: sequence and transcriptional regulation. Gene *131*, 69–78.

Banuett, F., and Herskowitz, I. (1989). Different *a* alleles of *Ustilago maydis* are necessary for maintenance of filamentous growth but not for meiosis. Proc. Natl. Acad. Sci. *86*, 5878–5882.

Banuett, F., and Herskowitz, I. (1996). Discrete developmental stages during teliospore formation in the corn smut fungus, *Ustilago maydis*. Development *122*, 2965–2976.

Bebber, D.P., Holmes, T., and Gurr, S.J. (2014). The global spread of crop pests and pathogens. Glob. Ecol. Biogeogr. *23*, 1398–1407.

Beck, M., and Hurt, E. (2016). The nuclear pore complex: understanding its function through structural insight. Nat. Rev. Mol. Cell Biol. *18*, 73–89.

Bjerrum, O.J., and Schafer-Nielsen, C. (1986). Buffer systems and transfer parameters for semidry electroblotting with a horizontal apparatus. Electrophor. VCH Weinh. Ger. 315–327.

Bogan, A.A., and Thorn, K.S. (1998). Anatomy of hot spots in protein interfaces. J. Mol. Biol. *280*, 1–9.

Bohlmann, R. (1996). Isolierung und Charakterisierung von filamentspezifisch exprimierten Genen aus *Ustilago maydis*. PhD dissertation: Department of Biology, Ludwig-Maximilians-University München, Germany (https://opac.tib.eu/DB=1/LNG=EN/XMLPRS=N/ PPN?PPN=236164600; retrieved: August 21, 2017).

Boudsocq, M., Willmann, M.R., McCormack, M., Lee, H., Shan, L., He, P., Bush, J., Cheng, S.-H., and Sheen, J. (2010). Differential innate immune signalling via Ca2+ sensor protein kinases. Nature *464*, 418–422.

Brachmann, A., Weinzierl, G., Kämper, J., and Kahmann, R. (2001). Identification of genes in the *bW/bE* regulatory cascade in *Ustilago maydis*. Mol. Microbiol. *42*, 1047–1063.

Brachmann, A., König, J., Julius, C., and Feldbrügge, M. (2004). A reverse genetic approach for generating gene replacement mutants in *Ustilago maydis*. Mol. Genet. Genomics.

Brameier, M., Krings, A., and MacCallum, R.M. (2007). NucPred Predicting nuclear localization of proteins. Bioinformatics *23*, 1159–1160.

Brefort, T., Doehlemann, G., Mendoza-Mendoza, A., Reissmann, S., Djamei, A., and Kahmann, R. (2009). *Ustilago maydis* as a Pathogen. Annu. Rev. Phytopathol. *47*, 423–445.

Brefort, T., Tanaka, S., Neidig, N., Doehlemann, G., Vincon, V., and Kahmann, R. (2014). Characterization of the Largest Effector Gene Cluster of *Ustilago maydis*. PLoS Pathog. *10*, e1003866.

Broomfield, P.E., and Hargreaves, J.A. (1992). A single amino-acid change in the iron-sulphur protein subunit of succinate dehydrogenase confers resistance to carboxin in *Ustilago maydis*. Curr. Genet. *22*, 117–121.

Bruce, S.A., Saville, B.J., and Neil Emery, R.J. (2011). *Ustilago maydis* Produces Cytokinins and Abscisic Acid for Potential Regulation of Tumor Formation in Maize. J. Plant Growth Regul. *30*, 51–63.

Cao, Y., Liang, Y., Tanaka, K., Nguyen, C.T., Jedrzejczak, R.P., Joachimiak, A., and Stacey, G. (2014). The kinase LYK5 is a major chitin receptor in *Arabidopsis* and forms a chitin-induced complex with related kinase CERK1. ELife *3*.

Chinchilla, D., Zipfel, C., Robatzek, S., Kemmerling, B., Nürnberger, T., Jones, J.D.G., Felix, G., and Boller, T. (2007). A flagellin-induced complex of the receptor FLS2 and BAK1 initiates plant defence. Nature *448*, 497–500.

Christensen, J. J. (1963). Corn smut caused by *Ustilago maydis*. Monograph no. 2. Amer. Phytopath. Society.

Clackson, T., and Wells, J. (1995). A hot spot of binding energy in a hormone-receptor interface. Science *267*, 383–386.

Cohen, S.N., Chang, A.C., and Hsu, L. (1972). Nonchromosomal antibiotic resistance in bacteria: genetic transformation of *Escherichia coli* by R-factor DNA. Proc. Natl. Acad. Sci. U. S. A. *69*, 2110–2114.

Cokol, M., Nair, R., and Rost, B. (2000). Finding nuclear localization signals. EMBO Rep. *1*, 411–415.

Cook, D.E., Mesarich, C.H., and Thomma, B.P.H.J. (2015). Understanding Plant Immunity as a Surveillance System to Detect Invasion. Annu. Rev. Phytopathol. *53*, 541–563.

Couto, D., Niebergall, R., Liang, X., Bücherl, C.A., Sklenar, J., Macho, A.P., Ntoukakis, V., Derbyshire, P., Altenbach, D., Maclean, D., et al. (2016). The *Arabidopsis* protein phosphatase PP2C38 negatively regulates the central immune kinase BIK1. PLoS Pathog *12*, e1005811.

Cui, H., Tsuda, K., and Parker, J.E. (2015). Effector-Triggered Immunity: From Pathogen Perception to Robust Defense. Annu. Rev. Plant Biol. *66*, 487–511.

Das, A.K., Helps, N.R., Cohen, P.T., and Barford, D. (1996). Crystal structure of the protein serine/threonine phosphatase 2C at 2.0 A resolution. EMBO J. *15*, 6798.

Day, P.R., and Anagnostakis, S.L. (1971). Corn Smut Dikaryon in Culture. Nature. New Biol. *231*, 19–20.

Day, B., Henty, J.L., Porter, K.J., and Staiger, C.J. (2011). The Pathogen-Actin Connection: A Platform for Defense Signaling in Plants. Annu. Rev. Phytopathol. *49*, 483–506.

Denancé, N., Sánchez-Vallet, A., Goffner, D., and Molina, A. (2013). Disease resistance or growth: the role of plant hormones in balancing immune responses and fitness costs. Front. Plant Sci. *4*.

Deshpande, N., Wilkins, M.R., Packer, N., and Nevalainen, H. (2008). Protein glycosylation pathways in filamentous fungi. Glycobiology *18*, 626–637.

Djamei, A., and Kahmann, R. (2012). *Ustilago maydis*: Dissecting the Molecular Interface between Pathogen and Plant. PLoS Pathog. *8*, e1002955.

Djamei, A., Schipper, K., Rabe, F., Ghosh, A., Vincon, V., Kahnt, J., Osorio, S., Tohge, T., Fernie, A.R., Feussner, I., et al. (2011). Metabolic priming by a secreted fungal effector. Nature *478*, 395–398.

Dodds, P.N., and Rathjen, J.P. (2010). Plant immunity: towards an integrated view of plant–pathogen interactions. Nat. Rev. Genet. *11*, 539–548.

Doehlemann, G., Wahl, R., Horst, R.J., Voll, L.M., Usadel, B., Poree, F., Stitt, M., Pons-Kühnemann, J., Sonnewald, U., Kahmann, R., et al. (2008). Reprogramming a maize plant: transcriptional and metabolic changes induced by the fungal biotroph *Ustilago maydis*. Plant J. *56*, 181–195.

Doehlemann, G., van der Linde, K., Aßmann, D., Schwammbach, D., Hof, A., Mohanty, A., Jackson, D., and Kahmann, R. (2009). Pep1, a Secreted Effector Protein of *Ustilago maydis*, Is Required for Successful Invasion of Plant Cells. PLoS Pathog. *5*, e1000290.

Doehlemann, G., Reissmann, S., Aßmann, D., Fleckenstein, M., and Kahmann, R. (2011). Two linked genes encoding a secreted effector and a membrane protein are essential for *Ustilago maydis*-induced tumour formation. Mol. Microbiol. *81*, 751–766.

Du, J., Verzaux, E., Chaparro-Garcia, A., Bijsterbosch, G., Keizer, L.C.P., Zhou, J., Liebrand, T.W.H., Xie, C., Govers, F., Robatzek, S., et al. (2015). Elicitin recognition confers enhanced resistance to *Phytophthora infestans* in potato. Nat. Plants *1*, 15034.

Dutheil, J.Y., Mannhaupt, G., Schweizer, G., M.K. Sieber, C., Münsterkötter, M., Güldener, U., Schirawski, J., and Kahmann, R. (2016). A Tale of Genome Compartmentalization: The Evolution of Virulence Clusters in Smut Fungi. Genome Biol. Evol. *8*, 681–704.

Farfsing, J.W. (2004). Regulation des Mais-induzierten *mig2*-Genclusters in *Ustilago maydis*. PhD dissertation: Department of Biology, Philipps University Marburg, Germany (http://archiv.ub.uni-marburg.de/diss/z2004/0537/; retrieved: May 16, 2017).

Fernandez-Alvarez, A., Elias-Villalobos, A., and Ibeas, J.I. (2009). The O-Mannosyltransferase PMT4 Is Essential for Normal Appressorium Formation and Penetration in *Ustilago maydis*. Plant Cell *21*, 3397–3412.

Fernandez-Alvarez, A., Elias-Villalobos, A., Jimenez-Martin, A., Marin-Menguiano, M., and Ibeas, J.I. (2013). Endoplasmic Reticulum Glucosidases and Protein Quality Control Factors Cooperate to Establish Biotrophy in *Ustilago maydis*. Plant Cell 25, 4676-4690.

Fesel, P.H., and Zuccaro, A. (2016). β-glucan: Crucial component of the fungal cell wall and elusive MAMP in plants. Fungal Genet. Biol. *90*, 53–60.

Fisher, M.C., Henk, D.A., Briggs, C.J., Brownstein, J.S., Madoff, L.C., McCraw, S.L., and Gurr, S.J. (2012). Emerging fungal threats to animal, plant and ecosystem health. Nature *484*, 186–194.

Flor, H.H. (1971). Current status of the gene-for-gene concept. Annu. Rev. Phytopathol. *9*, 275–296.

Fuchs, S., Grill, E., Meskiene, I., and Schweighofer, A. (2013). Type 2C protein phosphatases in plants: PP2Cs. FEBS J. *280*, 681–693.

Gibson, D.G., Young, L., Chuang, R.-Y., Venter, J.C., Hutchison, C.A., and Smith, H.O. (2009). Enzymatic assembly of DNA molecules up to several hundred kilobases. Nat. Methods *6*, 343–345.

Gietz, R.D., and Schiestl, R.H. (2007). High-efficiency yeast transformation using the LiAc/SS carrier DNA/PEG method. Nat. Protoc. *2*, 31–34.

Gillissen, B., Bergemann, J., Sandmann, C., Schroeer, B., Bölker, M., and Kahmann, R. (1992). A two-component regulatory system for self/non-self recognition in *Ustilago maydis*. Cell *68*, 647–657.

Giraldo, M.C., and Valent, B. (2013). Filamentous plant pathogen effectors in action. Nat. Rev. Microbiol. *11*, 800–814.

Glazebrook, J. (2005). Contrasting Mechanisms of Defense Against Biotrophic and Necrotrophic Pathogens. Annu. Rev. Phytopathol. *43*, 205–227.

Gómez-Gómez, L., and Boller, T. (2000). FLS2: An LRR Receptor–like Kinase Involved in the Perception of the Bacterial Elicitor Flagellin in *Arabidopsis*. Mol. Cell *5*, 1003–1011.

González, M., Brito, N., and González, C. (2012). High abundance of Serine/Threonine-rich regions predicted to be hyper-O-glycosylated in the secretory proteins coded by eight fungal genomes. BMC Microbiol. *12*, 213.

Halim, V.A., Altmann, S., Ellinger, D., Eschen-Lippold, L., Miersch, O., Scheel, D., and Rosahl, S. (2009). PAMP-induced defense responses in potato require both salicylic acid and jasmonic acid. Plant J. *57*, 230–242.

Han, S., Min, M.K., Lee, S.-Y., Lim, C.W., Bhatnagar, N., Lee, Y., Shin, D., Chung, K.Y., Lee, S.C., Kim, B.-G., et al. (2017). Modulation of ABA signaling by altering VxGΦL motif of PP2Cs in Oryza sativa. Mol. Plant, in press. doi: 10.1016/j.molp.2017.08.003.

Hemetsberger, C., Herrberger, C., Zechmann, B., Hillmer, M., and Doehlemann, G. (2012). The *Ustilago maydis* Effector Pep1 Suppresses Plant Immunity by Inhibition of Host Peroxidase Activity. PLoS Pathog. *8*, e1002684.

Henty-Ridilla, J.L., Li, J., Day, B., and Staiger, C.J. (2014). ACTIN DEPOLYMERIZING FACTOR4 Regulates Actin Dynamics during Innate Immune Signaling in *Arabidopsis*. Plant Cell *26*, 340–352.

Hind, S.R., Strickler, S.R., Boyle, P.C., Dunham, D.M., Bao, Z., O'Doherty, I.M., Baccile, J.A., Hoki, J.S., Viox, E.G., Clarke, C.R., et al. (2016). Tomato receptor FLAGELLIN-SENSING 3 binds flgII-28 and activates the plant immune system. Nat. Plants *2*, 16128.

Holliday, R. (1974). *Ustilago maydis*. In King, R.C. (ed.) Handbook of Genetics 1, Plenum Press, New York/USA: 575-595.

Horton, P., Park, K.-J., Obayashi, T., and Nakai, K. (2005). Protein Subcellular Localization Prediction With WoLF PSORT. (Published by Imperial College Press and distributed by World Scientific Publishing Co.), pp. 39–48.

Hotson, A., Chosed, R., Shu, H., Orth, K., and Mudgett, M.B. (2003). *Xanthomonas* type III effector XopD targets SUMO-conjugated proteins in planta: Plant-specific SUMO cysteine protease. Mol. Microbiol. *50*, 377–389.

Hu, W., Yan, Y., Hou, X., He, Y., Wei, Y., Yang, G., He, G., and Peng, M. (2015). TaPP2C1, a Group F2 Protein Phosphatase 2C Gene, Confers Resistance to Salt Stress in Transgenic Tobacco. PLOS ONE *10*, e0129589.

Irmler, A., and Forchhammer, K. (2001). A PP2C-type phosphatase dephosphorylates the PII signaling protein in the cyanobacterium *Synechocystis* PCC 6803. Proc. Natl. Acad. Sci. *98*, 12978–12983.

Jeworutzki, E., Roelfsema, M.R.G., Anschütz, U., Krol, E., Elzenga, J.T.M., Felix, G., Boller, T., Hedrich, R., and Becker, D. (2010). Early signaling through the *Arabidopsis* pattern recognition receptors FLS2 and EFR involves Ca2+-associated opening of plasma membrane anion channels: Flagellin-activated ion channels. Plant J. *62*, 367–378.

Jones, J.D.G., and Dangl, J.L. (2006). The plant immune system. Nature *444*, 323–329.

Jones, J.D.G., Vance, R.E., and Dangl, J.L. (2016). Intracellular innate immune surveillance devices in plants and animals. Science *354*, aaf6395-aaf6395.

de Jong, W.W., Zweers, A., and Cohen, L.H. (1978). Influence of single amino acid substitutions on electrophoretic mobility of sodium dodecyl sulfate-protein complexes. Biochem. Biophys. Res. Commun. *82*, 532–539.

Kämper, J. (2004). A PCR-based system for highly efficient generation of gene replacement mutants in *Ustilago maydis*. Mol. Genet. Genomics *271*, 103–110.

Kämper, J., Kahmann, R., Bölker, M., Ma, L.-J., Brefort, T., Saville, B.J., Banuett, F., Kronstad, J.W., Gold, S.E., Müller, O., et al. (2006). Insights from the genome of the biotrophic fungal plant pathogen *Ustilago maydis*. Nature *444*, 97–101.

Kelley, L.A., Mezulis, S., Yates, C.M., Wass, M.N., and Sternberg, M.J.E. (2015). The Phyre2 web portal for protein modeling, prediction and analysis. Nat. Protoc. *10*, 845–858.

Kerk, D., Bulgrien, J., Smith, D.W., Barsam, B., Veretnik, S., and Gribskov, M. (2002). The Complement of Protein Phosphatase Catalytic Subunits Encoded in the Genome of *Arabidopsis*. PLANT Physiol. *129*, 908–925.

Kerk, D., Templeton, G., and Moorhead, G.B.G. (2007). Evolutionary Radiation Pattern of Novel Protein Phosphatases Revealed by Analysis of Protein Data from the Completely Sequenced Genomes of Humans, Green Algae, and Higher Plants. PLANT Physiol. *146*, 351–367.

Knop, M., Siegers, K., Pereira, G., Zachariae, W., Winsor, B., Nasmyth, K., and Schiebel, E. (1999). Epitope tagging of yeast genes using a PCR-based strategy: more tags and improved practical routines. Yeast *15*, 963–972.

Koncz, C., and Schell, J. (1986). The promoter of TL-DNA gene 5 controls the tissue-specific expression of chimaeric genes carried by a novel type of *Agrobacterium* binary vector. MGG Mol. Gen. Genet. *204*, 383–396.

Konishi, M., Hatada, Y., and Horiuchi, J. -i. (2013). Draft Genome Sequence of the Basidiomycetous Yeast-Like Fungus *Pseudozyma hubeiensis* SY62, Which Produces an Abundant Amount of the Biosurfactant Mannosylerythritol Lipids. Genome Announc. *1*, e00409-13-e00409-13.

Kyriakis, J.M. (2014). In the Beginning, There Was Protein Phosphorylation. J. Biol. Chem. *289*, 9460–9462.

Laemmli, U.K. (1970). Cleavage of Structural Proteins during the Assembly of the Head of Bacteriophage T4. Nature *227*, 680–685.

Lanver, D., Tollot, M., Schweizer, G., Lo Presti, L., Reissmann, S., Ma, L.-S., Schuster, M., Tanaka, S., Liang, L., Ludwig, N., et al. (2017). *Ustilago maydis* effectors and their impact on virulence. Nat. Rev. Microbiol.

Laurie, J.D., Ali, S., Linning, R., Mannhaupt, G., Wong, P., Guldener, U., Munsterkotter, M., Moore, R., Kahmann, R., Bakkeren, G., et al. (2012). Genome Comparison of Barley and Maize Smut Fungi Reveals Targeted Loss of RNA Silencing Components and Species-Specific Presence of Transposable Elements. Plant Cell *24*, 1733–1745.

Lee, J.-Y., and Lu, H. (2011). Plasmodesmata: the battleground against intruders. Trends Plant Sci. *16*, 201–210.

Lee, M.W., Jelenska, J., and Greenberg, J.T. (2008). *Arabidopsis* proteins important for modulating defense responses to *Pseudomonas syringae* that secrete HopW1-1. Plant J. *54*, 452–465.

Leung, J. (1997). The *Arabidopsis* ABSCISIC ACID-INSENSITIVE2 (ABI2) and ABI1 Genes Encode Homologous Protein Phosphatases 2C Involved in Abscisic Acid Signal Transduction. PLANT CELL ONLINE *9*, 759–771.

Leung, J., Bouvier-Durand, M., Morris, P., Guerrier, D., Chefdor, F., and Giraudat, J. (1994). *Arabidopsis* ABA response gene ABI1: features of a calcium-modulated protein phosphatase. Science *264*, 1448–1452.

van der Linde, K., Kastner, C., Kumlehn, J., Kahmann, R., and Doehlemann, G. (2011). Systemic virus-induced gene silencing allows functional characterization of maize genes during biotrophic interaction with *Ustilago maydis*. New Phytol. *189*, 471–483.

Liu, B., Li, J.-F., Ao, Y., Li, Z., Liu, J., Feng, D., Qi, K., He, Y., Zeng, L., Wang, J., et al. (2013a). OsLYP4 and OsLYP6 play critical roles in rice defense signal transduction. Plant Signal. Behav. *8*, e22980.

Liu, L., Hu, X., Song, J., Zong, X., Li, D., and Li, D. (2009). Over-expression of a *Zea mays* L. protein phosphatase 2C gene (ZmPP2C) in *Arabidopsis thaliana* decreases tolerance to salt and drought. J. Plant Physiol. *166*, 531–542.

Liu, T., Liu, Z., Song, C., Hu, Y., Han, Z., She, J., Fan, F., Wang, J., Jin, C., Chang, J., et al. (2012). Chitin-Induced Dimerization Activates a Plant Immune Receptor. Science *336*, 1160–1164.

Liu, Z., Wu, Y., Yang, F., Zhang, Y., Chen, S., Xie, Q., Tian, X., and Zhou, J.-M. (2013b). BIK1 interacts with PEPRs to mediate ethylene-induced immunity. Proc. Natl. Acad. Sci. *110*, 6205–6210.

Livak, K.J., and Schmittgen, T.D. (2001). Analysis of Relative Gene Expression Data Using Real-Time Quantitative PCR and the $2^{-\Delta\Delta CT}$ Method. Methods *25*, 402–408.

Lo Presti, L., Zechmann, B., Kumlehn, J., Liang, L., Lanver, D., Tanaka, S., Bock, R., and Kahmann, R. (2017). An assay for entry of secreted fungal effectors into plant cells. New Phytol. *213*, 956–964.

Lorenz, S., Guenther, M., Grumaz, C., Rupp, S., Zibek, S., and Sohn, K. (2014). Genome Sequence of the Basidiomycetous Fungus *Pseudozyma aphidis* DSM70725, an Efficient Producer of Biosurfactant Mannosylerythritol Lipids. Genome Announc. *2*, e00053-14-e00053-14.

Luna, E., Pastor, V., Robert, J., Flors, V., Mauch-Mani, B., and Ton, J. (2011). Callose Deposition: A Multifaceted Plant Defense Response. Mol. Plant. Microbe Interact. *24*, 183–193.

Macho, A.P., and Zipfel, C. (2014). Plant PRRs and the Activation of Innate Immune Signaling. Mol. Cell *54*, 263–272.

Maeda, T., Tsai, A.Y., and Saito, H. (1993). Mutations in a protein tyrosine phosphatase gene (PTP2) and a protein serine/threonine phosphatase gene (PTC1) cause a synthetic growth defect in *Saccharomyces cerevisiae*. Mol. Cell. Biol. *13*, 5408–5417.

Mann, D.J., Campbell, D.G., McGowan, C.H., and Cohen, P.T.W. (1992). Mammalian protein serine/threonine phosphatase 2C: cDNA cloning and comparative analysis of amino acid sequences. Biochim. Biophys. Acta BBA Gene Struct. Expr. *1130*, 100–104.

Martínez-Espinoza, A.D., García-Pedrajas, M.D., and Gold, S.E. (2002). The *Ustilaginales* as Plant Pests and Model Systems. Fungal Genet. Biol. *35*, 1–20.

Matei, A., and Doehlemann, G. (2016). Cell biology of corn smut disease–*Ustilago maydis* as a model for biotrophic interactions. Curr. Opin. Microbiol. *34*, 60–66.

Mauch-Mani, B., and Mauch, F. (2005). The role of abscisic acid in plant–pathogen interactions. Curr. Opin. Plant Biol. *8*, 409–414.

McCullum, E.O., Williams, B.A.R., Zhang, J., and Chaput, J.C. (2010). Random Mutagenesis by Error-Prone PCR. In In Vitro Mutagenesis Protocols, J. Braman, ed. (Totowa, NJ: Humana Press), pp. 103–109.

Melcher, K., Ng, L.-M., Zhou, X.E., Soon, F.-F., Xu, Y., Suino-Powell, K.M., Park, S.-Y., Weiner, J.J., Fujii, H., Chinnusamy, V., et al. (2009). A gate–latch–lock mechanism for hormone signalling by abscisic acid receptors. Nature *462*, 602–608.

Melotto, M., Underwood, W., Koczan, J., Nomura, K., and He, S.Y. (2006). Plant Stomata Function in Innate Immunity against Bacterial Invasion. Cell *126*, 969–980.

Mendoza-Mendoza, A., Berndt, P., Djamei, A., Weise, C., Linne, U., Marahiel, M., Vraneš, M., Kämper, J., and Kahmann, R. (2009). Physical-chemical plant-derived signals induce differentiation in *Ustilago maydis*. Mol. Microbiol. *71*, 895–911.

Moeder, W., Ung, H., Mosher, S., and Yoshioka, K. (2010). SA-ABA antagonism in defense responses. Plant Signal. Behav. *5*, 1231–1233.

Moorhead, G.B.G., De Wever, V., Templeton, G., and Kerk, D. (2009). Evolution of protein phosphatases in plants and animals. Biochem. J. *417*, 401–409.

Moreira, I.S., Fernandes, P.A., and Ramos, M.J. (2007). Hot spots-A review of the protein-protein interface determinant amino-acid residues. Proteins Struct. Funct. Bioinforma. *68*, 803–812.

Morita, T., Koike, H., Hagiwara, H., Ito, E., Machida, M., Sato, S., Habe, H., and Kitamoto, D. (2014). Genome and Transcriptome Analysis of the Basidiomycetous Yeast *Pseudozyma antarctica* Producing Extracellular Glycolipids, Mannosylerythritol Lipids. PLoS ONE *9*, e86490.

Morrison, E.N., Emery, R.J.N., and Saville, B.J. (2015). Phytohormone Involvement in the *Ustilago maydis*–*Zea mays* Pathosystem: Relationships between Abscisic Acid and Cytokinin Levels and Strain Virulence in Infected Cob Tissue. PLOS ONE *10*, e0130945.

Mueller, A.N., Ziemann, S., Treitschke, S., Aßmann, D., and Doehlemann, G. (2013). Compatibility in the *Ustilago maydis*–Maize Interaction Requires Inhibition of Host Cysteine Proteases by the Fungal Effector Pit2. PLoS Pathog. *9*, e1003177.

Mullis, K., Faloona, F., Scharf, S., Saiki, R., Horn, G., and Erlich, H. (1986). Specific Enzymatic Amplification of DNA *In Vitro*: The Polymerase Chain Reaction. Cold Spring Harb. Symp. Quant. Biol. *51*, 263–273.

Nair, R., Carter, P., and Rost, B. (2003). NLSdb: database of nuclear localization signals. Nucleic Acids Res. *31*, 397–399.

Neidig, N. (2013). Funktionelle Analyse des *Ustilago maydis* Effektorproteins Tin3 im Gencluster 19A. PhD dissertation: Department of Biology, Philipps University Marburg, Germany (http://archiv.ub.uni-marburg.de/diss/z2013/0355/pdf/dnn.pdf; retrieved: August 21, 2017).

Nguyen Ba, A.N., Pogoutse, A., Provart, N., and Moses, A.M. (2009). NLStradamus: a simple Hidden Markov Model for nuclear localization signal prediction. BMC Bioinformatics *10*, 202.

Oerke, E.-C. (2006). Crop losses to pests. J. Agric. Sci. *144*, 31.

Panayotatos, N., Radziejewska, E., Acheson, A., Pearsall, D., Thadani, A., and Wong, V. (1993). Exchange of a single amino acid interconverts the specific activity and gel mobility of human and rat ciliary neurotrophic factors. J. Biol. Chem. *268*, 19000–19003.

Petit-Houdenot, Y., and Fudal, I. (2017). Complex Interactions between Fungal Avirulence Genes and Their Corresponding Plant Resistance Genes and Consequences for Disease Resistance Management. Front. Plant Sci. *8*.

Que, Y., Xu, L., Wu, Q., Liu, Y., Ling, H., Liu, Y., Zhang, Y., Guo, J., Su, Y., Chen, J., et al. (2014). Genome sequencing of *Sporisorium scitamineum* provides insights into the pathogenic mechanisms of sugarcane smut. BMC Genomics *15*, 996.

Rabe, F., Ajami-Rashidi, Z., Doehlemann, G., Kahmann, R., and Djamei, A. (2013). Degradation of the plant defence hormone salicylic acid by the biotrophic fungus *Ustilago maydis*: SA signalling and degradation in *U. maydis*. Mol. Microbiol. *89*, 179–188.

Rabe, F., Bosch, J., Stirnberg, A., Guse, T., Bauer, L., Seitner, D., Rabanal, F.A., Czedik-Eysenberg, A., Uhse, S., Bindics, J., et al. (2016). A complete toolset for the study of *Ustilago bromivora* and *Brachypodium* sp. as a fungal-temperate grass pathosystem. ELife *5*, e20522.

Rae, B.P., and Elliott, R.M. (1986). Characterization of the Mutations Responsible for the Electrophoretic Mobility Differences in the NS Proteins of Vesicular Stomatitis Virus New Jersey Complementation Group E Mutants. J. Gen. Virol. *67*, 2635–2643.

Raghavendra, A.S., Gonugunta, V.K., Christmann, A., and Grill, E. (2010). ABA perception and signalling. Trends Plant Sci. *15*, 395–401.

Raho, N., Ramirez, L., Lanteri, M.L., Gonorazky, G., Lamattina, L., ten Have, A., and Laxalt, A.M. (2011). Phosphatidic acid production in chitosan-elicited tomato cells, via both phospholipase D and phospholipase C/diacylglycerol kinase, requires nitric oxide. J. Plant Physiol. *168*, 534–539.

Ranf, S. (2017). Sensing of molecular patterns through cell surface immune receptors. Curr. Opin. Plant Biol. *38*, 68–77.

Redkar, A., Hoser, R., Schilling, L., Zechmann, B., Krzymowska, M., Walbot, V., and Doehlemann, G. (2015). A Secreted Effector Protein of *Ustilago maydis* Guides Maize Leaf Cells to Form Tumors. Plant Cell *27*, 1332–1351.

Righetti, P.G., Stoyanov, A., and Zhukov, M.Y. (2001). The proteome revisited: theory and practice of all relevant electrophoretic steps (Amsterdam ; New York: Elsevier Science).

Robert-Seilaniantz, A., Grant, M., and Jones, J.D.G. (2011). Hormone Crosstalk in Plant Disease and Defense: More Than Just JASMONATE-SALICYLATE Antagonism. Annu. Rev. Phytopathol. *49*, 317–343.

Robin, J.B., Arffa, R.C., Avni, I., and Rao, N.A. (1986). Rapid visualization of three common fungi using fluorescein-conjugated lectins. Invest. Ophthalmol. Vis. Sci. *27*, 500–506.

Rodriguez, P.L., Leube, M.P., and Grill, E. (1998). Molecular cloning in *Arabidopsis thaliana* of a new protein phosphatase 2C (PP2C) with homology to ABI1 and ABI2. Plant Mol. Biol. *38*, 879–883.

Roth, Z., Yehezkel, G., and Khalaila, I. (2012). Identification and Quantification of Protein Glycosylation. Int. J. Carbohydr. Chem. *2012*, 1–10.

Running, M.P., Clark, S.E., and Meyerowitz, E.M. (1995). Confocal microscopy of the shoot apex. Methods Cell Biol. *49*, 217–229.

Sambrook, J., Fritsch, E., and Maniatis, T. (1989). Molecular cloning: A laboratory manual: Vol. 2 (S.l.: Cold Spring Harbor).

Scheler, C., Durner, J., and Astier, J. (2013). Nitric oxide and reactive oxygen species in plant biotic interactions. Curr. Opin. Plant Biol. *16*, 534–539.

Schirawski, J., Mannhaupt, G., Munch, K., Brefort, T., Schipper, K., Doehlemann, G., Di Stasio, M., Rossel, N., Mendoza-Mendoza, A., Pester, D., et al. (2010). Pathogenicity Determinants in Smut Fungi Revealed by Genome Comparison. Science *330*, 1546–1548.

Schreiner, P., Chen, X., Husnjak, K., Randles, L., Zhang, N., Elsasser, S., Finley, D., Dikic, I., Walters, K.J., and Groll, M. (2008). Ubiquitin docking at the proteasome through a novel pleckstrin-homology domain interaction. Nature *453*, 548–552.

Schulz, B., Banuett, F., Dahl, M., Schlesinger, R., Schäfer, W., Martin, T., Herskowitz, I., and Kahmann, R. (1990). The *b* alleles of *U. maydis*, whose combinations program pathogenic development, code for polypeptides containing a homeodomain-related motif. Cell *60*, 295–306.

Schuster, M., Schweizer, G., Reissmann, S., and Kahmann, R. (2015). Genome editing in *Ustilago maydis* using the CRISPR–Cas system. Fungal Genet. Biol.

Schuster, M., Schweizer, G., and Kahmann, R. (2017). Comparative analyses of secreted proteins in plant pathogenic smut fungi and related basidiomycetes. Fungal Genet. Biol.

Schweighofer, A., and Meskiene, I. (2015). Phosphatases in Plants. In Plant Phosphoproteomics, W.X. Schulze, ed. (New York, NY: Springer New York), pp. 25–46.

Schweighofer, A., Hirt, H., and Meskiene, I. (2004). Plant PP2C phosphatases: emerging functions in stress signaling. Trends Plant Sci. *9*, 236–243.

Schweighofer, A., Kazanaviciute, V., Scheikl, E., Teige, M., Doczi, R., Hirt, H., Schwanninger, M., Kant, M., Schuurink, R., Mauch, F., et al. (2007). The PP2C-Type Phosphatase AP2C1, Which Negatively Regulates MPK4 and MPK6, Modulates Innate Immunity, Jasmonic Acid, and Ethylene Levels in *Arabidopsis*. PLANT CELL ONLINE *19*, 2213–2224.

Serdyuk, I.N., Zaccai, N.R., and Zaccai, G. (2007). Methods in molecular biophysics: structure, dynamics, function (Cambridge ; New York: Cambridge University Press).

Sharma, R., Mishra, B., Runge, F., and Thines, M. (2014). Gene Loss Rather Than Gene Gain Is Associated with a Host Jump from Monocots to Dicots in the Smut Fungus *Melanopsichium pennsylvanicum*. Genome Biol. Evol. *6*, 2034–2049.

Sheard, L.B., and Zheng, N. (2009). Plant biology: Signal advance for abscisic acid. Nature *462*, 575–576.

Sheen, J. (1998). Mutational analysis of protein phosphatase 2C involved in abscisic acid signal transduction in higher plants. Proc. Natl. Acad. Sci. *95*, 975–980.

Shi, Y., Mowery, R.A., Ashley, J., Hentz, M., Ramirez, A.J., Bilgicer, B., Slunt-Brown, H., Borchelt, D.R., and Shaw, B.F. (2012). Abnormal SDS-PAGE migration of cytosolic proteins can identify domains and mechanisms that control surfactant binding. Protein Sci. *21*, 1197–1209.

Shinya, T., Nakagawa, T., Kaku, H., and Shibuya, N. (2015). Chitin-mediated plant–fungal interactions: catching, hiding and handshaking. Curr. Opin. Plant Biol. *26*, 64–71.

Shubchynskyy, V., Boniecka, J., Schweighofer, A., Simulis, J., Kvederaviciute, K., Stumpe, M., Mauch, F., Balazadeh, S., Mueller-Roeber, B., Boutrot, F., et al. (2017). Protein phosphatase AP2C1 negatively regulates basal resistance and defense responses to *Pseudomonas syringae*. J. Exp. Bot. erw485.

Singh, A., Giri, J., Kapoor, S., Tyagi, A.K., and Pandey, G.K. (2010). Protein phosphatase complement in rice: genome-wide identification and transcriptional analysis under abiotic stress conditions and reproductive development. BMC Genomics *11*, 435.

Skibbe, D.S., Doehlemann, G., Fernandes, J., and Walbot, V. (2010). Maize Tumors Caused by *Ustilago maydis* Require Organ-Specific Genes in Host and Pathogen. Science *328*, 89–92.

Snetselaar, K., and McCann, M. (2017). *Ustilago maydis*, the corn smut fungus, has an unusual diploid mitotic stage. Mycologia *109*, 140–152.

Song, S.-K., Lee, M.M., and Clark, S.E. (2006). POL and PLL1 phosphatases are CLAVATA1 signaling intermediates required for *Arabidopsis* shoot and floral stem cells. Development *133*, 4691–4698.

Song, S.-K., Hofhuis, H., Lee, M.M., and Clark, S.E. (2008). Key Divisions in the Early *Arabidopsis* Embryo Require POL and PLL1 Phosphatases to Establish the Root Stem Cell Organizer and Vascular Axis. Dev. Cell *15*, 98–109.

Soon, F.-F., Ng, L.-M., Zhou, X.E., West, G.M., Kovach, A., Tan, M.H.E., Suino-Powell, K.M., He, Y., Xu, Y., Chalmers, M.J., et al. (2012). Molecular Mimicry Regulates ABA Signaling by SnRK2 Kinases and PP2C Phosphatases. Science *335*, 85–88.

Southern, E.M. (1975). Detection of specific sequences among DNA fragments separated by gel electrophoresis. J. Mol. Biol. *98*, 503–517.

Souza, C. de A., Li, S., Lin, A.Z., Boutrot, F., Grossmann, G., Zipfel, C., and Somerville, S.C. (2017). Cellulose-Derived Oligomers Act as Damage-Associated Molecular Patterns and Trigger Defense-Like Responses. Plant Physiol. *173*, 2383–2398.

Spanu, P.D., and Panstruga, R. (2017). Editorial: Biotrophic Plant-Microbe Interactions. Front. Plant Sci. *8*.

Spartz, A.K., Ren, H., Park, M.Y., Grandt, K.N., Lee, S.H., Murphy, A.S., Sussman, M.R., Overvoorde, P.J., and Gray, W.M. (2014). SAUR Inhibition of PP2C-D *Phosphatases* Activates Plasma Membrane H+-ATPases to Promote Cell Expansion in Arabidopsis. Plant Cell.

Spellig, T., Bottin, A., and Kahmann, R. (1996). Green fluorescent protein (GFP) as a new vital marker in the phytopathogenic fungus *Ustilago maydis*. MGG Mol. Gen. Genet. *252*, 503–509.

Steentoft, C., Vakhrushev, S.Y., Joshi, H.J., Kong, Y., Vester-Christensen, M.B., Schjoldager, K.T.-B.G., Lavrsen, K., Dabelsteen, S., Pedersen, N.B., Marcos-Silva, L., et al. (2013). Precision mapping of the human O-GalNAc glycoproteome through SimpleCell technology. EMBO J. *32*, 1478–1488.

Stothard, P. (2000). The sequence manipulation suite: JavaScript programs for analyzing and formatting protein and DNA sequences. BioTechniques *28*, 1102, 1104.

Tanaka, S., Brefort, T., Neidig, N., Djamei, A., Kahnt, J., Vermerris, W., Koenig, S., Feussner, K., Feussner, I., and Kahmann, R. (2014). A secreted *Ustilago maydis* effector promotes virulence by targeting anthocyanin biosynthesis in maize. ELife *3*.

Taniguti, L.M., Schaker, P.D.C., Benevenuto, J., Peters, L.P., Carvalho, G., Palhares, A., Quecine, M.C., Nunes, F.R.S., Kmit, M.C.P., Wai, A., et al. (2015). Complete Genome Sequence of *Sporisorium scitamineum* and Biotrophic Interaction Transcriptome with Sugarcane. PLOS ONE *10*, e0129318.

Testerink, C., and Munnik, T. (2011). Molecular, cellular, and physiological responses to phosphatidic acid formation in plants. J. Exp. Bot. *62*, 2349–2361.

Thomma, B.P.H.J., Nürnberger, T., and Joosten, M.H.A.J. (2011). Of PAMPs and Effectors: The Blurred PTI-ETI Dichotomy. Plant Cell *23*, 4–15.

Ton, J., Flors, V., and Mauch-Mani, B. (2009). The multifaceted role of ABA in disease resistance. Trends Plant Sci. *14*, 310–317.

Torres, M.A. (2006). Reactive Oxygen Species Signaling in Response to Pathogens. PLANT Physiol. *141*, 373–378.

Toruño, T.Y., Stergiopoulos, I., and Coaker, G. (2016). Plant Pathogen Effectors: Cellular Probes Interfering with Plant Defenses in Spatial and Temporal Manners. Annu. Rev. Phytopathol. *54*.

Tsukuda, T., Carleton, S., Fotheringham, S., and Holloman, W.K. (1988). Isolation and characterization of an autonomously replicating sequence from *Ustilago maydis*. Mol. Cell. Biol. *8*, 3703–3709.

Umbrasaite, J., Schweighofer, A., Kazanaviciute, V., Magyar, Z., Ayatollahi, Z., Unterwurzacher, V., Choopayak, C., Boniecka, J., Murray, J.A.H., Bogre, L., et al. (2010). MAPK Phosphatase AP2C3 Induces Ectopic Proliferation of Epidermal Cells Leading to Stomata Development in *Arabidopsis*. PLoS ONE *5*, e15357.

Varden, F.A., De la Concepcion, J.C., Maidment, J.H., and Banfield, M.J. (2017). Taking the stage: effectors in the spotlight. Curr. Opin. Plant Biol. *38*, 25–33.

Vleeshouwers, V.G.A.A., and Oliver, R.P. (2014). Effectors as Tools in Disease Resistance Breeding Against Biotrophic, Hemibiotrophic, and Necrotrophic Plant Pathogens. Mol. Plant. Microbe Interact. *27*, 196–206.

Voigt, C.A. (2014). Callose-mediated resistance to pathogenic intruders in plant defense-related papillae. Front. Plant Sci. *5*.

Watkins, A.M., Bonneau, R., and Arora, P.S. (2016). Side-Chain Conformational Preferences Govern Protein–Protein Interactions. J. Am. Chem. Soc. *138*, 10386–10389.

Wei, K., and Pan, S. (2014). Maize protein phosphatase gene family: identification and molecular characterization. BMC Genomics *15*, 773.

West, G.M., Pascal, B.D., Ng, L.-M., Soon, F.-F., Melcher, K., Xu, H.E., Chalmers, M.J., and Griffin, P.R. (2013). Protein Conformation Ensembles Monitored by HDX Reveal a Structural Rationale for Abscisic Acid Signaling Protein Affinities and Activities. Structure *21*, 229–235.

White, D. G. (1999). Compendium of Corn Diseases, 3rd ed. APS Press, St. Paul.

Widjaja, I., Lassowskat, I., Bethke, G., Eschen-Lippold, L., Long, H.-H., Naumann, K., Dangl, J.L., Scheel, D., and Lee, J. (2009). A protein phosphatase 2C, responsive to the bacterial effector AvrRpm1 but not to the AvrB effector, regulates defense responses in *Arabidopsis*: An AvrRpm1-responsive PP2C regulates defense. Plant J. *61*, 249–258.

Willmann, R., Lajunen, H.M., Erbs, G., Newman, M.-A., Kolb, D., Tsuda, K., Katagiri, F., Fliegmann, J., Bono, J.-J., Cullimore, J.V., et al. (2011). *Arabidopsis* lysin-motif proteins LYM1 LYM3 CERK1 mediate bacterial peptidoglycan sensing and immunity to bacterial infection. Proc. Natl. Acad. Sci. *108*, 19824–19829.

Wise, A.A., Liu, Z., and Binns, A.N. (2006). Culture and Maintenance of *Agrobacterium* Strains. In *Agrobacterium* Protocols, (New Jersey: Humana Press), pp. 3–14.

Wu, C.-H., Abd-El-Haliem, A., Bozkurt, T.O., Belhaj, K., Terauchi, R., Vossen, J.H., and Kamoun, S. (2017). NLR network mediates immunity to diverse plant pathogens. Proc. Natl. Acad. Sci. 201702041.

Yan, C., Wu, F., Jernigan, R.L., Dobbs, D., and Honavar, V. (2008). Characterization of Protein–Protein Interfaces. Protein J. *27*, 59–70.

Yasuda, M., Ishikawa, A., Jikumaru, Y., Seki, M., Umezawa, T., Asami, T., Maruyama-Nakashita, A., Kudo, T., Shinozaki, K., Yoshida, S., et al. (2008). Antagonistic Interaction between Systemic Acquired Resistance and the Abscisic Acid-Mediated Abiotic Stress Response in *Arabidopsis*. PLANT CELL ONLINE *20*, 1678–1692.

Yoshida, S., Morita, T., Shinozaki, Y., Watanabe, T., Sameshima-Yamashita, Y., Koitabashi, M., Kitamoto, D., and Kitamoto, H. (2014a). Mannosylerythritol lipids secreted by phyllosphere yeast *Pseudozyma antarctica* is associated with its filamentous growth and propagation on plant surfaces. Appl. Microbiol. Biotechnol. *98*, 6419–6429.

Yoshida, T., Mogami, J., and Yamaguchi-Shinozaki, K. (2014b). ABA-dependent and ABA-independent signaling in response to osmotic stress in plants. Curr. Opin. Plant Biol. *21*, 133–139.

Yu, X., Feng, B., He, P., and Shan, L. (2017). From Chaos to Harmony: Responses and Signaling Upon Microbial Pattern Recognition. Annu. Rev. Phytopathol. *55*.

Zipfel, C. (2014). Plant pattern-recognition receptors. Trends Immunol. *35*, 345–351.

6. Appendix

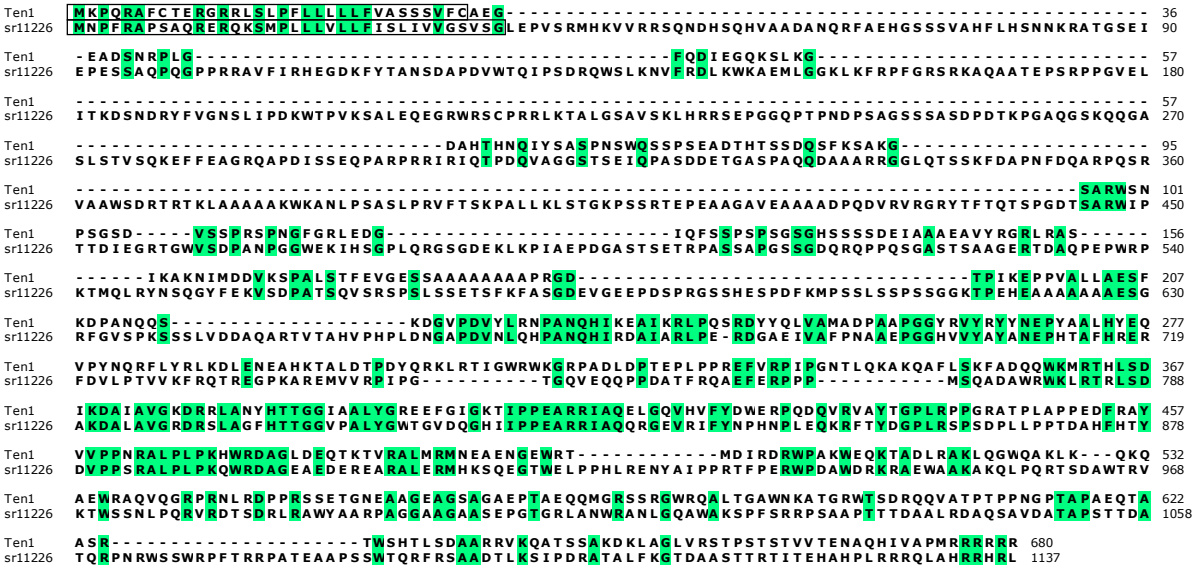

Fig. 33: Local sequence alignment of Ten1 and sr11226 from *S. reilianum*. Black boxes indicate predicted signal peptides.

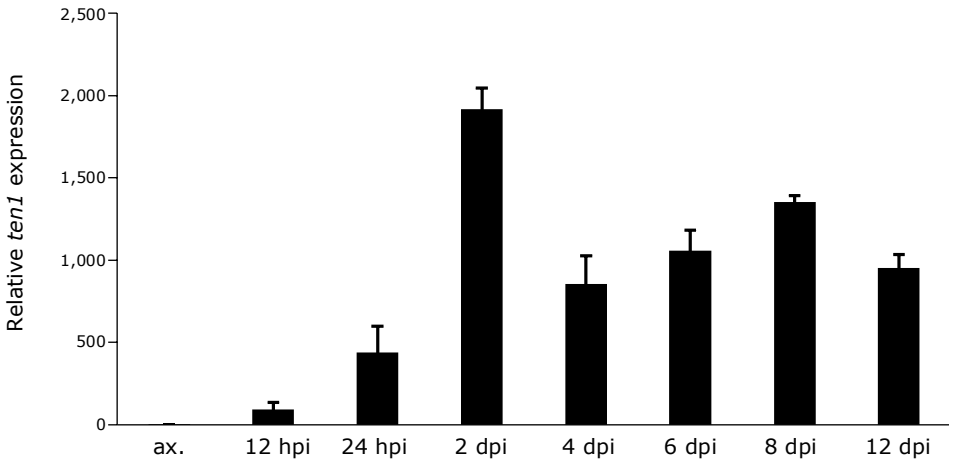

Fig. 34: Relative *ten1* expression after *U. maydis* infection of maize seedlings. Shown are DESeq-normalized gene counts determined by RNAseq analyses of maize seedling leaves infected with FB1 and FB2. ax., axenic culture; hpi, hours post-infection; dpi, days post-infection (data provided by D. Lanver).

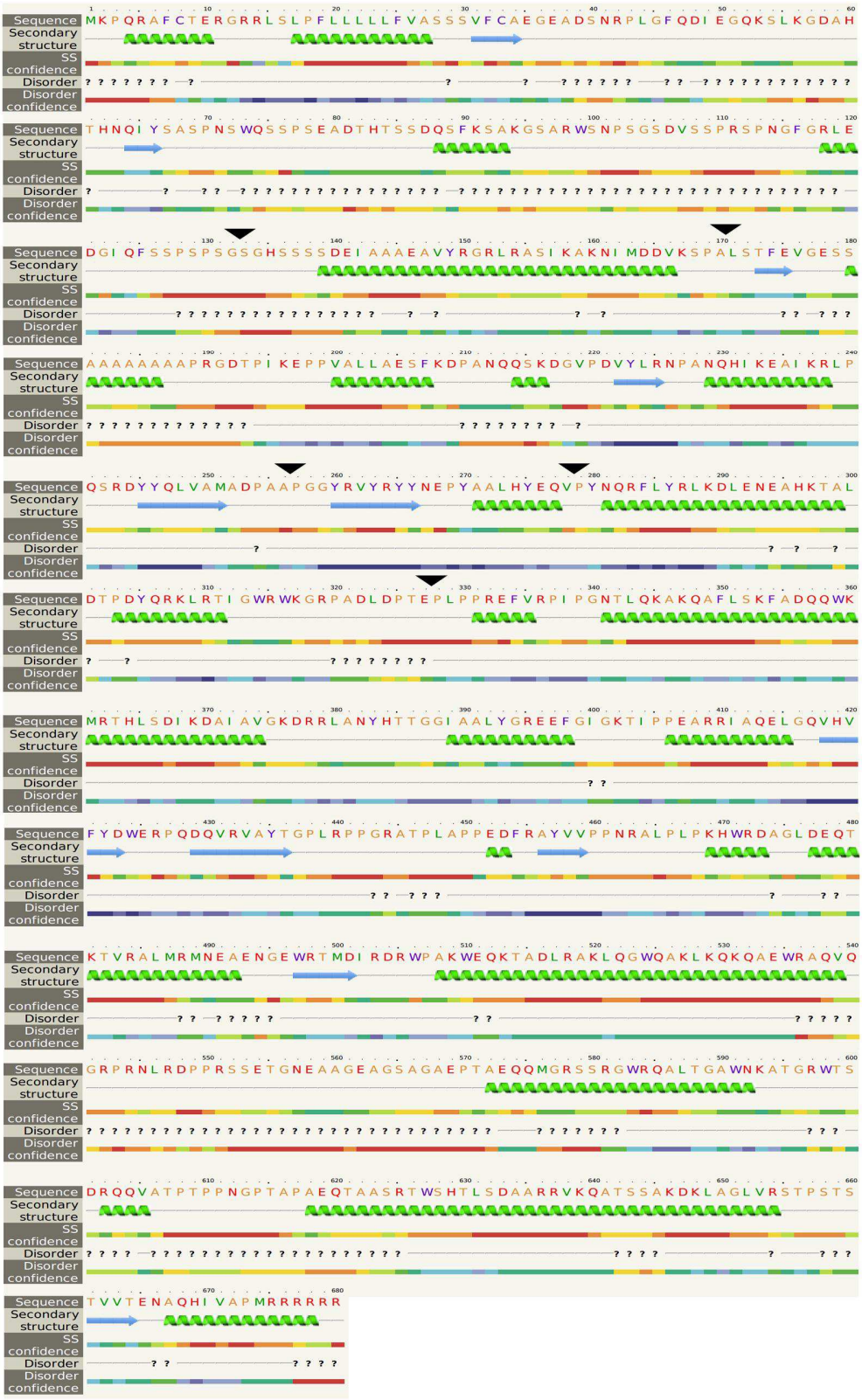

Fig. 35: Secondary structure prediction of Ten1 by Phyre[2]. Green helices indicate alpha helices; blue arrows indicate β-sheets. Black arrowheads indicate truncation sites for the mapping of the ZmPP26-interacting domain and for the insertion of a triple HA-tag between residues 132 and 133.